Analisys Note:
A Measurement of Inclusive Charged Current Interaction Rate at SciBooNE

Part 1

Yasuhiro Nakajima

May 1, 2010

Contents

Chapter 1

Overview

The final goal of this analysis is to search for ν_μ disappearance using both SciBooNE and MiniBooNE data.

Since this analysis involves too many studies and information to fit in a single technote, I am going to separate the description of the analysis into three documents:

1. A note describes the SciBooNE samples and the spectrum fit. (this note)
2. A note describes the improved method for the SciBooNE spectrum fit.
3. A note describes the joint oscillation fit constrained by SciBooNE measurements.

This tech-note describe a measurement of neutrino interaction rate (flux $\times$ cross-section) at SciBooNE detector, as a part of SciBooNE-MiniBooNE joint ν_μ disappearance analysis.

As described in the rest of this document, we find data/MC disagreement after the spectrum fit. The sources are not yet fully understood while there are several hints to understand that. So there will be another technote (Part 2) which describes further study of SciBooNE data to understand the data and MC discrepancy.

The measured neutrino interaction rate will be used to predict at neutrino flux and shape at the MiniBooNE detector.

Chapter 2

Data and MC samples

2.1 Data

For this analysis, the entire neutrino-mode data sets are used. The corresponding POT is 9.9×10^{19}.

2.2 Simulation

2.2.1 Beam Simulation

We use beam MC sample produced on April 07 by MiniBooNE people. The detail of the flux model are described in their paper.

2.2.2 Neutrino Interaction Simulation

To make a comparison with MiniBooNE with consistent cross-section model, we use NUANCE program for neutrino interaction simulation. The models and parameters used are "MiniBooNE May 07 default" ones. Table 2.1 shows the important parameters used. The parameters used in NEUT are also shown in this table as a reference.

Table 2.1: Parameter used for Neutrino interaction simulation

Parameter	NUANCE	NEUT
p_F	220 MeV/c	217 MeV/c
E_B	34 MeV/c	27 MeV/c
M_A	1.234 GeV	1.21 GeV
κ	1.022	1.00
Res. π M_A	1.10 GeV	1.21 GeV

There are another couple of important differences between NEUT and NUANCE. First, lepton mass corrections for resonant π and coherent π production are not applied for NUANCE, while they are used for NEUT. Second, We apply scale factor of 0.65 for coherent π production, which come from MiniBooNE's neutral current coherent π measurement.

The more detailed comparison between NUANCE and NEUT are summarized in the tech-note by Kendall.

2.2.3 Detector Response Simulation

Our Geant4 based detector simulation is described elsewhere.

Chapter 3

Event Reconstruction

3.1 Track Reconstruction

3.1.1 Tracking

Tracking and matching algorithm are described at Hiraide-san's analysis note.

3.1.2 Muon Momentum Reconstruction

"Muon momentum" is reconstructed for every tracks, including tracks stopped in SciBar/EC and penetrated MRD as well as those stopped in MRD. The reconstruction method and its performance are described here.

MRD-matched Muons

For the tracks originated from SciBar and matched to MRD, the total energy (E_μ) is reconstructed as:

$$E_\mu = E_\mu^{SciBar} + E_\mu^{EC} + E_\mu^{Wall} + E_\mu^{MRD},$$

where E_μ^{SciBar}, E_μ^{EC} and E_μ^{Wall} are expected energy deposit by muons at SciBar, EC and the wall of the dark box between EC and MRD, respectively. E_μ^{MRD} is calculated using range-to-energy conversion table.

We estimated these energy deposits using the MC simulation. The values used for the reconstruction are: E_μ^{SciBar}/(path length) = 2.04 MeV/cm, $E_\mu^{EC} = 90.8/\cos\theta_\mu$ MeV and $E_\mu^{Wall} = 3.3/\cos\theta_\mu$ MeV. The range-to-energy conversion factor used to compute E_μ^{MRD} is shown in the Figure 3.1. Figure 3.2 shows the expected muon momentum resolution for MRD-stopped muons.

SciBar-stopped Muons

For the tracks contained in the SciBar detector, E_μ is reconstructed using a separate range to energy conversion table estimated by MC.

Figure 3.3 shows the range to energy conversion table for SciBar-contained tracks. The expected muon momentum resolution is shown in the Figure 3.4. The resolution is much better compared to MRD-stopped sample since we can measure the muon range more precisely for SciBar-contained tracks.

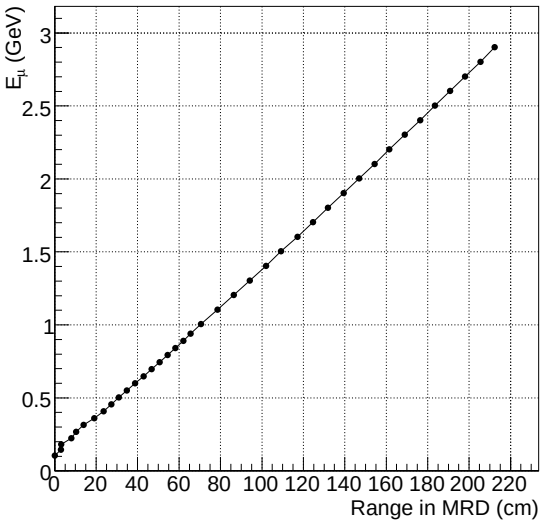

Figure 3.1: Range to muon energy conversion table used to reconstruct E_μ^{MRD}.

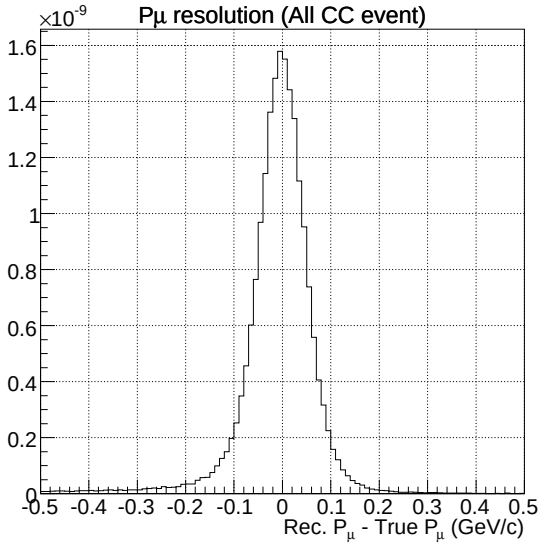

Figure 3.2: Muon momentum resolution for MRD-stopped tracks.

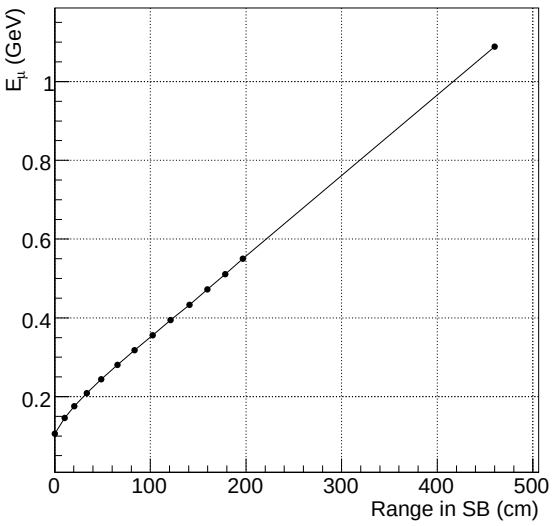

Figure 3.3: Range to muon energy conversion table used to reconstruct E_μ for SciBar-contained tracks.

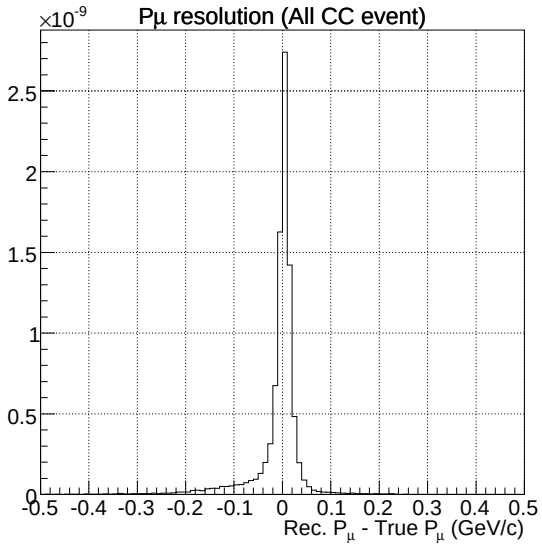

Figure 3.4: Muon momentum resolution for SciBar contained tracks.

3.2 Event Selection

3.2.1 Overview

To measure muon neutrino flux, we use Charged Current (CC) event occurred in SciBar inclusively. The signature of the CC events is a long muon track.

First, we select tracks with MuCL greater than 0.05, and define the highest momentum (longest) track among those as a muon candidate. Then a series of "base cuts" are applied to increase CC purity. Finally, the sample is sub-divided into 3 sub-samples using the the stopping point of the highest momentum track : SciBar-Stopped, MRD-stopped and MRD-penetrated samples. Although it is possible to make EC-stopped sample, this sample is not used for this analysis because of its small statistics and large NC contamination.

The detail of these event selections are described in the following sections.

3.2.2 Base Cuts

The following cuts are applied to the all samples to increase signal purity.

Timing cut We require the track timing t is within $0 < t < 2\mu sec$.

Fiducial volume cut Tentatively, we define the vertex as the upstream edge of the longest track, and require the (x,y,z) position to be $|x| < 130\ cm$, $|y| < 130\ cm$, and $2.62 < |z| < 157.2$ cm.

P_μ cut This cut is to remove neutral current backgrounds, especially from SciBar-stopped sample. We require reconstructed $P_\mu > 0.25\ GeV$

Then the sample is further divided into three using the stopping point of the muon track.

3.2.3 MRD-Stopped Sample

MRD-stopped sample is selected by requiring the longest track reached to MRD. Then we require the end points to be:

- $|x| < 132\ cm$
- $|y| < 111\ cm$
- $z <$ the last layer of the MRD

These cuts are to remove muons escaped from side or downstream ends of the MRD. Figure 3.5 and Figure 3.6 show the distribution of reconstructed muon momentum and angle of the MRD-stopped tracks.

Then, neutrino energy(E_ν) and Q^2 are reconstructed assuming CC-QE interaction as given by the following formula,

$$E_\nu^{QE} = \frac{m_p^2 - (m_n - V)^2 - m_\mu^2 + 2(m_n - V)E_\mu}{2(m_n - V - E_\mu + p_\mu \cos\theta_\mu)},$$

where m_p, m_n and m_μ are the mass of proton, neutron and muon, respectively, and V is the nuclear potential energy ($= 27MeV$). The reconstructed Q^2 is given by,

$$Q^2 = 2E_\nu(E_\mu - p_\mu \cos\theta_\mu) - m_\mu^2.$$

Figures 3.7 and 3.8 are reconstructed E_ν and Q^2 distribution, respectively. Although reconstructed E_ν and Q^2 are not directly used in the spectrum fit, these are good variables to check the flux prediction and cross-section predictions.

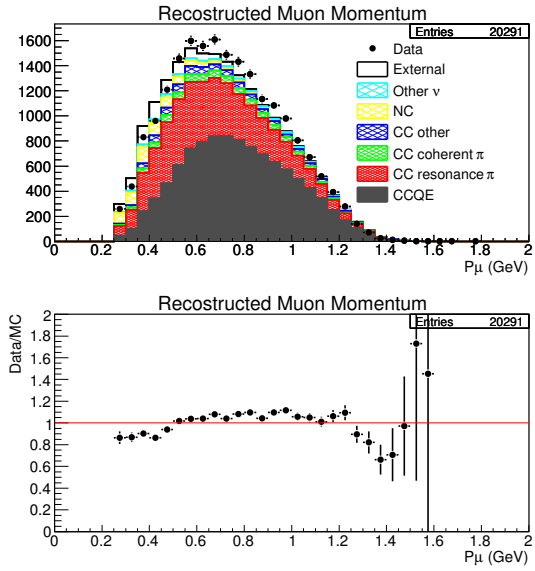

Figure 3.5: Reconstructed p_μ distribution for MRD-stopped sample. MC is relatively normalized by the number of MRD-matched events.

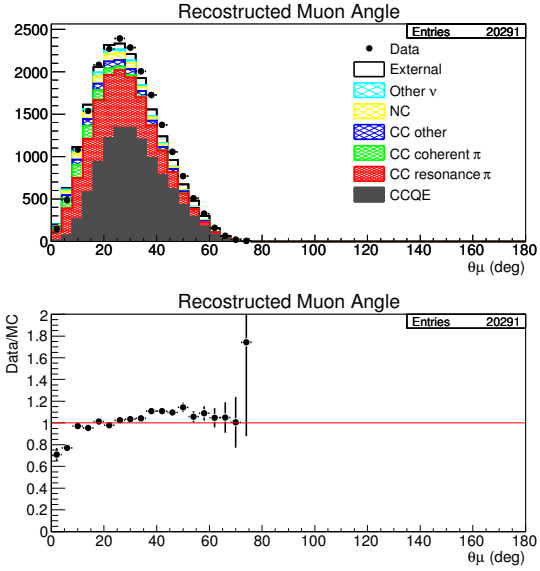

Figure 3.6: Reconstructed θ_μ distribution for MRD-stopped sample MC is relatively normalized by the number of MRD-matched events.

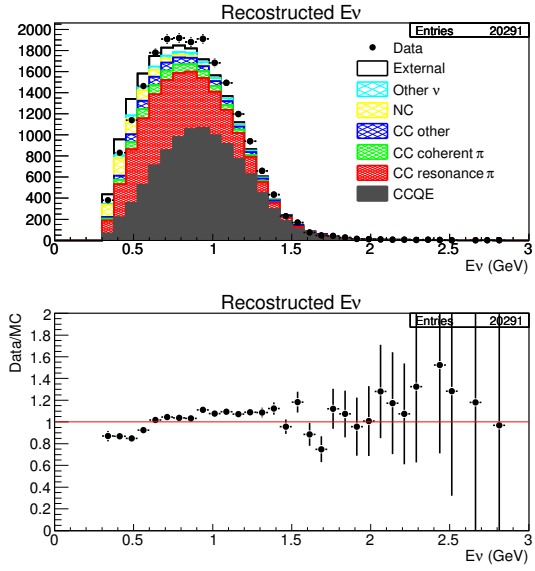

Figure 3.7: Reconstructed E_ν distribution for MRD-stopped sample. MC is relatively normalized by the number of MRD-matched events.

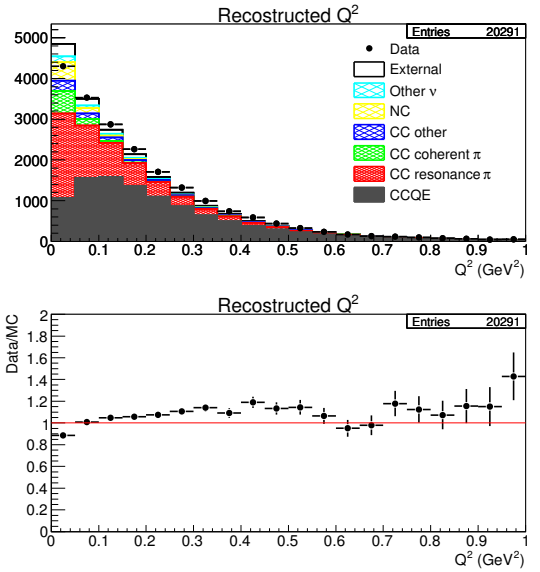

Figure 3.8: Reconstructed Q^2 distribution for MRD-stopped sample MC is relatively normalized by the number of MRD-matched events.

3.2.4 MRD-Penetrated Sample

MRD-penetrated events are selected by requiring muons reached to the downstream end of the MRD. Although we cannot reconstructed muon momentum since these muons are not stopped in the detectors, this sample have strong constraint on the normalization at highest energy region. Hence, the muon angle distributions are used in the spectrum fit.

Figure 3.9 shows the distribution of muon angle for the MRD-penetrated sample.

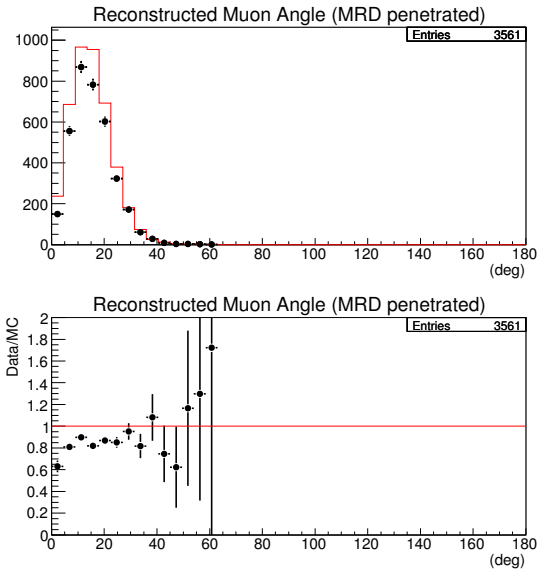

Figure 3.9: Reconstructed muon angle for MRD-stopped sample. MC is relatively normalized by the number of MRD-matched events.

3.2.5 SciBar-Stopped Sample

The final sample is SciBar-stopped sample. To select muons contained in SciBar, we require both downstream and upstream ends the tracks to be within the fiducial volume.

Validity of the p_μ Cut

This sample is especially suffered by the large contamination of backgrounds from NC interaction and the neutrino interaction in the dirt. To remove these backgrounds, we require "P_μ" to be greater than 0.25 GeV.

Figure 3.10 shows the muon momentum distribution before applying "P_μ" cut. We can see the large portion of NC and Dirt events are removed by this "P_μ" requirement

The other motivation of p_μ requirement come from MiniBooNE sample. They require (the number of tanks hits) > 200, to deject the Michel electron signals. Figure 3.11 shows the true p_μ distribution of MiniBooNE final ν_μ CC-QE sample used for the oscillation fit. From this figure, we can see the tank hits threshold corresponds to $p_\mu \sim 0.25$ GeV/c. Hence, we don't gain sensitivity to the oscillation analysis by lowering the p_μ threshold below 0.25 GeV/c.

Additionally, the validity of MuCL requirement is checked since the MuCL is tuned for high momentum muons. Figure 3.12 shows the distribution of MuCL vs. p_μ for true muon tracks in SciBar-stopped sample. Although the current MuCL tend to return 0 for low momentum muons, it is safe to use once we require $p_\mu > 0.25$ GeV/c.

Track Direction ID

For SciBar-stopped sample, the decay electrons from muons are used to identify the direction of the muon tracks. The decay electron signal is selected by requiring delayed TDC hits at the ends

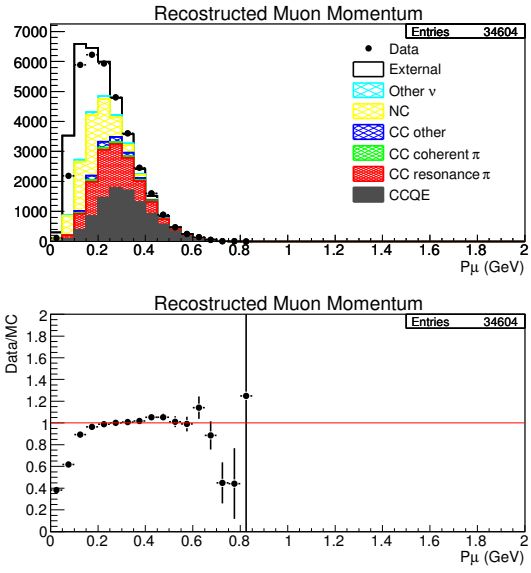

Figure 3.10: Reconstructed muon momentum after applying base cuts except for P_μ and MuCL cuts. Events with $P_\mu > 0.25$ GeV are selected.

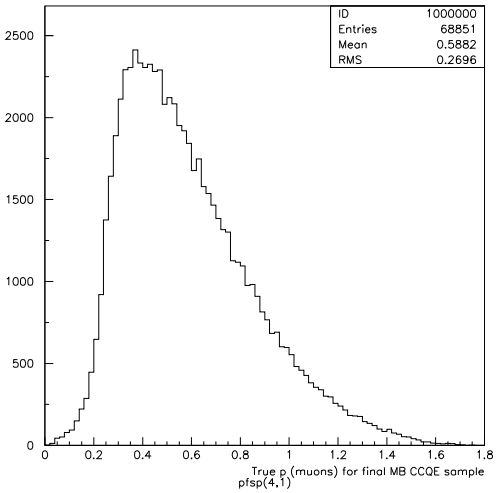

Figure 3.11: True muon momentum of MiniBooNE final ν_μ CC-QE sample used for the oscillation fit.

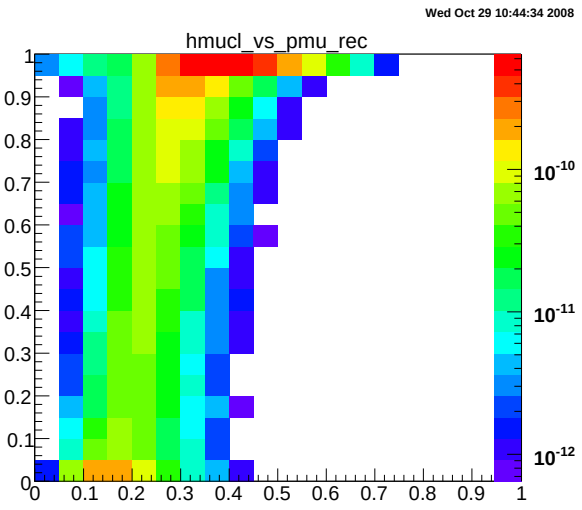

Figure 3.12: The distributions of MuCL vs. p_μ for true muon tracks in SciBar-stopped sample. The color represent the number of event in logarithm scale.

of SciBar tracks. We also require coincidence of TDC signal from the top- and side-view to remove hits from random noise or after pulses.

Figures 3.13 and 3.14 are timing distributions of the delayed hits at the upstream and downstream edge of SciBar tracks.

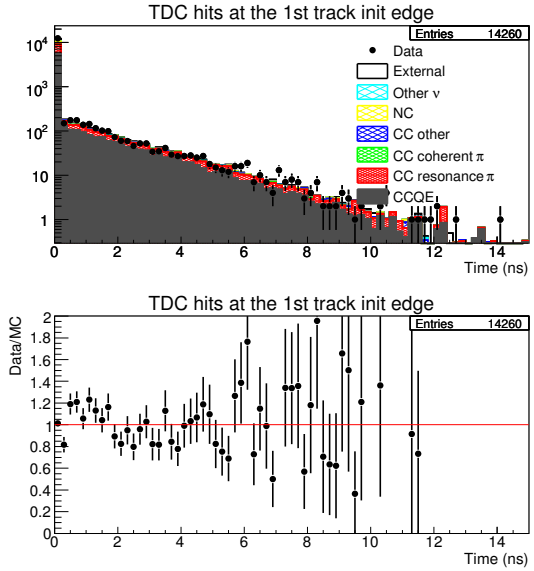

Figure 3.13: Timing distribution of hits on TDC at the upstream edge of the SciBar stopped track.

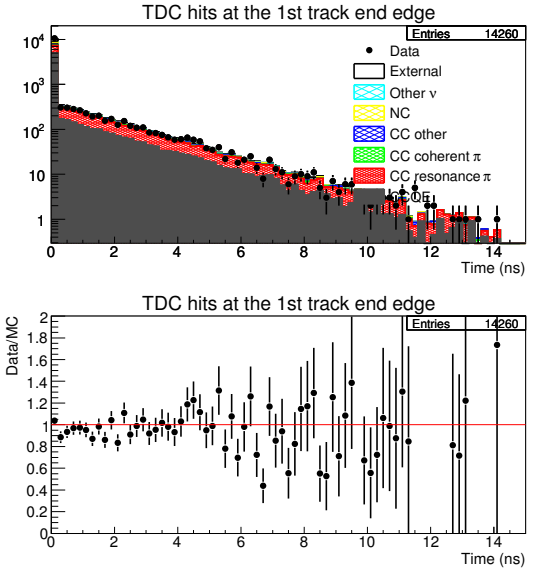

Figure 3.14: Timing distribution of hits on TDC at the downstream edge of the SciBar stopped track.

Using these information, tracks

- have delayed hit at $t > 200$ *nsec* at the upstream ends, and
- don't have delayed hit at $t > 200$ *nsec* at the downstream ends

are identified as backward-going tracks. According to the MC simulation of CCQE event reconstructed as 1 track events, ~ 57 % of the backward-going track can be found with this method and miss identification probability is $\sim$1 %.

Basic Distributions

Figures 3.15 and 3.16 are reconstructed muon momentum and angle distributions for SciBar-stopped sample. Also, Figures 3.17 and 3.18 are reconstructed neutrino energy and Q^2 distributions. We see good agreement between data and MC for E_ν distribution. However, large data deficit at the low Q^2 region is found. For the spectrum fitting, we assign additional systematic uncertainty to cover this discrepancy. The detail of this error is described in the later sections.

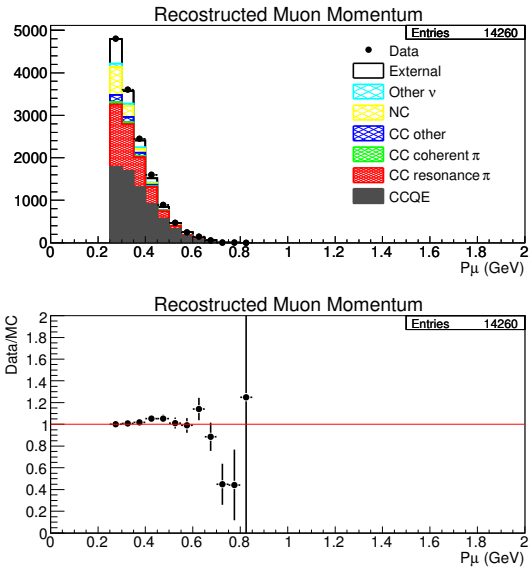

Figure 3.15: Reconstructed p_μ distribution for SciBar-stopped sample MC is relatively normalized by the number of MRD-matched events.

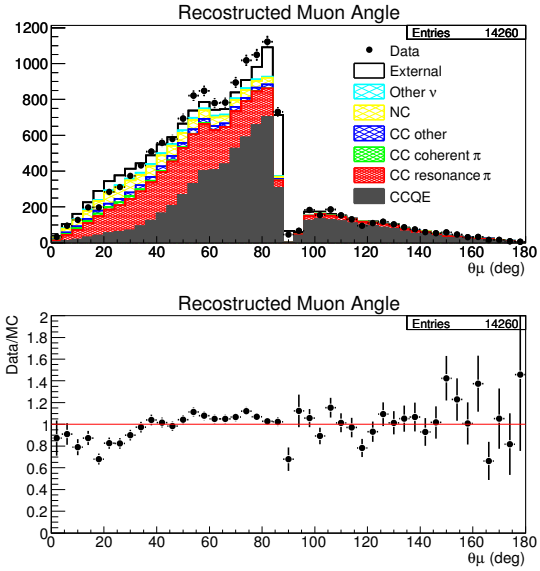

Figure 3.16: Reconstructed θ_μ distribution for SciBar-stopped sample MC is relatively normalized by the number of MRD-matched events.

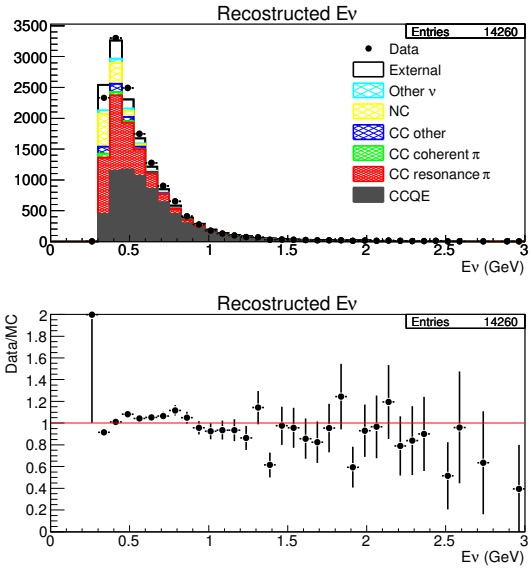

Figure 3.17: Reconstructed E_ν distribution for SciBar-stopped sample MC is relatively normalized by the number of MRD-matched events.

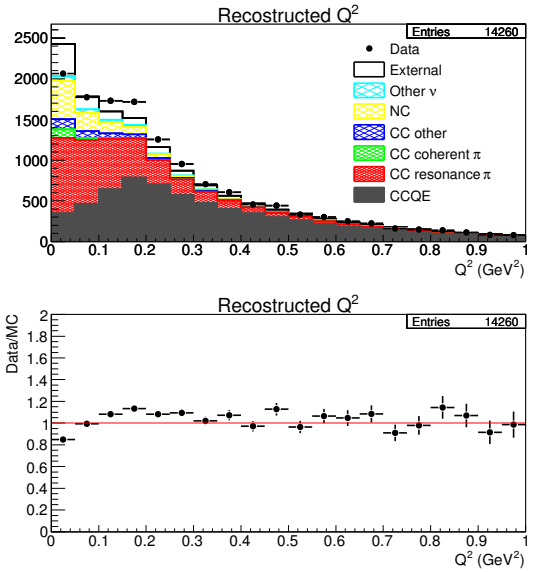

Figure 3.18: Reconstructed Q^2 distribution for SciBar-stopped sample MC is relatively normalized by the number of MRD-matched events.

3.2.6 Acceptance

Figures 3.19 and 3.20 shows acceptance as a function of true P_μ and θ_μ.

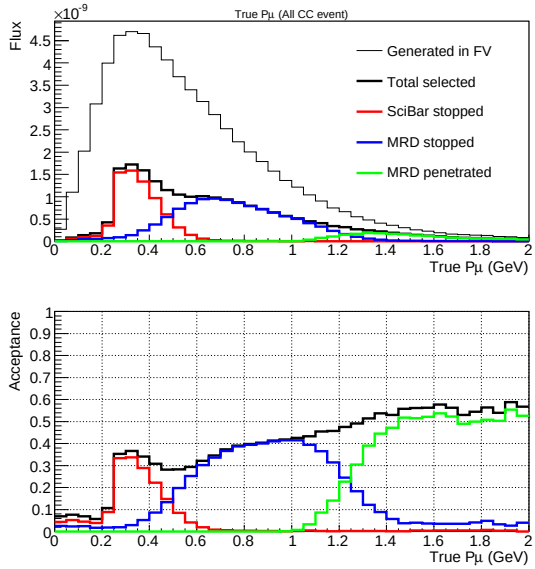

Figure 3.19: Acceptance as a function of true muon momentum.

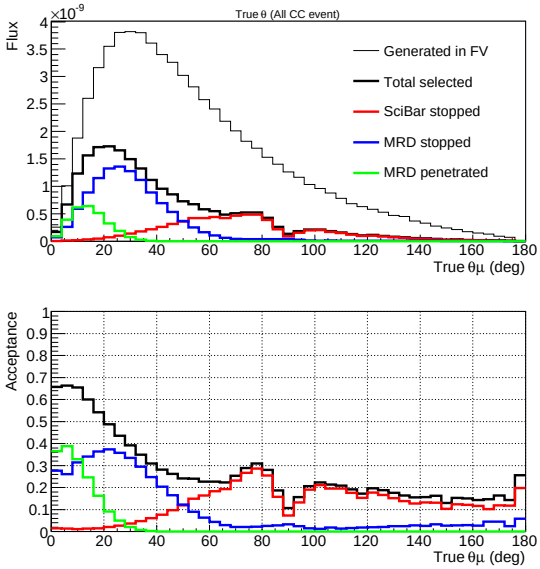

Figure 3.20: Acceptance as a function of true muon angle. The dip around 90 degree is due to SciBar geometry. We cannot reconstruct vertical tracks since we need at least 3 layer hit to form tracks.

Figure 3.21 is the acceptance as a function of true neutrino energy. [1]

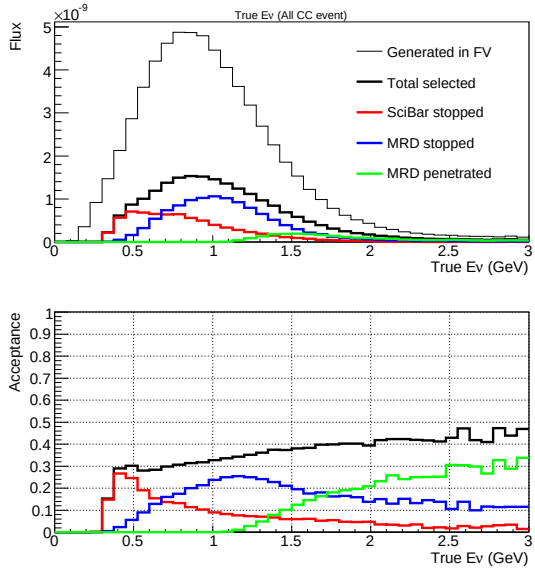

Figure 3.21: Acceptance as a function of true neutrino energy for each samples.

[1] These plots are based on NEUT prediction. Should be very similar to NUANCE prediction.

Chapter 4

Data and MC Comparison in Absolute Scale

In this chapter, we describe the data/MC comparisons in the absolute scale before the spectrum fit.

4.1 Systematic Uncertainty

The following systematic uncertainties are considered.

4.1.1 Flux Uncertainty

The detail of the flux model and its uncertainty is described elsewhere (reference: MiniBooNE flux paper). The only difference to this reference is that we use the uncertainty based on spline fit for π^+/π^- production at the target (need reference).

4.1.2 Neutrino Interaction Cross-section Uncertainty

Primary Interaction Uncertainty

Errors for cross-section parameters are estimated by MC re-weighting using "NuanceInterface". In the NuanceInterface, we vary the cross-section parameters and re-calculate interaction cross-section with the varied parameter sets. The weight is computed as the ratio of valid and nominal cross-sections.

However, we found that "QE κ" variation is not properly predicted by the NuanceInterface. Then, we produced a special function of Q^2 to estimate the variation. The detail of estimating κ variation is described in the Appendix B.4.

The parameter variation is randomly drawn with the systematic uncertainties. Table 4.1 is the summary of the nominal cross-section values and its variations.

Final State Interaction Uncertainty

We vary π absorption and charge exchange cross-section in the nucleus by $\pm 20\%$ and $\pm 35\%$, respectively. Independent Monte Carlo samples are produced with this varied cross-section model, and the difference to the nominal value is assigned as the systematic uncertainty.

Table 4.1: Systematic uncertainties for cross-section parameters

Parameter	Nominal value	Variation
p_F	220 MeV/c	±30
E_B	34 MeV/c	±9
QE M_A	1.234 GeV	±0.234
QE κ	1.022	±0.022
Resonant π M_A	1.10 GeV	±0.275
Coherent π M_A	1.03 GeV	±0.275
Multi-π M_A	1.30 GeV	±0.52
ΔS	0	±0.1

Single π Production Q^2 Shape

We found data-MC discrepancy at low Q^2 region of CC-1π enriched sample. Then, we made a fit to extract the size of discrepancy and obtained scale factors of

$$P_{1\pi} = \begin{cases} 2.14 \times Q^2 + 0.43 & (Q^2 \leq 0.2\ GeV) \\ 1 & (Q^2 > 0.2\ GeV) \end{cases} \text{ and} \tag{4.1}$$

$$P_{Coh-\pi} = 0.56, \tag{4.2}$$

where $P_{1\pi}$ is a factor for CC resonant 1π production and $P_{Coh-\pi}$ is one for CC coherent 1π production. The detail of the fitting is described in the Appendix A.

The difference between before and after applying these scale factors is assigned as systematic uncertainty.

4.1.3 Detector Uncertainty

dE/dx uncertainty

The uncertainties of "stopping power" of SciBar and MRD is estimated to be 3 %, and 10 % for EC. This estimation is based on K2K analysis.(need reference)

To evaluate the effect of this uncertainty, we generate MC sample with different detector densities: The variation is ± 3 % for SciBar and MRD, and ± 10 % for EC. Then the differences to the nominal MC prediction are assigned to the error.

In K2k this effect is simply tread as a shift of muon momentum scale. However, in SciBooNE, the change of stopping power also have large effect to the acceptance due to limited MRD size. To take this effect into account, we re-run MC simulation with different density (stopping power).

Pion interaction cross-section

The uncertainty of total pion interaction cross-section in the detector is estimated to be 10 %.(ref: Hiraide-san's thesis). We generate MC sample with ± 10 % pion interaction cross-section. The difference to the nominal MC is assigned as systematic error.

Dirt density uncertainty

We generate dirt MC simulation by varying the dirt density by ± 20 %.

4.2 Basic Distributions

4.2.1 SciBar-Stopped Sample

Figures 4.1 and 4.2 shows the distributions of reconstructed p_μ, θ_μ, E_ν and Q^2 of SciBar-stopped sample. Unlike the distribution shown in the previous sections, the MC predictions are absolutely normalized by the number of POT. The size of systematic errors are also shown in these figures.

We found that the number of events are larger than MC prediction by bit more than 1 σ variation, which is dominated by the cross-section uncertainty.

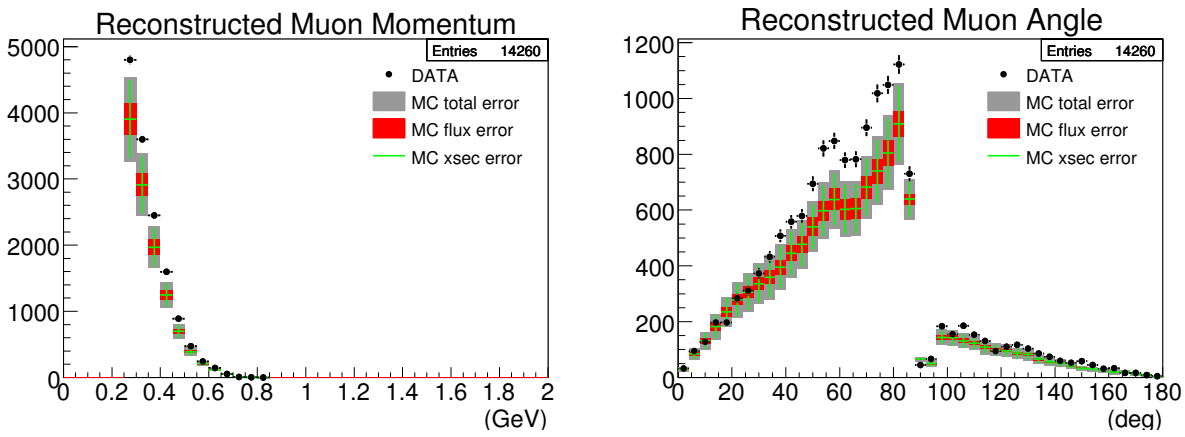

Figure 4.1: Reconstructed p_μ (left) and θ_μ (right) distribution for SciBar-stopped sample. MC distribution is absolutely normalized by the POT.

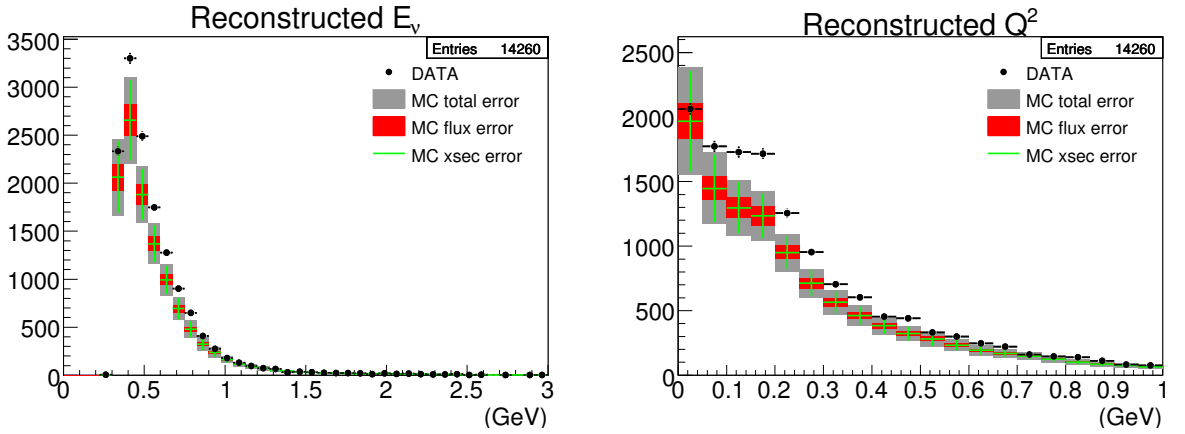

Figure 4.2: Reconstructed E_ν (left) and Q^2 (right) distribution for SciBar-stopped sample. MC distribution is absolutely normalized by the POT.

4.2.2 MRD-Stopped Sample

Figures 4.3 and 4.4 shows the distributions of reconstructed p_μ, θ_μ, E_ν and Q^2 of MRD-Stopped sample. Again, the MC distributions are normalized by the POT.

In this sample, we also found that the number of events are larger than MC prediction by bit more than 1 σ variation. This is similar behaviour to the SciBar-stopped sample.

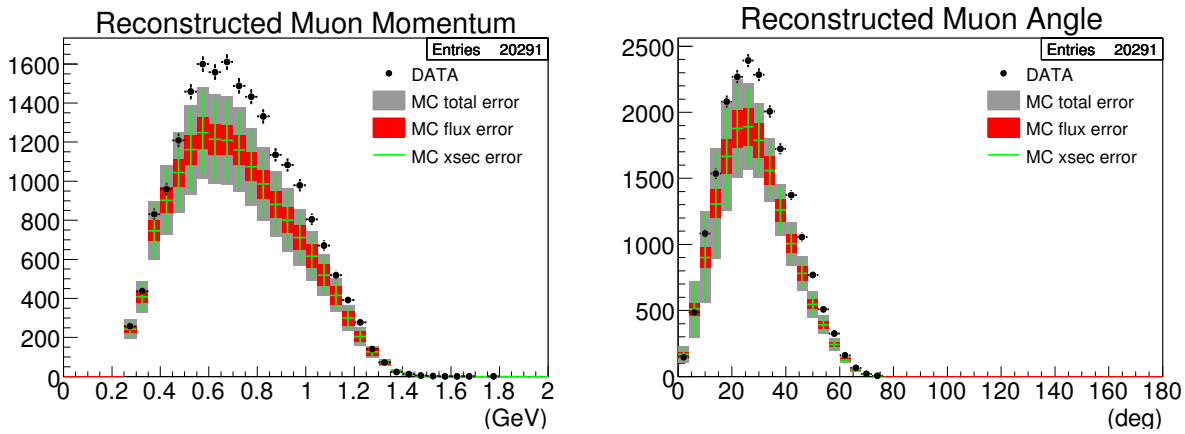

Figure 4.3: Reconstructed p_μ (left) and θ_μ (right) distribution for MRD-stopped sample. MC distribution is absolutely normalized by the POT.

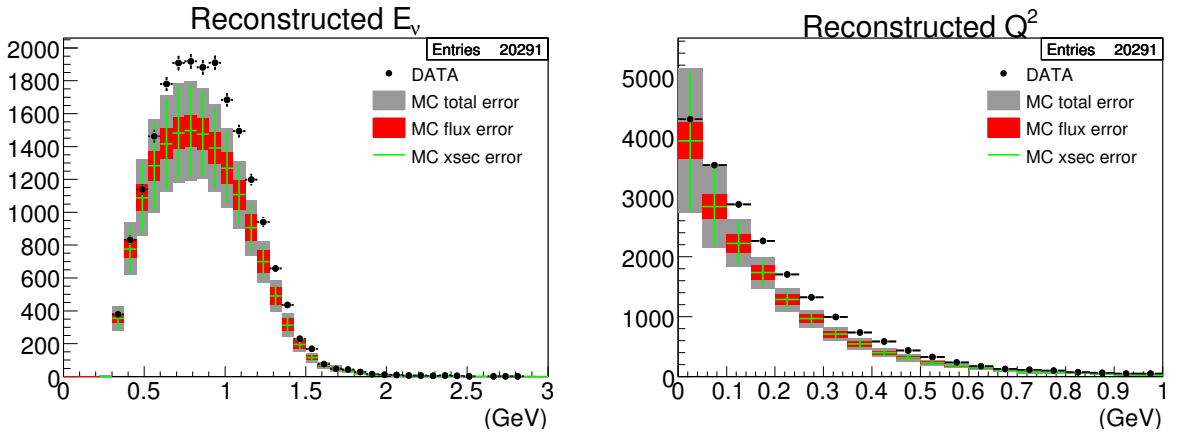

Figure 4.4: Reconstructed E_ν (left) and Q^2 (right) distribution for MRD-stopped sample. MC distribution is absolutely normalized by the POT.

4.2.3 MRD-Penetrated Sample

Figure 4.5 shows the distributions of θ_μ of the MRD-Stopped sample. Again, the MC distributions are normalized by the POT.

In this sample, we found the data normalization is almost consistent to the MC sample. Although this is different behaviour to the SciBar-stopped and MRD-stopped samples, it is quite possible for the following reasons; (1) MRD-penetrated sample is dominated by the flux from kaon decay while the other samples are mostly from pion decay, (2) MRD-penetrated sample has acceptance only to small Q^2 region, where large cross-section uncertainties are expected.

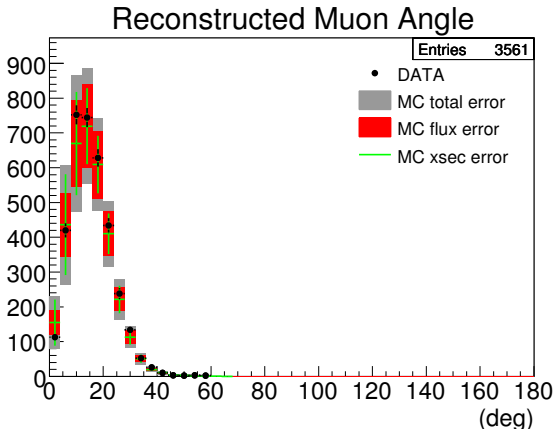

Figure 4.5: θ_μ distribution for MRD-penetrated sample.

4.3 Summary

Overall, we found data excess of bit more than 1 σ variation at most of regions. Since these variations are not very significant, we assume that this variation is due to cross-section and flux uncertainty, and proceed to the spectrum fitting with the current error.

Chapter 5

Neutrino Spectrum Fit

We extract scale factors for true E_ν regions by fitting two dimensional P_μ vs. θ_μ distributions from SciBar-stopped and MRD-stopped samples, and θ_μ distribution from MRD-penetrated sample simultaneously.

In this section, we first discuss about the choice of samples and binnings, and then describe the definition of the χ^2.

5.1 Choice of Samples and Binnings

5.1.1 Energy Resolution

We reconstruct neutrino spectrum using muon kinematics only. Therefore, the neutrino energy resolutions are determined by two sources: (1) resolution of the muon momentum and angle, and (2) contamination of different interaction modes.

The resolution of muon momentum is shown in the section 3.1.2. Here we discuss about the effect of the source (2).

Since the dominant CC interaction mode is CCQE in our energy region, we discuss the effect of contamination of different interaction modes by comparing true E_ν and E_ν^{QE}.

Figure 5.1 shows the difference of E_ν and E_ν^{QE} from MRD-stopped sample for each true E_ν regions. We can see that as the energy increases, the QE contamination decreases. There are 2 reasons which explain this effect. First, the cross section ratio of CCQE/CC-inclusive decreases as energy increases. Second, given the same energy neutrino, muons from CCQE interaction tend to have larger momentum than any other CC interaction. Since these muons are less likely to stop in the MRD, we loose acceptance for CCQE event from high energy neutrinos.

Figure 5.2 is showing the mean reconstructed neutrino energy and its spread as a function of the true energy. We basically loose the neutrino energy resolution at $E_\nu >\sim 1.3$ GeV for MRD-stopped sample. Hence, the additional information from the MRD-penetrated events can help understanding the spectrum at the high energy region.

5.1.2 Acceptance Comparison to MiniBooNE

Figures 5.3, 5.4 and 5.5 shows the distributions of true muon kinematics and neutrino energy of the accepted events at SciBooNE and MiniBooNE.

We can see the SciBar-stopped + MRD-stopped sample gives us similar muon momentum acceptance to MiniBooNE. On the other hand, MRD-stopped and MRD-penetrated samples have biased acceptance to forward going muons, since we require muon to be reached to MRD.

In terms of neutrino energy, the sum of SciBar-stopped and MRD-stopped samples provides similar coverage to MiniBooNE, and the acceptance of MRD-penetrated sample tend to have higher energy than MiniBooNE sample.

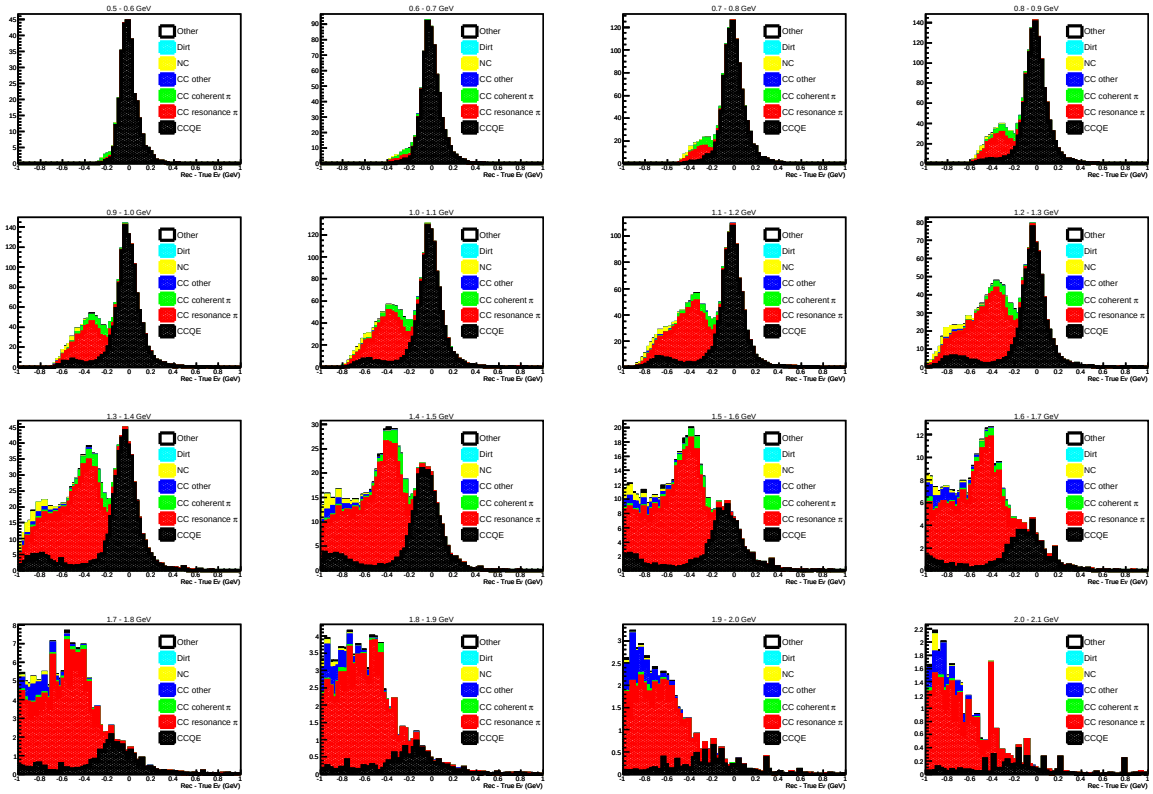

Figure 5.1: Neutrino energy resolutions for each true E_ν regions for MRD-stopped events.

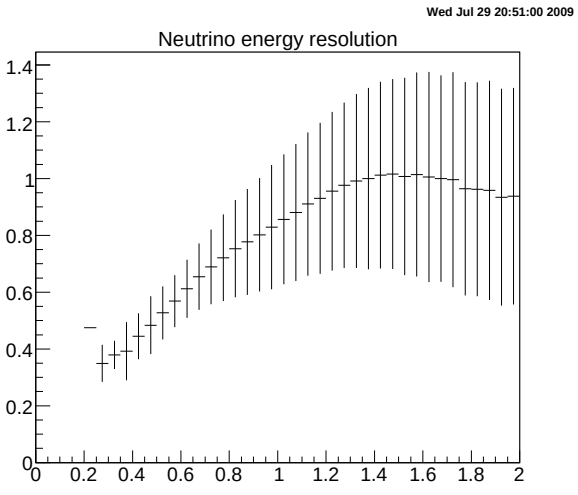

Figure 5.2: Mean value of reconstructed energy assuming CCQE kinematics (E_ν^{QE}), as a function of true E_ν. The error bars represents the RMS of E_ν^{QE} distribution.

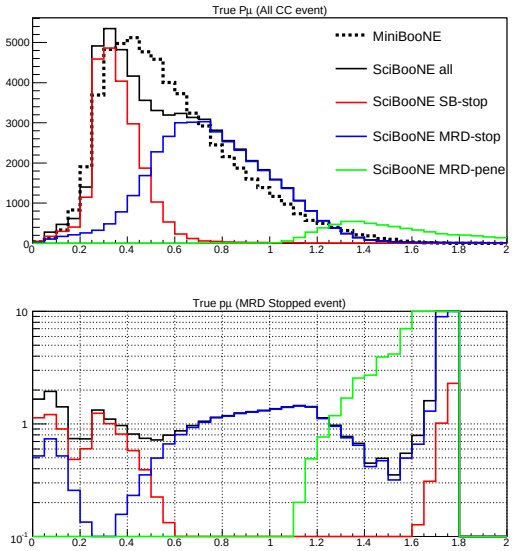

Figure 5.3: Comparison of true P_μ distributions of selected sample at SciBooNE and MiniBooNE

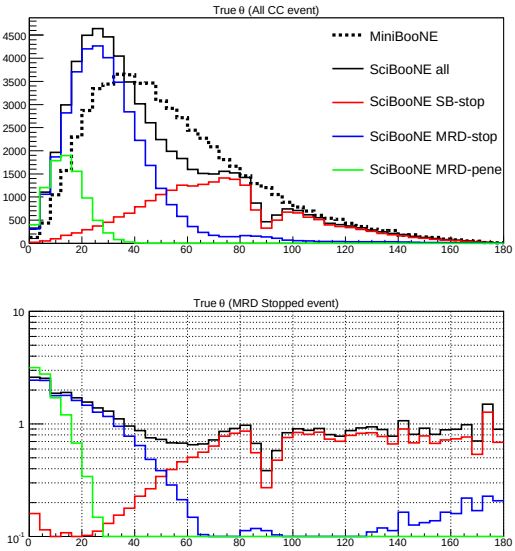

Figure 5.4: Comparison of true θ_μ distributions of selected sample at SciBooNE and MiniBooNE

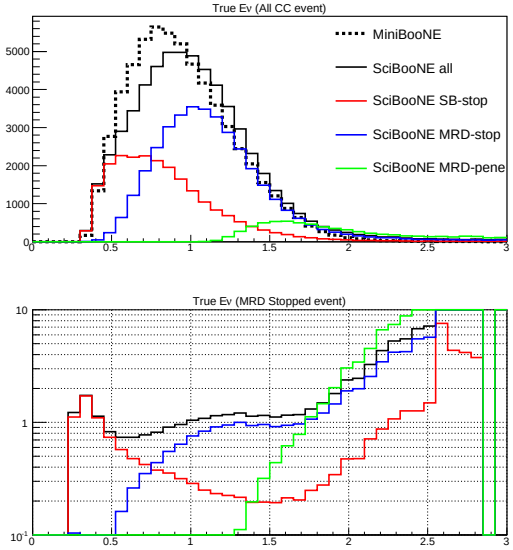

Figure 5.5: Comparison of true E_ν distributions of selected sample at SciBooNE and MiniBooNE

5.1.3 Sample and Binnings

To summarize the discussion above, the sum of SciBar-stopped and MRD-stopped sample provide most similar acceptance to MiniBooNE. However, MRD-stopped sample has very poor energy resolution at the $E_\nu >\sim 1.3$ GeV. This situation is expected be improved by adding MRD-penetrated sample, which provides the flux at the highest energy region.

Thus we adopt all these samples simultaneously (SciBar-stopped, MRD-stopped and MRD-penetrated samples), with the binning shown in the Table 5.1.

In this table, $f_i (i = 0, 1, 2 \cdots)$ represents the scale factor for each E_ν region. We fit these parameters to minimize the χ^2 between data and MC.

Table 5.1: Scale factor for the spectrum fit case B (SciBar-stop + MRD-stop + MRD-pene)

Parameter	f_0	f_1	f_2	f_3	f_4	f_5
E_ν range (GeV)	0 - 0.5	0.5 - 0.75	0.75 - 1.0	1.0 - 1.25	1.25 - 1.75	1.75 -

5.1.4 Monte Carlo Templates

We produce Monte Carlo Templates for each true E_ν region described in the previous section.

Figure 5.6 shows the MC p_μ vs. θ_μ distribution of SciBar-stopped and MRD-stopped sample, respectively. Figures 5.7 and 5.8 are MC templates of these distributions for each true neutrino energy bins. We can see that we have good energy resolution by combining SciBar-stopped and MRD-stopped samples, up to 1.75 GeV. However, we have very poor information of the flux above 1.75 GeV, with SciBar-stopped and MRD-stopped samples only. Therefore, MRD-penetrated can help determining the spectrum shape.

Figure 5.9 shows MC predictions of θ_μ distribution of MRD-penetrated sample. Although the shape of angular distribution itself doesn't have so much information for the energy distribution, this sample have strong information for the normalization of the highest energy bins.

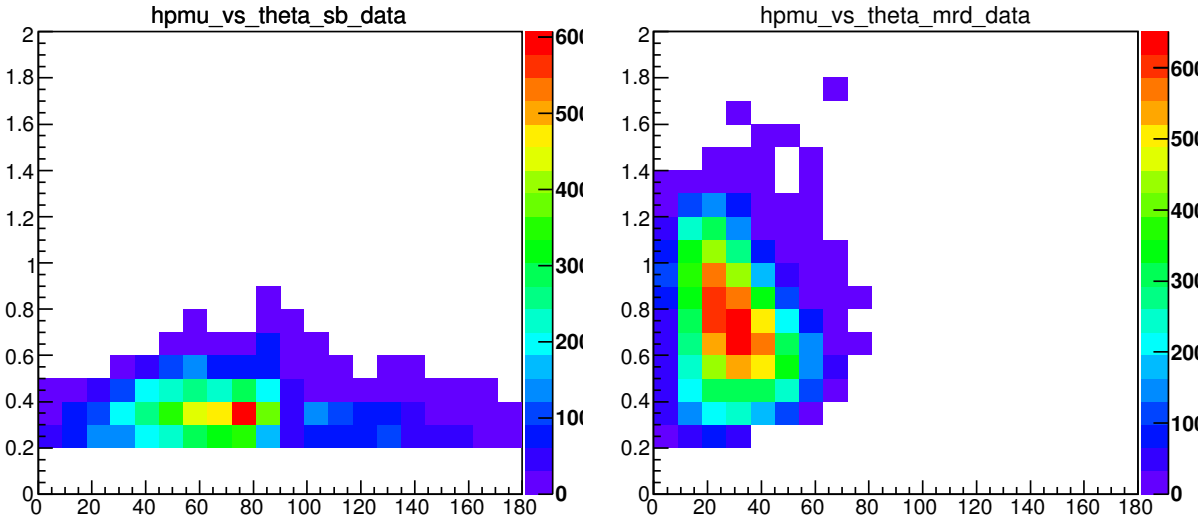

Figure 5.6: Data distributions of p_μ vs. θ_μ for SciBar-stopped (left) and MRD-stopped (right) samples.

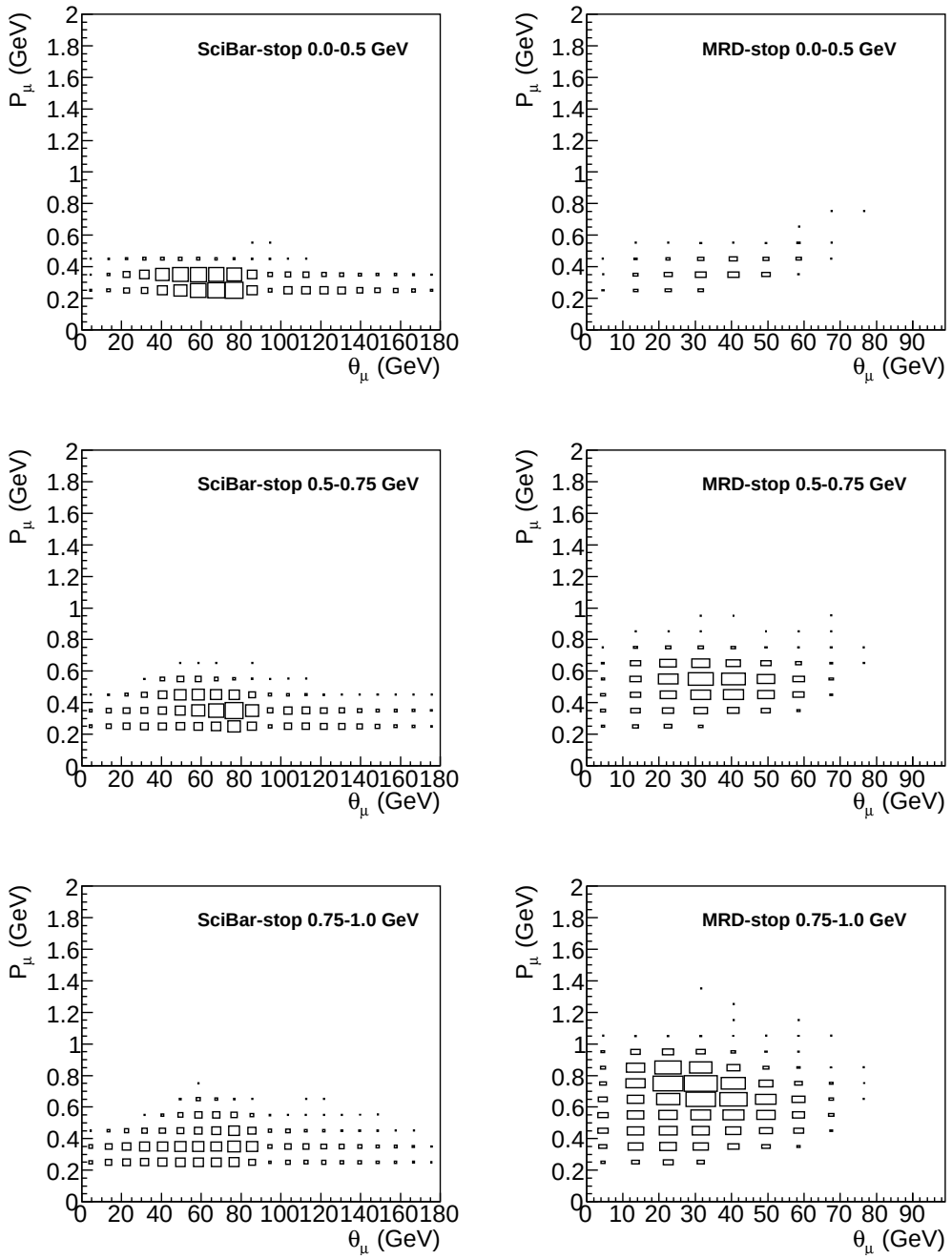

Figure 5.7: MC temples of p_μ vs. θ_μ distribution for SciBar-stopped and MRD-stopped sample for the first three E_ν regions. The same normalization factors are used for both SciBar-stopped and MRD-stopped samples.

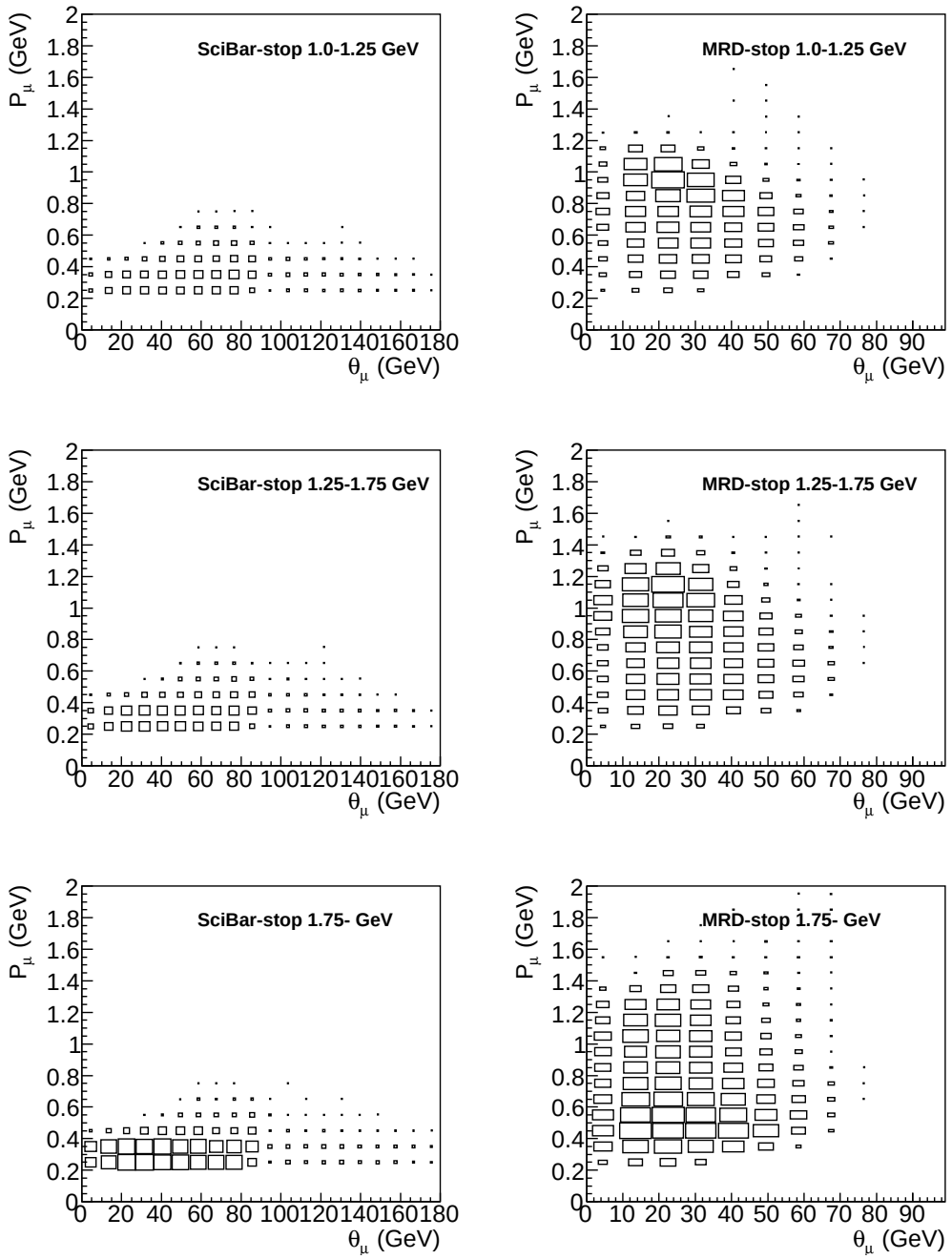

Figure 5.8: MC temples of p_μ vs. θ_μ distribution for SciBar-stopped and MRD-stopped sample for the last three E_ν regions. The same normalization factors are used for both SciBar-stopped and MRD-stopped samples.

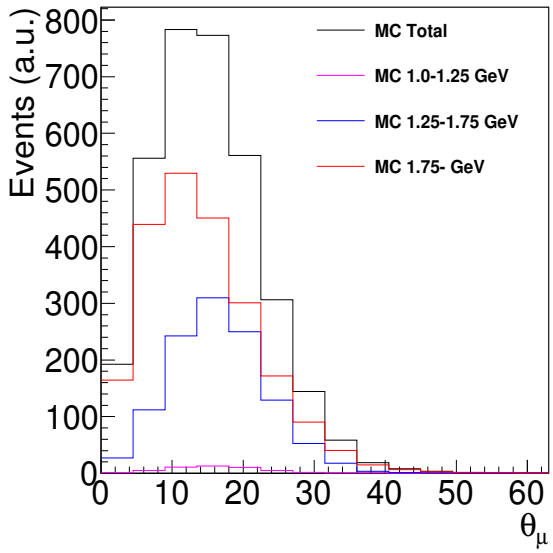

Figure 5.9: MC temples of θ_μ distribution for MRD-penetrated sample. The black line shows the total MC prediction. The red line shows the prediction for $E_\nu > 1.75GeV$, the blue line for $1.25 < E_\nu < 1.75GeV$, and the purple line for $1.0 < E_\nu < 1.25GeV$ neutrinos.

5.2 Definition of the χ^2

We consider two definitions of the χ^2 for the spectrum fitting: Log likelihood ratio and the Pearson's χ^2.

In this section, we first describe about these two definitions, and then discuss about the choice of the χ^2.

5.2.1 Likelihood Ratio

In the case of no systematic uncertainty present, the probability density function obeys Poisson distribution: $P(N,\mu) = \frac{\mu^N e^{-\mu}}{N!}$, where N is the number of event observed, and μ is the expected number of event.

Using this function, the χ^2 is written as:

$$\chi^2 = -2 \sum_{i}^{Nbin(P_\mu,\theta_\mu)} \ln\left[\frac{P(N_i^{data}; N_i^{MC})}{P(N_i^{data}; N_i^{data})}\right]. \tag{5.1}$$

Then we add systematic uncertainty. The systematic uncertainties are estimated bin-by-bin with their correlations. To incorporate this systematic error, we re-define the likelihood function as the convolution of Poisson and multivariated Gaussian distribution:

$$P(\vec{n};\vec{\mu};V) = \frac{1}{(2\pi)^{n/2}\sqrt{|V|}} \int_0^\infty \prod_i^{Nbin} dx_i \frac{x_i^{n_i} e^{-x_i}}{n_i!} \exp\left[-\frac{1}{2}(x_j-\mu_j)V_{jk}^{-1}(x_k-\mu_k)\right] \tag{5.2}$$

Here V denotes the bin-by-bin error matrix with the dimension of $Nbins \times Nbins$.

To calculate the above integration, we use Monte Carlo integration technique. Here, the likelihood function is calculated as:

$$P(\vec{n};\vec{\mu};V) = \frac{1}{Ndraws} \sum_i^{Ndraws} P(\vec{n};\vec{x}_i), \qquad \text{where} \quad P(\vec{n};\vec{x}_i) = \prod_j^{Nbin} \frac{x_{ij}^{n_j} e^{-x_{ij}}}{n_j!}. \tag{5.3}$$

In this equation, $\vec{x}_i$ is the i-th random draw of the expected number of event at each P_μ vs. θ_μ bins, obtained by the error matrix V and the central value $\vec{\mu}$. We use 1000 random draws for this integration. The detail of the systematic uncertainties are described in the next section.

Using this likelihood function, we rewrite the definition of χ^2 to:

$$\chi^2 = -2\ln\left[\frac{P(\vec{n};\vec{\mu};V)}{P(\vec{n};\vec{n};V)}\right] \tag{5.4}$$

5.2.2 Pearson's χ^2

The other candidate is Pearson's χ^2. In this case, the χ^2 is defined as:

$$\chi^2 = \sum_{i,j}^{Nbins} (n_i-\mu_i)(V_{sys}+V_{stat})_{ij}^{-1}(n_j-\mu_j) \tag{5.5}$$

where V_{sys} is the same error matrix used for the likelihood method. V_{stat} is defined as:

$$V_{stat} = \begin{pmatrix} n_1 & & & 0 \\ & n_2 & & \\ & & \ddots & \\ 0 & & & n_{Nbins} \end{pmatrix}. \tag{5.6}$$

This method is less accurate compared to the likelihood method since we assume all systematic and statistical fluctuations are Gaussian around the predation μ. However, the fit process is a lot simpler and stabler compare to the likelihood method using Monte Carlo integration.

5.2.3 Comparison Between the Two Methods

We compare the two method by performing fits with statistical errors only. This way, we remove the uncertainties come from MC integration method and can see pure difference between Poisson and Gaussian assumptions.

Figure 5.10 shows the fit results of the two methods. The parameters and their correlation coefficients for Poisson and Gaussian statistical errors are shown in the Tables 5.2 and 5.3, respectively. Here we can see the two fits give essentially same results, and it is safe to use Gaussian instead of Poisson distribution for the statistical error.

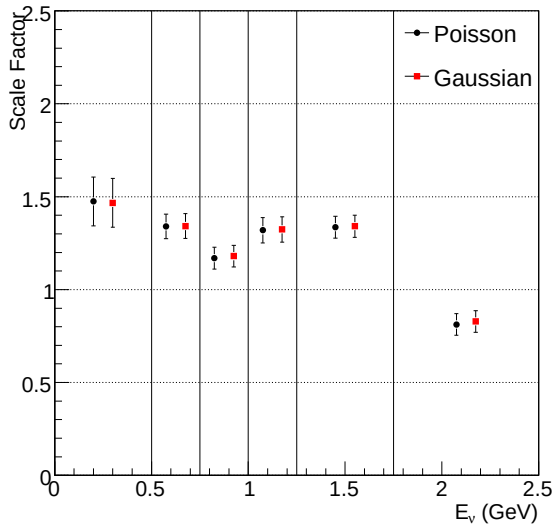

Figure 5.10: Spectrum fit results with statistical errors only. The black points shows the fit results by Poisson log likelihood method described in the Section 5.2.1. The red points shows the fit results by the Pearson's χ^2 with Gaussian statistical error, described in the Section 5.2.2.

Table 5.2: Best fit values and their error of the fit by the Poisson log likelihood method with statistic errors only. The binning used is the case B. The bottom half shows the correlation coefficients for each parameters.

	f_0	f_1	f_2	f_3	f_4	f_5
Best fit	1.475	1.340	1.170	1.319	1.336	0.812
Error	0.132	0.066	0.059	0.069	0.059	0.058
f_0	1.0000	-0.5155	-0.0078	0.0420	-0.0179	-0.0185
f_1	-0.5155	1.0000	-0.4737	0.0362	-0.0042	-0.0223
f_2	-0.0078	-0.4737	1.0000	-0.5818	0.1570	-0.1089
f_3	0.0420	0.0362	-0.5818	1.0000	-0.6144	0.2553
f_4	-0.0179	-0.0042	0.1570	-0.6144	1.0000	-0.6130
f_5	-0.0185	-0.0223	-0.1089	0.2553	-0.6130	1.0000

For the Poisson Likelihood method, we need huge number of MC random draws to make an accurate expectation of the integral for systematic uncertainty. We found that the number of random draws are beyond what can be produced with the current computing power. **Thus, we choose the error matrix method with Gaussian statistical error for the spectrum fitting**.

Table 5.3: Best fit values and their error of the fit by the Pearson's χ^2 with Gaussian statistical errors only. The binning used is the case B. The bottom half shows the correlation coefficients for each parameters.

	f_0	f_1	f_2	f_3	f_4	f_5
Best fit	1.467	1.342	1.180	1.324	1.341	0.829
Error	0.132	0.067	0.059	0.068	0.060	0.058
f_0	1.0000	-0.5302	0.0077	0.0396	-0.0178	-0.0172
f_1	-0.5302	1.0000	-0.4846	0.0366	0.0017	-0.0227
f_2	0.0077	-0.4846	1.0000	-0.5706	0.1474	-0.1072
f_3	0.0396	0.0366	-0.5706	1.0000	-0.6201	0.2695
f_4	-0.0178	0.0017	0.1474	-0.6201	1.0000	-0.6265
f_5	-0.0172	-0.0227	-0.1072	0.2695	-0.6265	1.0000

5.3 Shape-only Systematic Uncertainty

In this section, we describe how to construct "V_{sys}" appeared in the Eq. (5.5).

5.3.1 Principle

In principle, the scale factor as a function of E_ν (f_i) should represent the factor for (flux $\times$ x-section), and should be correlated to MiniBooNE.

Based on this principle, all flux and cross-section variations are re-normalized, and the variations cannot be tuned by the E_ν scale factor are assigned as systematic variation. The explicit explanation of this method will be described in the next section.

On the other hand, the detector uncertainty should be independent to MiniBooNE measurement. So, for the errors not correlated to MiniBooNE, its absolute variations are assigned as systematic error.

The followings are explicit list of errors which categorized to Shape-only and Absolute uncertainties.

Shape-only Errors:

- All flux variations
- All neutrino (primary) interaction x-sections
- Single π low Q^2 shape variation

Absolute Errors:

- Detector response variations (dE/dx)
- π interaction cross-section in the detector material
- π interaction cross-section in the nucleon.

Ideally, the π interaction cross-section in the nucleon can be correlated to MiniBooNE. However, the mechanism in which these π are detected is completely different between SciBooNE and MiniBooNE; SciBooNE is based on the tracks, while MiniBooNE utilize decay electron signal produced in the π decay chain. Hence, we consider that these errors are uncorrelated to MiniBooNE.

5.3.2 How to Construct "Shape-only" Variation

In this section, we describe the technical detail of how to construct the "shape-only" systematic error used for the spectrum fit.

First, we prepare MC expectations of number of events at each (p_μ, θ_μ) bins and at E_ν bins: x_{ij}, where i denotes the index of (p_μ, θ_μ) bins and j denotes the index of E_ν bins. Using this x_{ij}, the total number of events at each (p_μ, θ_μ) bins n_i and at each E_ν bins N_j are written as:

$$n_i = \sum_j^{E_\nu bins} x_{ij}, \quad and \quad N_j = \sum_i^{(p_\mu,\theta_\mu)bins} x_{ij}. \tag{5.7}$$

We prepare both central value (cv) and systematic variations (sys) of these predictions. Then, we assume that the variation of N_j is constrained by the spectrum fit, and need to be removed from the systematic error. Therefore, the constrained systematic variation $n'_i(sys)$ is calculated as:

$$n'_i(sys) = \sum_j^{E_\nu bins} f_j x_{ij}(sys) \frac{N_j(cv)}{N_j(sys)}, \tag{5.8}$$

where f_j is the scale factor for each E_ν bins.

Also, the central values weighted by the f_j are written as:

$$n'_i(cv) = \sum_{j}^{E_\nu bins} f_j x_{ij}(cv). \tag{5.9}$$

Using these $n'_i(sys)$ and $n'_i(cv)$, the error matrix from unisim variation is

$$V_{ij} = (n'_i(sys) - n'_i(cv))(n'_j(sys) - n'_j(cv)). \tag{5.10}$$

Similarly, the error matrix estimated from multisim method is calculated by:

$$V_{ij} = \frac{1}{M}\sum_{k}^{M}(n'_{ik}(sys) - n'_{ik}(cv))(n'_{jk}(sys) - n'_{jk}(cv)), \tag{5.11}$$

where k denotes the index of multisim random draws and M denotes the total number of draws.

Finally, we add all systematic errors obtained by the above method to construct V_{sys} in the Eq. (5.5).

In the spectrum fit, we continuously update V_{sys} using the current f_j values. (i.e. The error matrix is re-calculated at the every step of the fitting.)

5.3.3 The size of systematic uncertainties

Figure 5.11 shows the diagonal element of the error at each P_μ vs. θ_μ bin of SciBar-stopped and MRD-stopped samples. Figure 5.12 is the central values and its RMS of θ_μ distribution from MRD-penetrated sample. The errors shown here are calculated with the all scale factors (f_j) being set to 1 (before fit). The size of errors from individual sources will be described in the Appendix D.

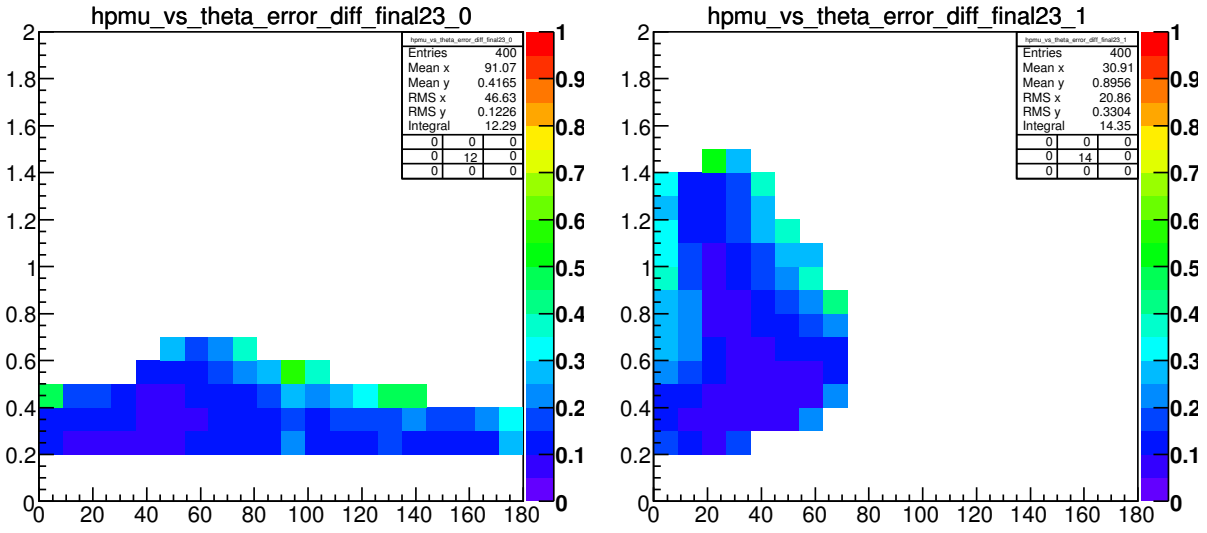

Figure 5.11: Diagonal element of the systematic uncertainties at each P_μ vs. θ_μ bin. The left plot shows the uncertainties for SciBar-stopped sample, and the right plot shows those for MRD-stopped sample.

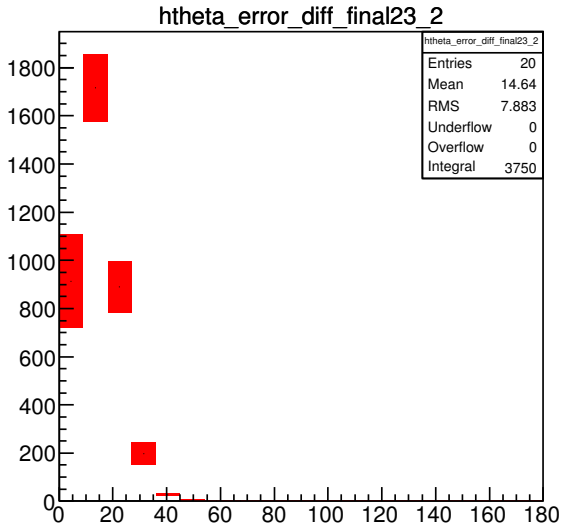

Figure 5.12: MC prediction and its total systematic uncertainties for θ_μ distribution of MRD-penetrated sample. The red filled region shows the size of the systematic uncertainty.

5.4 Fit Result

We find the scale factors to minimize the χ^2 using MINUIT program. The bins with at least 5 entries are used for fit.

The best fit parameters and its correlation coefficient are shown in the Table 5.4. The χ^2 value after fitting is 210.4/153 d.o.f.. The probability of giving this χ^2 is only 4×10^{-3}, indicating that there is some systematics we are missing.

To investigate the cause of this bad χ^2 requires bit more study, and that will be described in a separate technote. Here, we just summarize the fit results with the current best-known errors, and show data-MC comparison in the rest of this note.

Figure 5.13 shows the extracted number of events as a function of true neutrino energy, for combined sample of SciBar-stopped, MRD-stopped and MRD-penetrated events.

Table 5.4: Best fit values and their error of the spectrum fit. The bottom half shows the correlation coefficients for each parameters.

	f_0	f_1	f_2	f_3	f_4	f_5
Best fit	1.689	1.435	1.336	1.273	1.141	0.847
Error	0.196	0.078	0.049	0.058	0.069	0.064
f_0	1.0000	0.2457	-0.0903	-0.4029	-0.3806	-0.0252
f_1	0.2457	1.0000	-0.0942	-0.3697	-0.3834	-0.1301
f_2	-0.0903	-0.0942	1.0000	-0.0979	-0.0191	-0.2997
f_3	-0.4029	-0.3697	-0.0979	1.0000	-0.0155	0.1284
f_4	-0.3806	-0.3834	-0.0191	-0.0155	1.0000	-0.3234
f_5	-0.0252	-0.1301	-0.2997	0.1284	-0.3234	1.0000

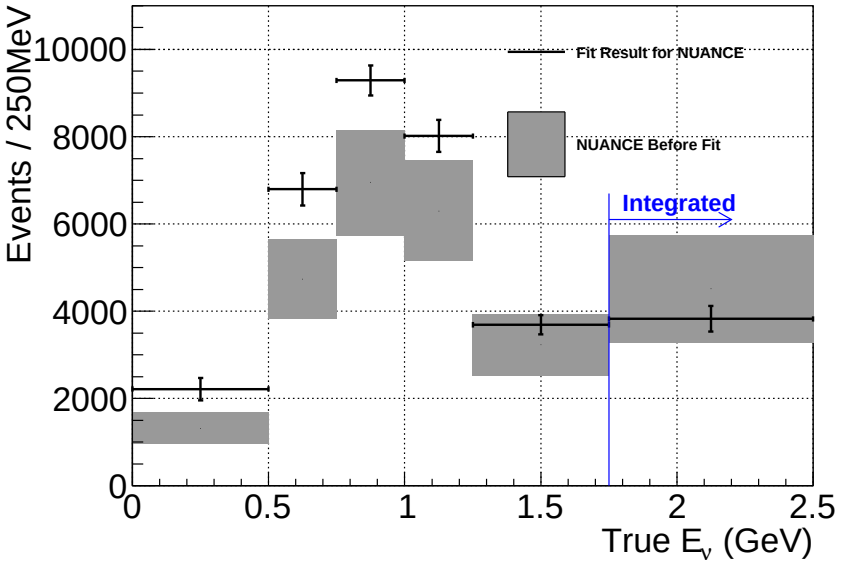

Figure 5.13: The number of events as a function of true neutrino energy, for combined sample of SciBar-stopped, MRD-stopped and MRD-penetrated events.

5.5 p_μ vs. θ_μ Distributions

Figures 5.14 and 5.16 show the MC predicted P_μ vs θ_μ distributions for the SciBar-stopped and MRD-stopped samples, respectively. Figures 5.15 and 5.17 show the distributions of (data-MC)/MC in P_μ vs θ_μ plane for the SciBar-stopped and MRD-stopped samples, respectively. Figure 5.18 is the θ_μ distribution for the MRD-stopped sample.

Finally, Figure 5.19 show the distributions of (data-MC)/MC divided by systematic (shown in the Figure 5.11) and statistical errors. We can clearly see some trend larger than systematic uncertainties in the data-MC difference even after fitting.

The further investigation of this described will be discussed in a separate technote.

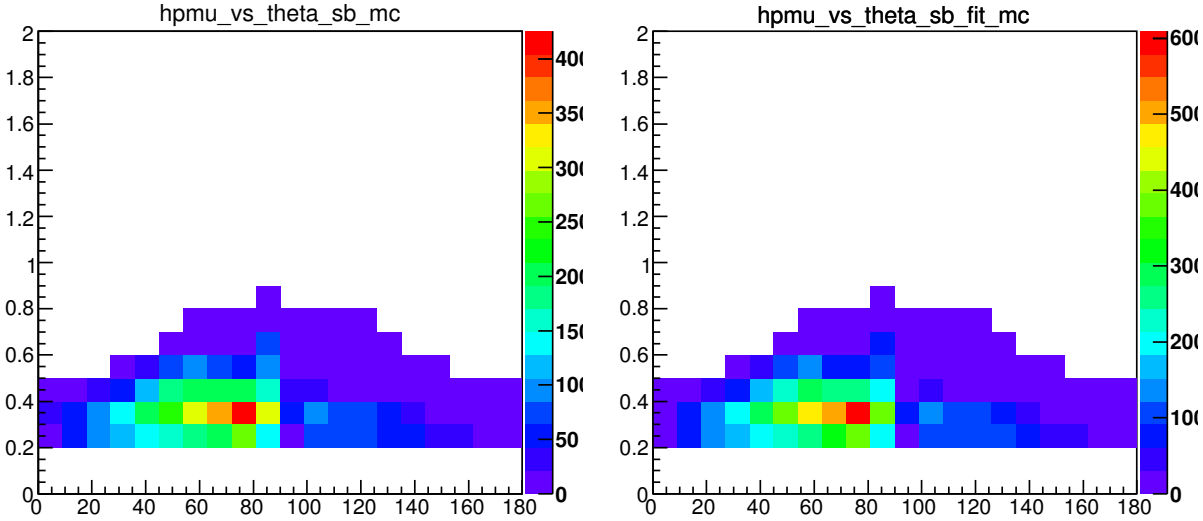

Figure 5.14: MC distribution of SciBar-stopped P_μ vs. θ_μ distribution (left) before and (right) after fit. Only bins used for the shown in these plots.

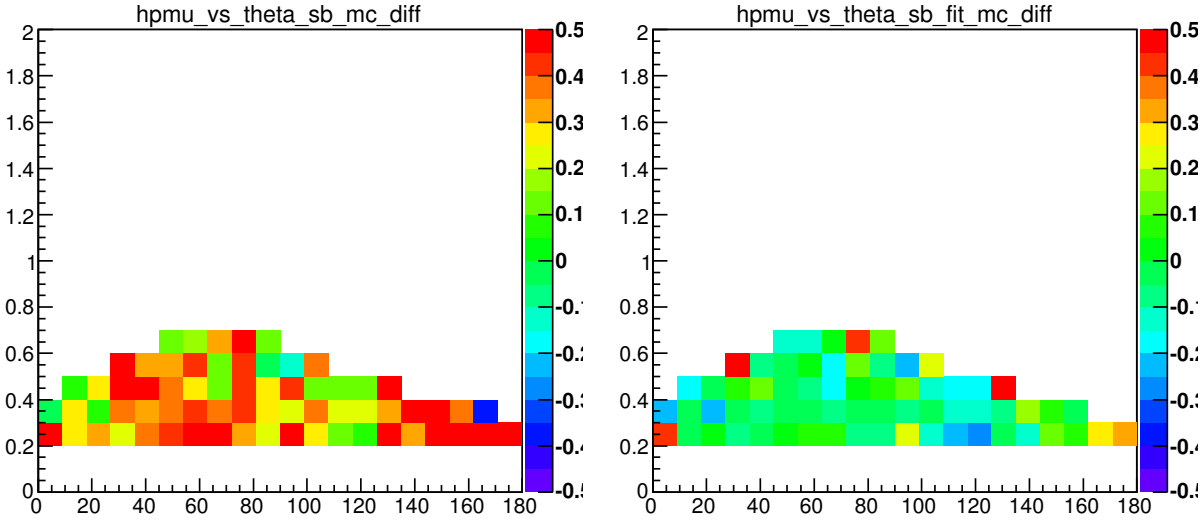

Figure 5.15: Distribution of (Data-MC)/MC of the SciBar-stopped events at each P_μ vs. θ_μ bins (left) before and (right) after fit. Only bins used for the shown in these plots.

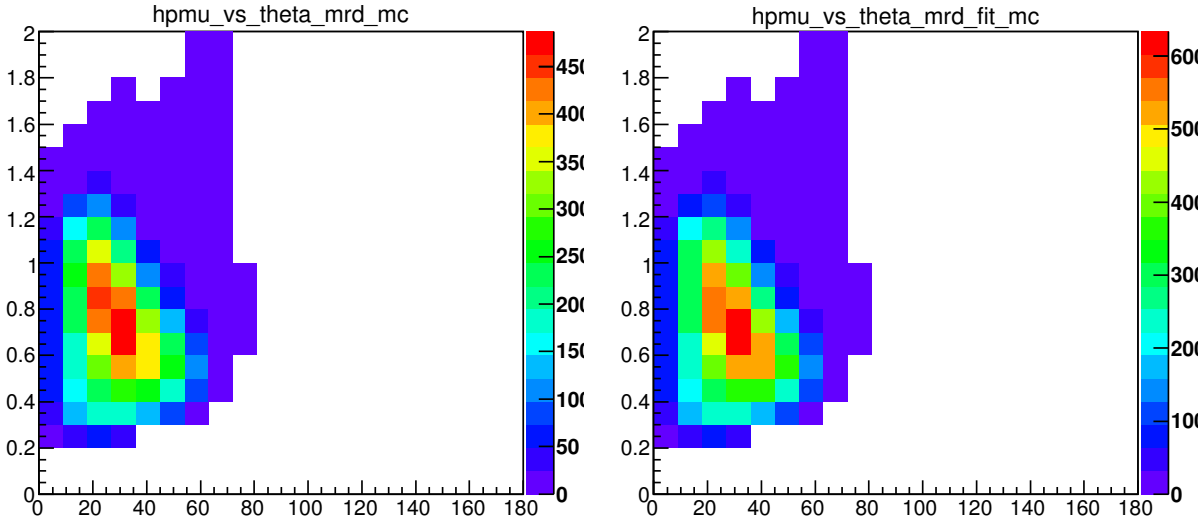

Figure 5.16: MC distribution of MRD-stopped P_μ vs. θ_μ distribution (left) before and (right) after fit. Only bins used for the shown in these plots.

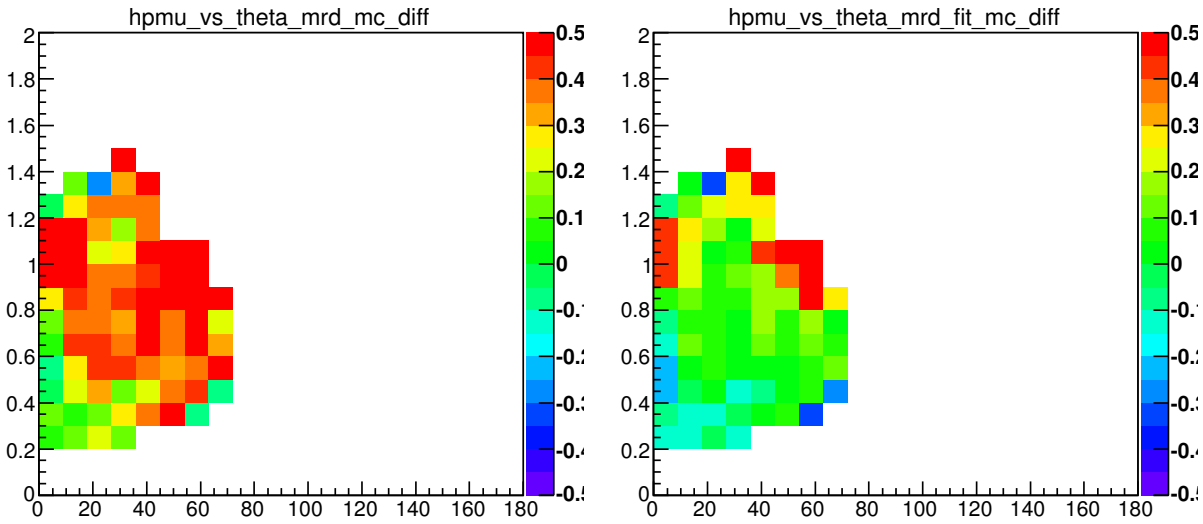

Figure 5.17: Distribution of (Data-MC)/MC of the MRD-stopped events at each P_μ vs. θ_μ bins (left) before and (right) after fit. Only bins used for the shown in these plots.

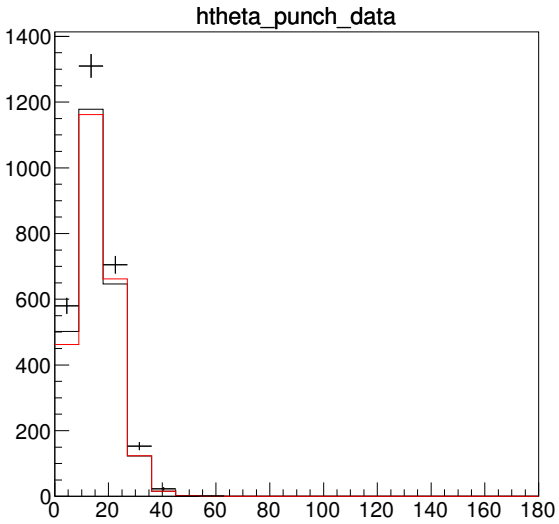

Figure 5.18: θ_μ distribution for MRD-penetrated sample. Black dots shows the data point. Black line is the MC prediction before fit, and the red line is the one after fit.The MC distribution is almost unchanged between before and after fit.

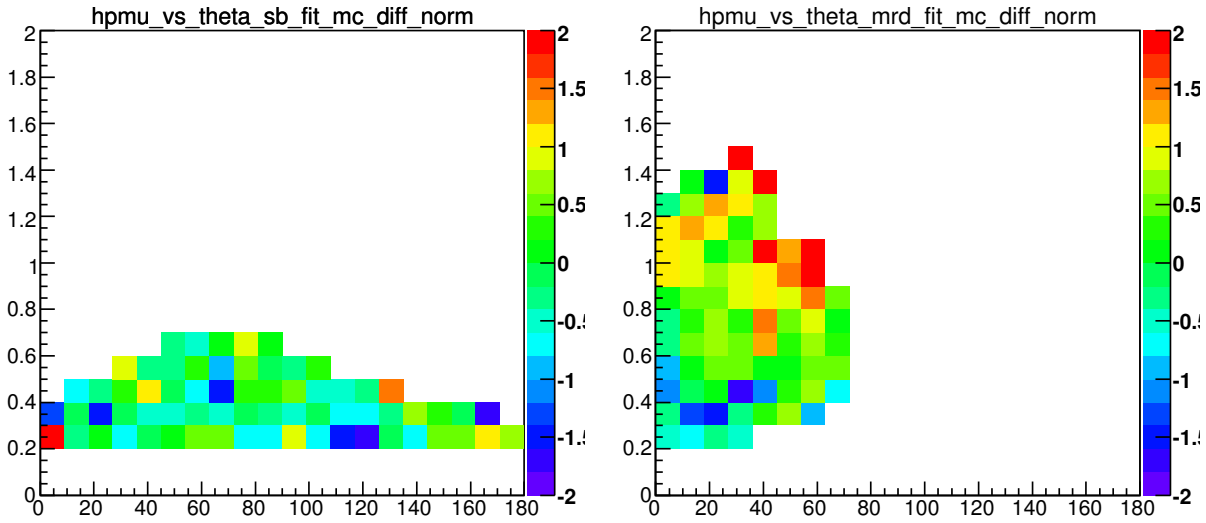

Figure 5.19: The distributions of (Data-MC)/MC/(sys. + stat. error) at each P_μ vs. θ_μ bins. The left plot is that of SciBar-stopped sample, and the right one is that of MRD-stopped sample. Only bins used for the shown in these plots.

5.6 Distributions After Fit

5.6.1 SciBar-Stopped Sample

Figures 5.20 and 5.21 shows the distributions of the reconstructed p_μ, θ_μ, E_ν and Q^2 of SciBar-stopped sample. The MC predictions are absolutely normalized by the number of POT.

The systematic errors shown in these plots are same ones used for the spectrum fit (shape-only flux and cross-section errors). There is another category of the error called "MC fit error" in these figures. These are errors of the spectrum fit results shown in the Table 5.4, propagated to each distributions.

We can see that the flux error becomes negligible since the variation is mostly constrained by the spectrum fit. Therefore, the remaining error is dominated by the cross-section shape errors.

The data points are basically covered by the current systematic errors, however, we found the number of data is systematically smaller than the MC prediction for SciBar-stopped sample.

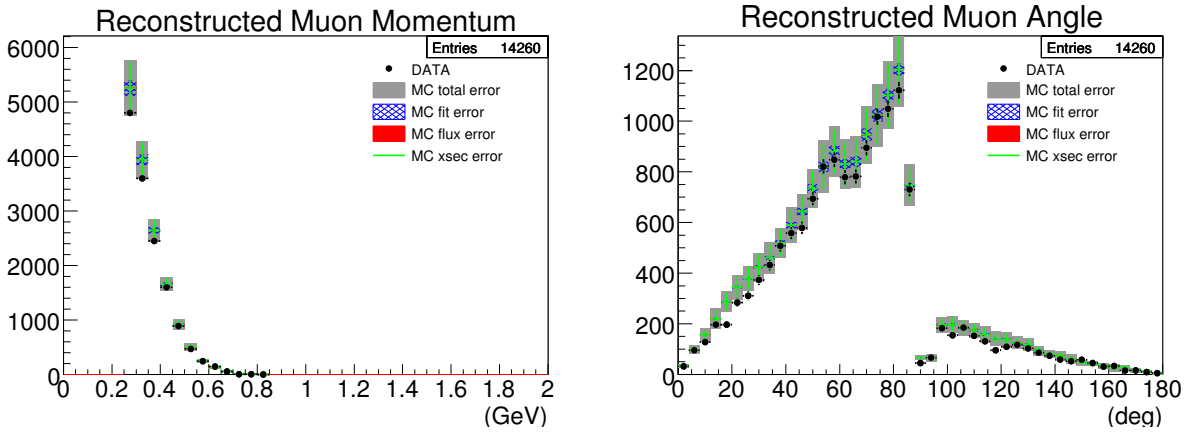

Figure 5.20: Reconstructed p_μ (left) and θ_μ (right) distribution for SciBar-stopped sample after spectrum fit. MC distribution is weighted by the scale factors and absolutely normalized by the POT.

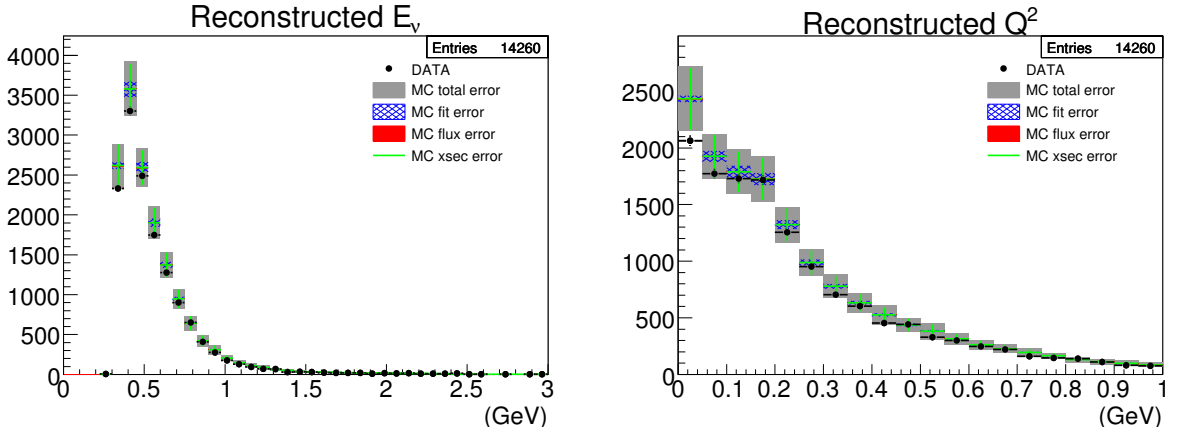

Figure 5.21: Reconstructed E_ν (left) and Q^2 (right) distribution for SciBar-stopped sample after spectrum fit. MC distribution is weighted by the scale factors and absolutely normalized by the POT.

5.6.2 MRD-Stopped Sample

Figures 5.22 and 5.23 shows the distributions of reconstructed p_μ, θ_μ, E_ν and Q^2 of MRD-stopped sample. Again, the MC predictions are absolutely normalized by the number of POT.

Similar to the SciBar-stopped sample, the remaining error is dominated by the cross-section shape errors.

The data points are basically covered by the current systematic errors, too. However, the central value is bit apart from the data points; we see data deficit at small p_μ and E_ν regions, and data excess at larger p_μ and E_ν regions.

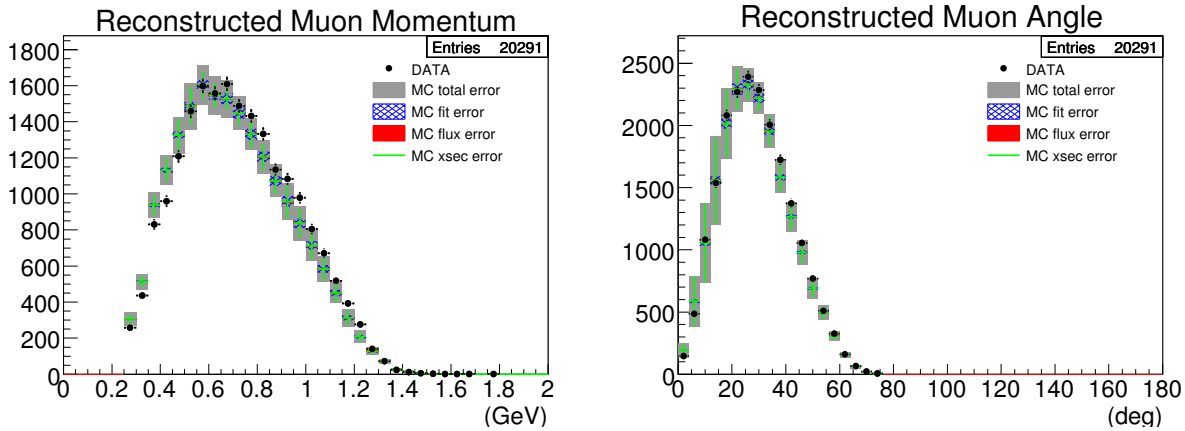

Figure 5.22: Reconstructed p_μ (left) and θ_μ (right) distribution for MRD-stopped sample after spectrum fit. MC distribution is weighted by the scale factors and absolutely normalized by the POT.

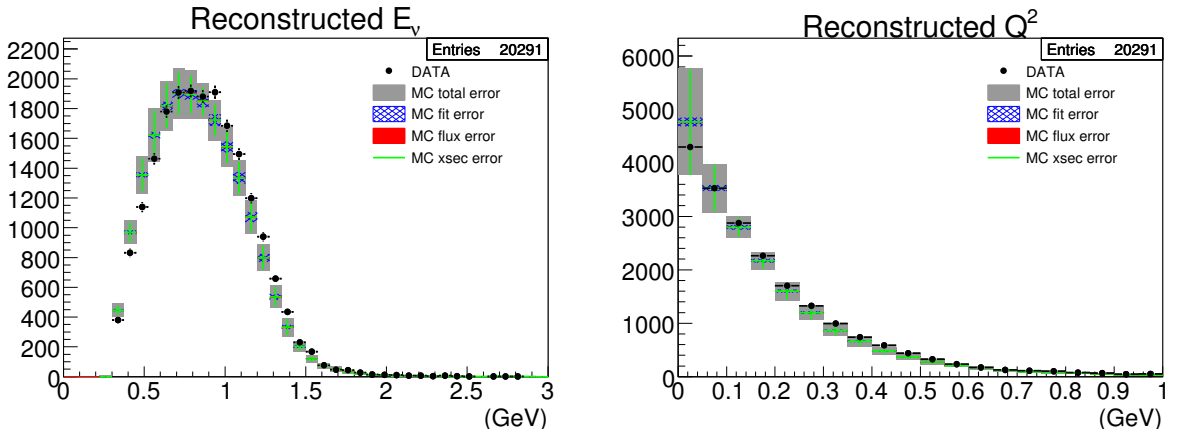

Figure 5.23: Reconstructed E_ν (left) and Q^2 (right) distribution for MRD-stopped sample after spectrum fit. MC distribution is weighted by the scale factors and absolutely normalized by the POT.

5.6.3 MRD-Penetrated Sample

Figure 5.24 shows the distributions of reconstructed θ_μ, of MRD-penetrated sample. Again, the MC predictions are absolutely normalized by the number of POT.

The error is dominated by the cross-section shape errors. There is also non-negligible error from flux uncertainty due to kaon contamination variations in this sample.

We can see the data points are well covered by the current systematic errors.

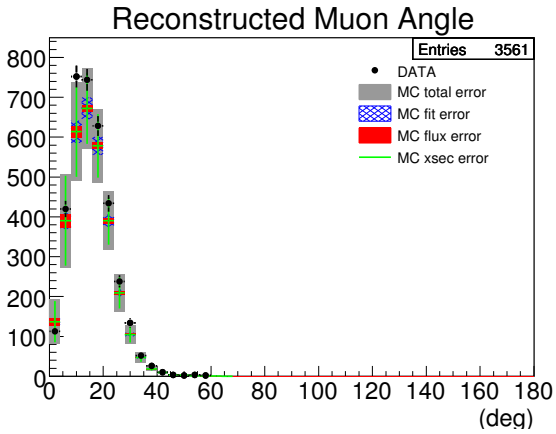

Figure 5.24: θ_μ distribution for MRD-penetrated sample after the spectrum fit. MC distribution is weighted by the scale factors and absolutely normalized by the POT.

Chapter 6

Summary and Discussions

As a part of SciBooNE-MiniBooNE joint ν_μ disappearance analysis, we measure charged current event rates at SciBooNE for several true E_ν regions. The scale factors and its errors for true E_ν regions are obtained by the spectrum fit, and the results are shown in the Table 5.4.

However, we found number of issues for the results. Firstly, the χ^2 value after fitting is 210/153 d.o.f., which is hard to explain with the fluctuation by the systematic uncertainty ($prob = 4 \times 10^{-3}$). This means there are some unknown systematic uncertainty exists. As shown in Figure 5.19, there are several p_μ vs. θ_μ bins with significant data-MC discrepancy.

Therefore, the next steps include a search for the source of these discrepancy, and find out the way to improve sample and error estimate. These studies will be described in the technote coming next (part 2).

There are also room to improve the spectrum prediction. As shown in the Figures 5.20-5.24, the uncertainty after fit is dominated by the cross-section errors, which means we can reduce the error if we can tune the cross-section parameters. The dominant cross-section uncertainties come from QE M_A and κ variations. A simultaneous fit of the E_ν scale factors, M_A^{QE} and κ are made, and the results will be described in the next technote as well.

Once we conclude the study listed above, we will make an prediction of MiniBooNE distributions constrained by the SciBooNE data.

Appendix A

CC Single π Production Q^2 Shape Fitting

A.1 Sample to Fit

We found data-MC discrepancy at low-Q2 region for CC-1π enriched sample. To evaluate the size of the discrepancy, we fit the Q^2 distributions from SciBar-stopped and MRD-stopped samples.

First, each sample is subdivided into three sub-samples: 1 track, $\mu + p$ and $\mu + \pi$ samples. each sub-sample is defined as:

1 track: no additional tracks from the vertex.

$\mu + p$**:** 1 additional track from the vertex with MuCL < 0.05.

$\mu + \pi$**:** 1 additional track from the vertex with MuCL > 0.05.

Then, we reconstruct Q^2 assuming $\Delta(1232)$ mass (Q^2_Δ). Figure A.1 shows the resolution of Q^2_Δ for SciBar-stopped and MRD-stopped samples. We can see Q^2_Δ is a good estimate of true Q^2 value for CC-resonant π interaction.

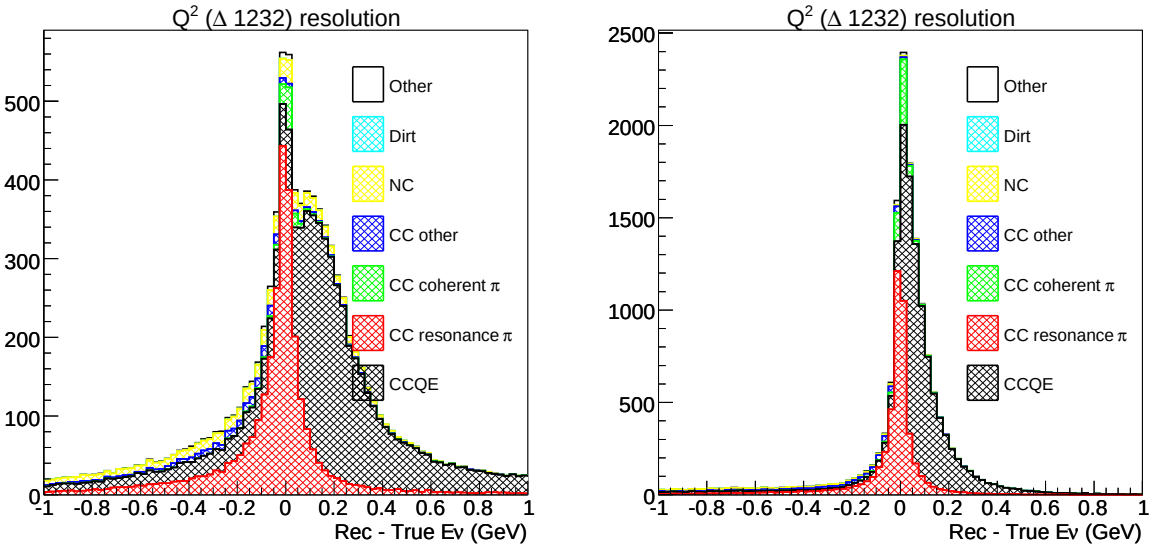

Figure A.1: Difference of Q^2_Δ and true Q^2 values from SciBar-stopped (left) and MRD-stopped (right) samples.

Figures A.2 and A.3 show the distributions of Q^2_Δ for each sample before fitting. We fit these 6 distributions simultaneously to extract Q2 dependence of data-MC discrepancy for CC-1π production.

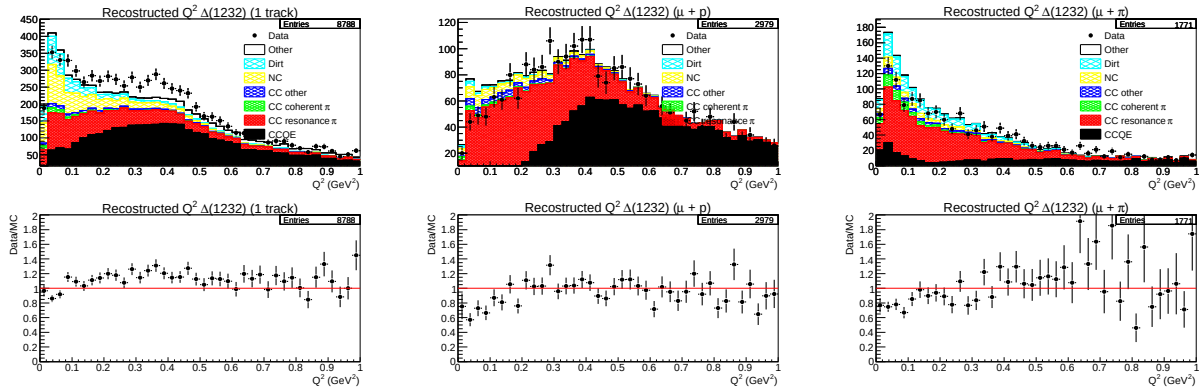

Figure A.2: Reconstructed Q^2_Δ distributions for 1 track (left), $\mu + p$ (center), and $\mu + \pi$ (right) samples from SciBar-stopped events.

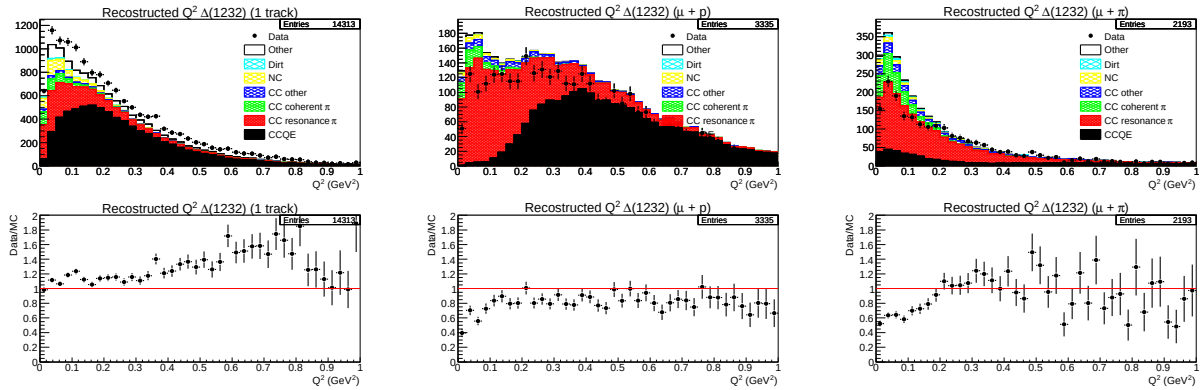

Figure A.3: Reconstructed Q^2_Δ distributions for 1 track (left), $\mu + p$ (center), and $\mu + \pi$ (right) samples from MRD-stopped events.

A.2 Fit Method and Result

Since the significant data-MC discrepancy is present at $Q^2_\Delta < 0.2\ GeV$, we assume the correction function to be:

$$P_{1\pi} = \begin{cases} A_{1\pi} \times Q^2_{(\Delta)} + B_{1\pi} & (Q^2_{(\Delta)} \leq 0.2\ GeV) \\ 1 & (Q^2_{(\Delta)} > 0.2\ GeV) \end{cases}. \tag{A.1}$$

Including these correction factors ($A_{1\pi},\ B_{1\pi}$), the following 6 parameters are used for the fitting.:

$A_{1\pi},\ B_{1\pi}$**:** Correction factor for CC resonant 1 π production.a

$P_{Coh-\pi}$**:** Scale factor for CC coherent π production.

P_{norm}**:** Overall normalization factor.

$P_{QE/non-QE}$**:** Migration factor between QE and non-QE events.

$P_{1trk/2trk}$**:** Migration factor between 1 track and 2 track samples.

We fit these parameters with the statistical errors only. The χ^2 is the ratio of the Poisson log likelihood defined as

$$\chi^2 = -2 \sum_{i}^{Nbins} \ln \left[\frac{P(N_i^{data}; N_i^{MC})}{P(N_i^{data}; N_i^{data})} \right], \quad \text{where} \quad \mathrm{P(N}, \mu) = \frac{\mu^{\mathrm{N}} \mathrm{e}^{-\mu}}{\mathrm{N!}} \tag{A.2}$$

Table A.1 shows best fit value of the parameters.

Table A.1: Best fit values of the CC-1π Q^2 fitting.

Parameter	$A_{1\pi}$	$B_{1\pi}$	$P_{Coh-\pi}$	P_{norm}	$P_{QE/non-QE}$	$P_{1trk/2trk}$
Best fit	2.14	0.43	0.56	1.24	0.88	1.31

Although these factors are obtained as a function of $Q^2_{(\Delta)}$, we apply these factor as a function of true Q^2. Figures A.4 and A.5 are the $Q^2_{(\Delta)}$ distribution after applying these scale factors. We can see the obtained scale factor as a function of true Q^2 still well describing the data-MC discrepancy at low Q^2.

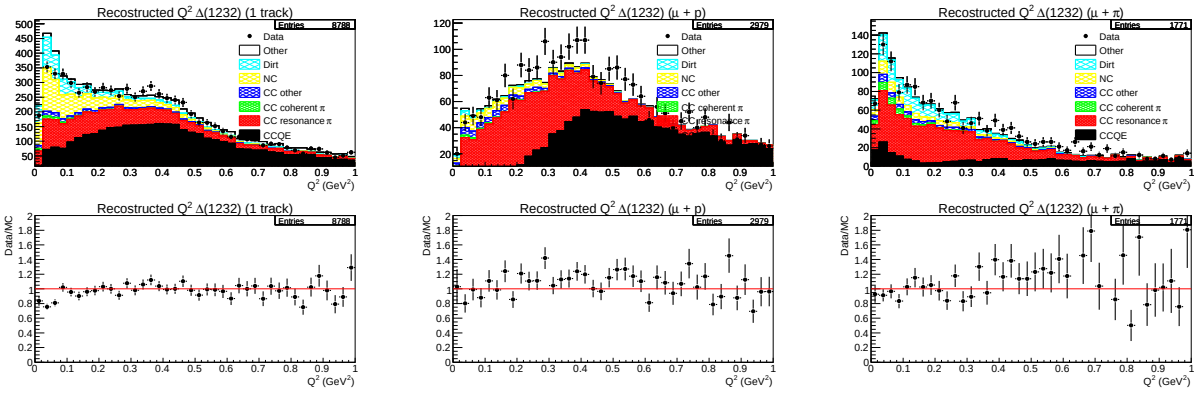

Figure A.4: Reconstructed Q^2_Δ distributions for 1 track (left), $\mu + p$ (center), and $\mu + \pi$ (right) samples from SciBar-stopped events, after the fitting.

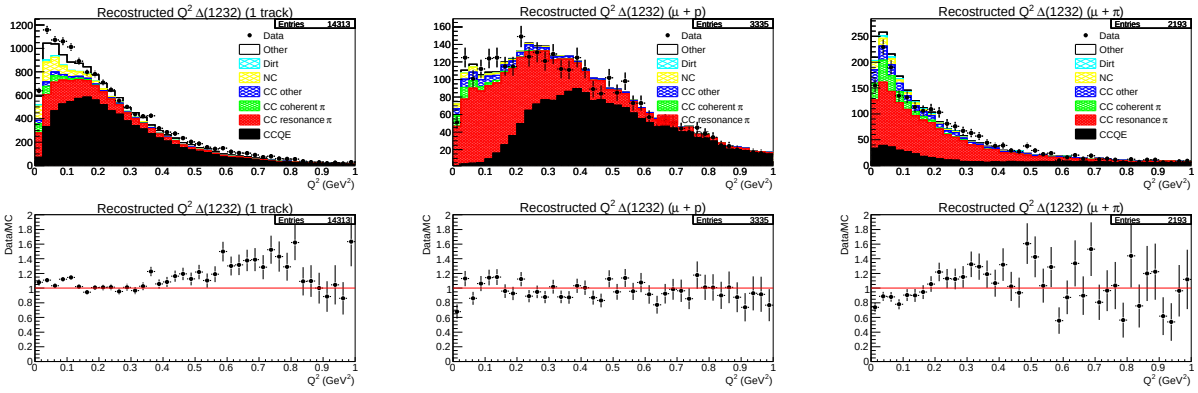

Figure A.5: Reconstructed Q^2_Δ distributions for 1 track (left), $\mu + p$ (center), and $\mu + \pi$ (right) samples from MRD-stopped events, after the fitting.

Then, another assumption is that the effect of P_{norm}, $P_{QE/non-QE}$ and $P_{1trk/2trk}$ are already covered by the current systematic error for flux, M_A and FSI errors. Hence, only the effect from $P_{Coh-\pi}$, $A_{1\pi}$ and $B_{1\pi}$ are taken into account for the systematic uncertainty for the spectrum fitting (and near to far extrapolation).

A.3 Comparison to the Correction Factor Obtained from MiniBooNE Data

Finally we check the consistency of the CC-1π correction factor with the one obtained from MiniBooNE data (refer MiniBooNE CC-QE paper?).

Figure A.6 is the reconstructed Q^2_{QE} of MiniBooNE CC-1π event. Both SciBooNE- and MiniBooNE-based corrections are overlaid in the plot. We confirm that the behaviour at low-Q^2 ($Q^2 < 0.2$ GeV) is very similar. Although there is a little discrepancy between two corrections, that effect is presumably covered by the M_A and FSI uncertainties.

Then we use SciBooNE-based correction on both MiniBooNE and SciBooNE for the oscillation analysis.

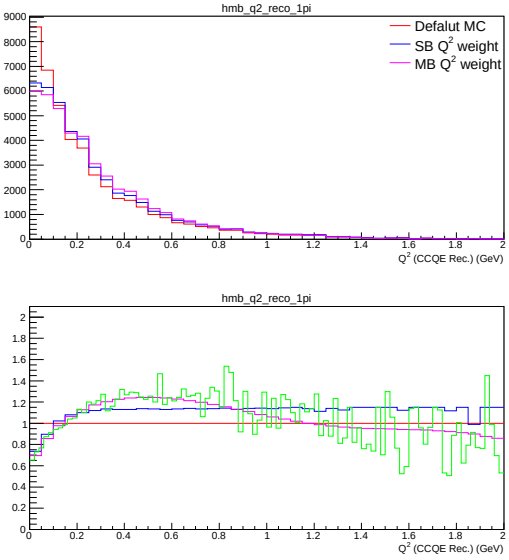

Figure A.6: Comparison of the correction based on SciBooNE and MiniBooNE. The top plot is the Q^2_{QE} distribution of (MC true) CC-1π events. Distributions of default prediction, the one after SciBooNE based correction and the one after MiniBooNE based correction are overlaid. The bottom plot is the ratio to the default prediction.

Appendix B

Study of *NuanceInterface*

B.1 Introduction

To estimate the systematic variation modeled in *NUANCE* program, we use a tool called "NunaceInterface". This tool allows to call the differential cross-section used in Nuance event-by-event. Using this tool, we can re-weight the MC samples event-by-event to predict distribution with some cross-section parameter which is different from the central values used for MC production. However, this method is not expected to work perfectly for all parameter variations. In this section, a study of validity of the "NunaceInterface" is described.

B.2 Method

To test the validity of "NuanceInterface", we generate various Nuance vectors with various cross-section parameters, and compared the distributions.

The following is the test method in the case of CCQE M_A variation:

We use $M_A = 1.234$ GeV for the MC central values, and assign ± 0.22 GeV uncertainty.

First we produce MC samples with $M_A = 1.234$ and $M_A = 1.45$ separately. Then, we re-weight the sample produced with $M_A = 1.234$ to $M_A = 1.45$ using "NuanceInterface". Ideally, the number of events from the sample produced at $M_A = 1.234$ and re-weighted to $M_A = 1.45$ (N($M_A = 1.234 \rightarrow 1.45$)), and the number of events from the sample originally produced at $M_A = 1.45$ (N($M_A = 1.45$)) should be consistent.

We do the same thing for the inverse way; i.e, compare N($M_A = 1.45 \rightarrow 1.234$) and N($M_A = 1.234$). Again these two should be consistent if the NunaceInterface worked ideally.

In summary, we produced four distributions for each cross-section parameters to be tested: N($M_A = 1.234 \rightarrow 1.45$), N($M_A = 1.45$), N($M_A = 1.45 \rightarrow 1.234$) and N($M_A = 1.234$).

The distribution of each variations are shown in to following sections.

B.3 Comparison of each variation

B.3.1 M_A variation

Figure B.1 shows the comparison of the true E_ν and true Q^2 distributions for $M_A = 1.234 GeV$ (central value) and $M_A = 1.45 GeV$ $(+1\sigma)$.

We can see that the re-weighted distributions are consistent to the ideal ones, except for small statistical fluctuations. Hence, we find NuanceInterface works perfectly for M_A variations.

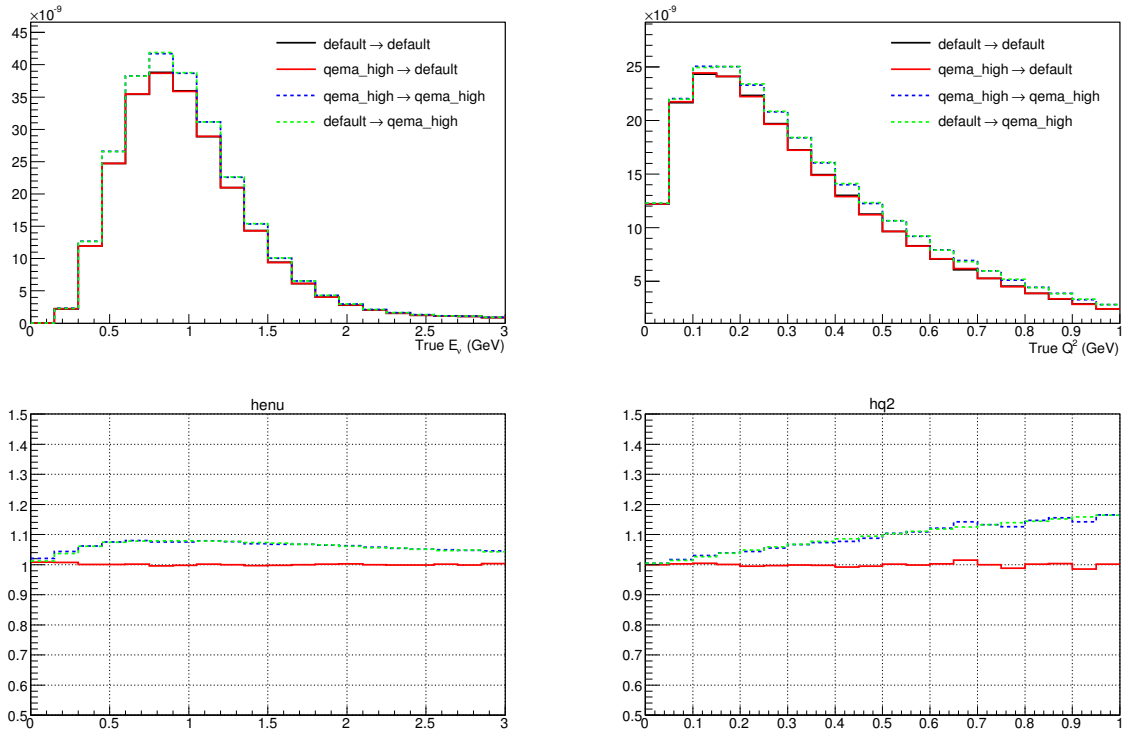

Figure B.1: Variation of for QE M_A as a function of true E_ν (left) and true Q^2 (right).

B.3.2 κ variation

Figure B.2 shows the comparison of the true E_ν and true Q^2 distributions for $\kappa = 1.022$ (central value) and $\kappa = 1.000$ (-1σ).

Here, we find significant discrepancies between the ideal $\kappa = 1.000$ distributions and the one re-weighted from $\kappa = 1.022$. This is more or less expected because there are some missing phase-space once we apply large κ factor (i.r. larger Pauli blocking), which cannot be recovered by re-weighting.

Therefore, we developed an special method for estimating κ error. The detail of this method is described in the next section.

B.3.3 p_F variation

Figure B.3 shows the comparison of the true E_ν and true Q^2 distributions for $p_F = 220MeV$ (central value) and $p_F = 250MeV$ $(+1\sigma)$.

We found that the predictions from NuanceInterface doesn't agree well with the correct distributions. However, the discrepancy is small ($\sim 1\%$) and also we set uncertainty of p_F conservatively ($\pm 30\%$). Thus, We consider it is fine to use the current error as it is.

B.3.4 E_B variation

Figure B.4 shows the comparison of the true E_ν and true Q^2 distributions for $E_B = 34MeV$ (central value) and $E_B = 25MeV$ (-1σ).

We also have trouble to predicting the variation from E_B. However, since the size of variation itself is very small, the effect of E_B error is marginal.

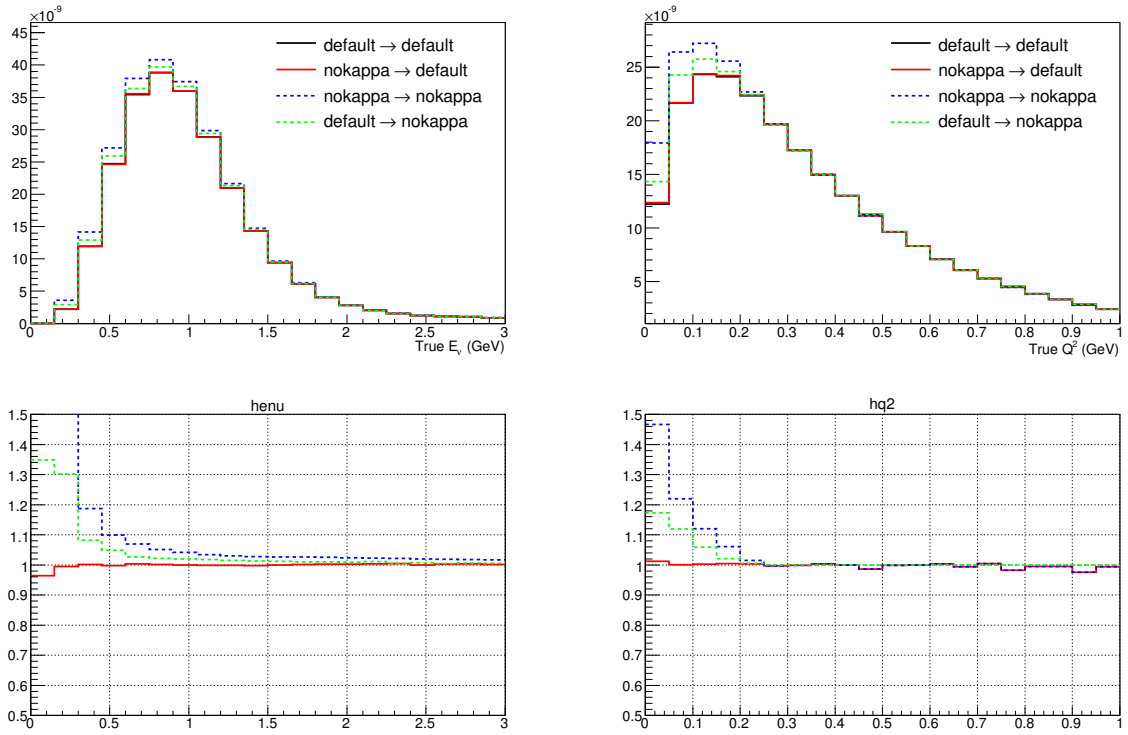

Figure B.2: Variation of for QE κ as a function of true E_ν (left) and true Q^2 (right).

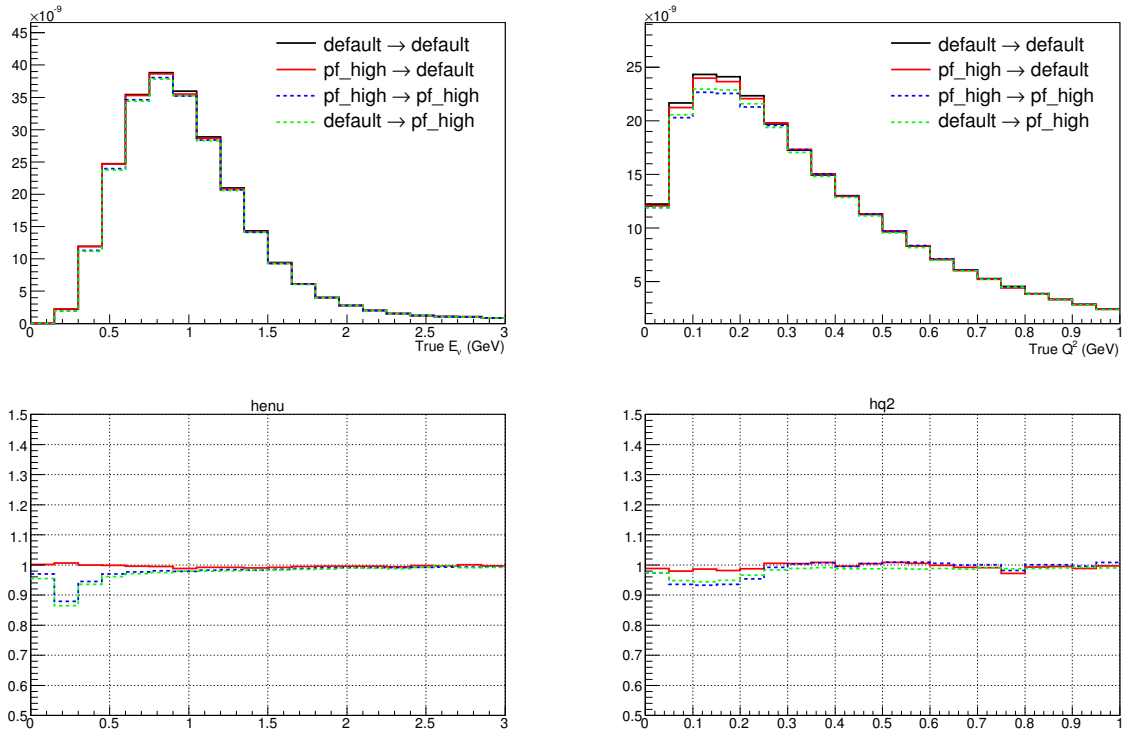

Figure B.3: Variation of for p_F as a function of true E_ν (left) and true Q^2 (right).

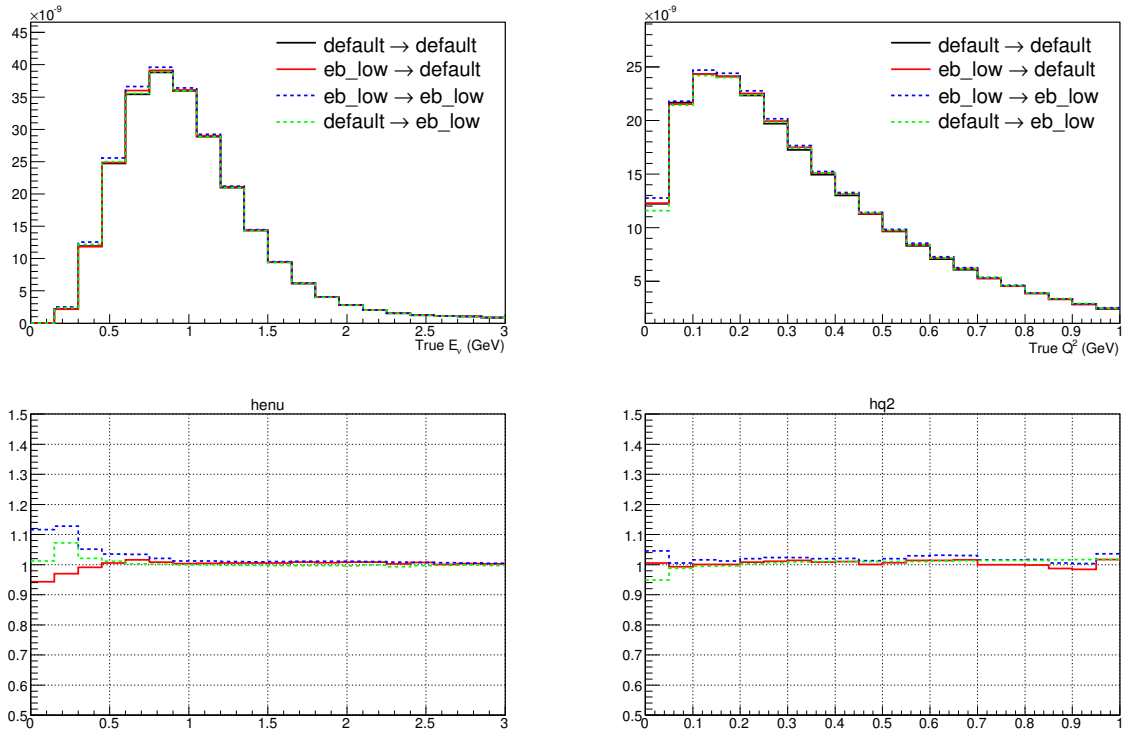

Figure B.4: Variation of for E_B as a function of true E_ν (left) and true Q^2 (right).

B.4 Special Function for κ variation

B.4.1 Extraction of the function

To see which quantity is best to describe the variation from κ we compare the two predictions ($\kappa = 1.000$ and 1.022) in a true E_ν vs. true Q^2 plane.

Figure B.5 shows the ratio between $\kappa = 1.000$ and 1.022 for CCQE events. From this plot, the effect of κ is almost pure function of Q^2 and has very small dependence to the neutrino energy.

Hence, a function of Q^2 can provide a reasonable approximation for κ variation. Figure B.6 show the true Q^2 distribution of CCQE events with $\kappa = 1.000$ and 1.022, and its ratio. This ratio between $\kappa = 1.022$ and $\kappa = 1.000$ are directly used to re-weight the MC predictions.

B.4.2 Test of the function with the reconstructed quantities

To test the validity of this new function of Q^2, we apply this function to the MC produced with $\kappa = 1.022$ to make $\kappa = 1.000$ prediction, and compared to the one originally produced with $\kappa = 1.000$.

Reconstructed p_μ, θ_μ, E_ν and Q^2 are used to this comparison. We use reconstructed quantities to test possible effect from FSI differences.

Figures B.7– B.10 shows the result. We see the function of Q^2 does much better jobs than NuanceInterface in predicting $\kappa = 1.000$ distributions. Also, the prediction from Q^2 function is consistent to the correct distributions. We confirm that this new function Q^2 is safe to use for prediction systematic variation from κ.

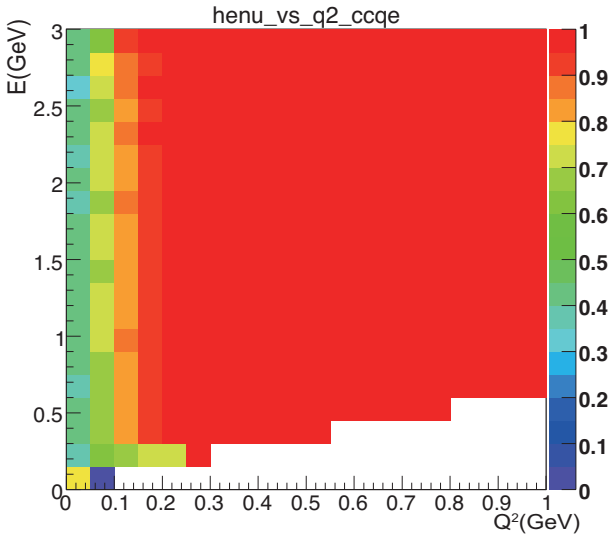

Figure B.5: Ratio of $\kappa = 1.022$ prediction divided by $\kappa = 1.0$ prediction, in $E_\nu vs. Q^2$ plane.

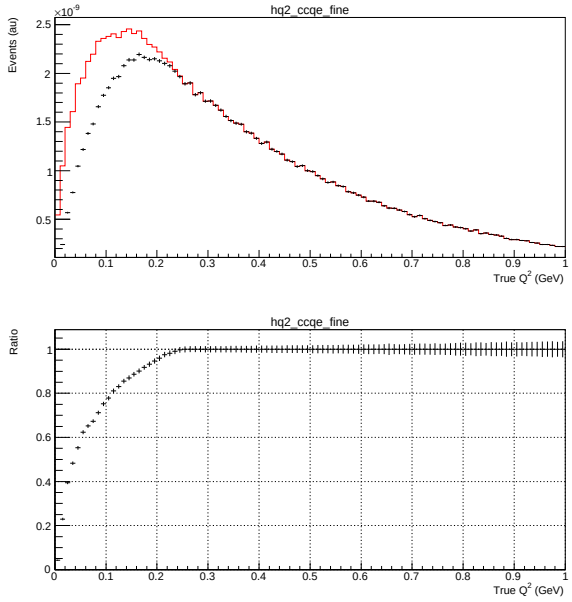

Figure B.6: (Top:) The true Q^2 distribution of $\kappa = 1.000$ (red) and $\kappa = 1.022$ predictions. (Bottom:) The ratio of $\kappa = 1.022$ prediction divided by $\kappa = 1.0$. This ratio is directly used to estimate the effect of kappa variation.

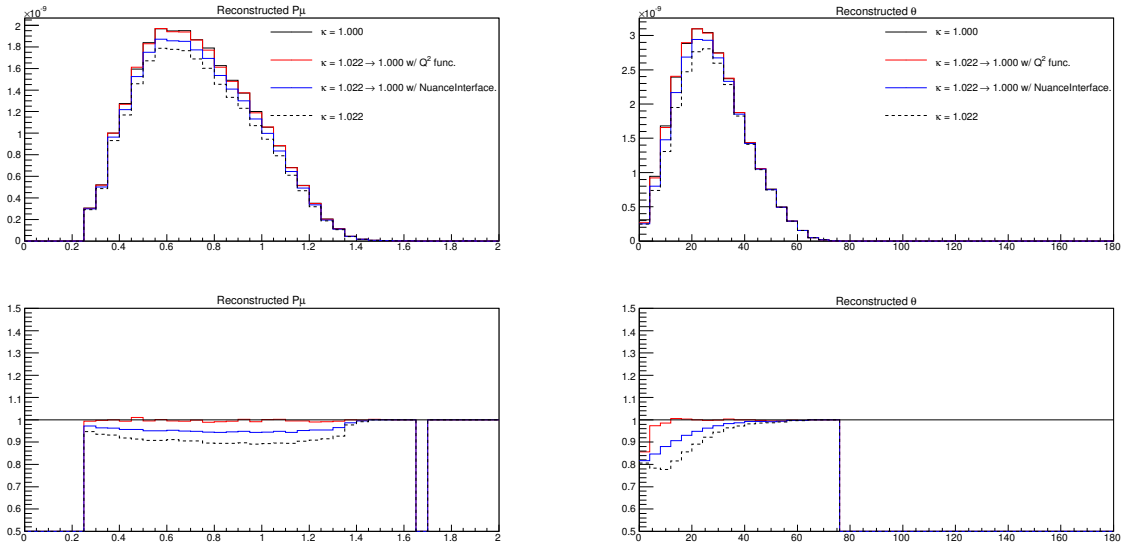

Figure B.7: Reconstructed p_μ (left) and θ_μ (right), for various κ predictions, obtained from MRD-stopped sample.

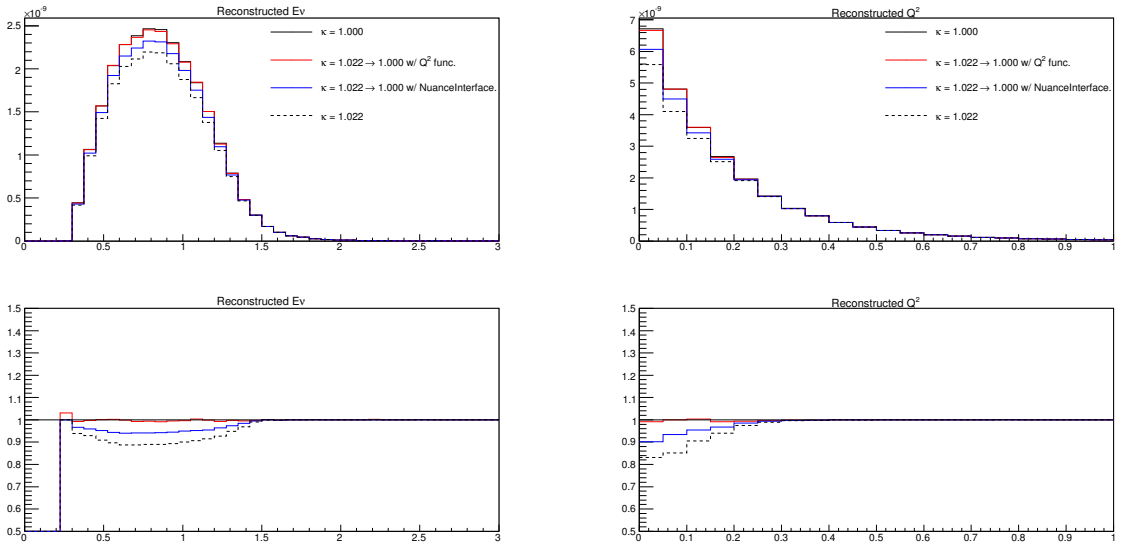

Figure B.8: Reconstructed E_ν (left) and Q^2 (right), for various κ predictions, obtained from MRD-stopped sample.

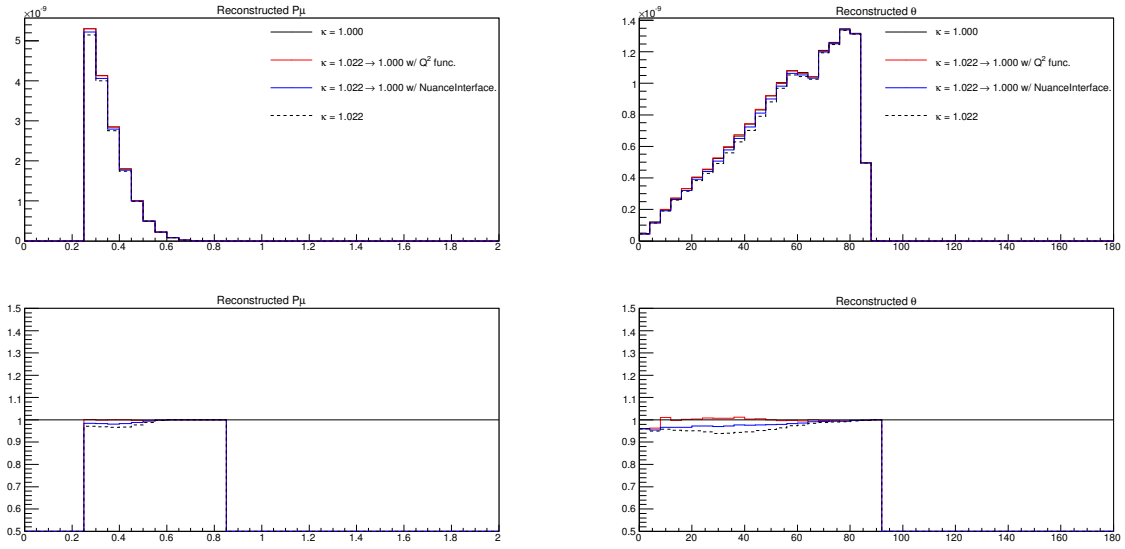

Figure B.9: Reconstructed p_μ (left) and θ_μ (right), for various κ predictions, obtained from SciBar-stopped sample.

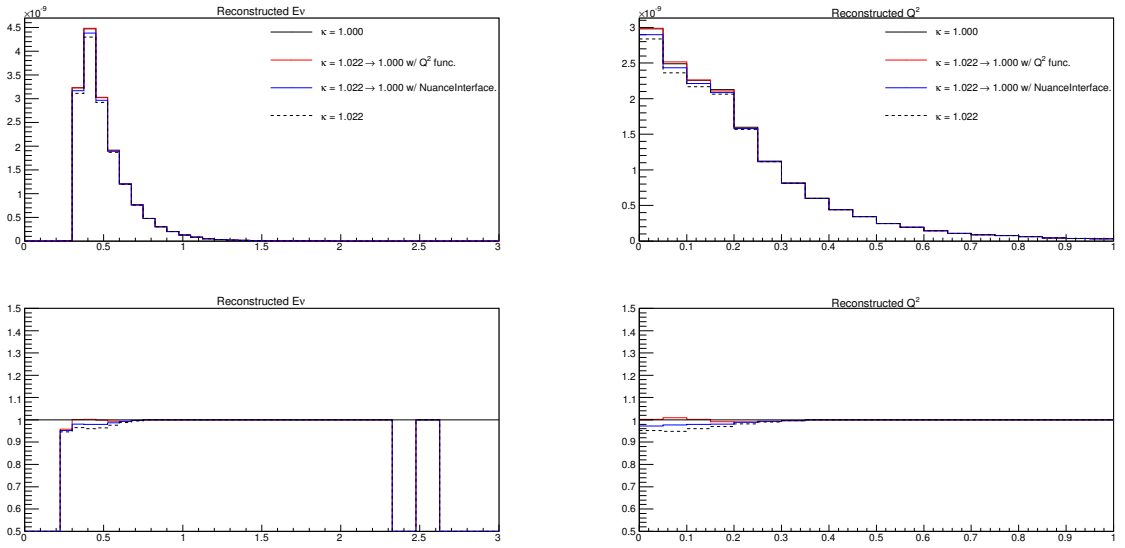

Figure B.10: Reconstructed E_ν (left) and Q^2 (right), for various κ predictions, obtained from SciBar-stopped sample.

B.5 Summary

In summary, we found the NuanceInterface can perfectly predict M_A variations. However, there is a significant problem when try to "decrease" κ using NuanceIneterface. This is because there is missing phase space once suppression by large κ is applied, and cannot be recovered by re-weighting. Because of this, we develop a special function as a function of Q^2 to predict κ variation. (Section B.4). We use this for estimating kappa errors.

We also find small problem in predicting p_F and E_B variations using NuanceInterface. However, since the size of variations are small, and also since we are not attempting to fix the central value, we just use the errors estimated by using NunaceInetrface.

Appendix C

Spectrum Fit with NEUT Predictions

C.1 Generator Level Comparison Between NEUT and NUANCE

The major differences between NEUT and NUANCE are summarized at Table 2.1. Other than those, there are several differences on the FSI simulations. The detailed comparison of generator level differences are summarized at a separate technote written by Kendall. Here, I will show the difference of the total number of interactions predicted by the two simulators.

Figure C.1 shows the comparison of true neutrino energy distributions generated at SciBar fiducial volume. The left plots in the figure shows the distributions before applying the cross-section weight, demonstrating that the exact same neutrino fluxes are used for this comparison.

The right plots are comparison after applying the cross-section weights. Because of the choice of κ (for QE) and $M_A^{1\pi}$, NUANCE predict $\sim$15% smaller number of events compared to NEUT.

C.2 Basic Distributions Before Fit

C.2.1 SciBar-stopped Sample

Figures C.2 and C.3 shows the distributions of p_μ, θ_μ, E_ν and Q^2 distributions of SciBar-stopped sample from data and NEUT predictions. Compared to the NUANCE prediction, we can clearly see that NEUT predict larger number of events and thus have less normalization difference to the data.

C.2.2 MRD-stopped Sample

Figures C.4 and C.5 shows the distributions of p_μ, θ_μ, E_ν and Q^2 distributions of MRD-stopped sample from data and NEUT predictions. Again, NEUT predict larger normalization compared to NUANCE.

C.2.3 MRD-penetrated Sample

Figure C.6 shows the θ_μ distribution of MRD-penetrated sample from data and NEUT predictions.

C.3 Spectrum Fit

C.3.1 Fit Method

The fitting is done using the same machinery used for fit with NUANCE prediction, which uses the Pearson's chi2 described in the Section 5.2.2.

For simplicity, I use the exactly same error matrix used for NUANCE prediction, and just scaled the size of error with the number of events at each p_μ and θ_μ bins.

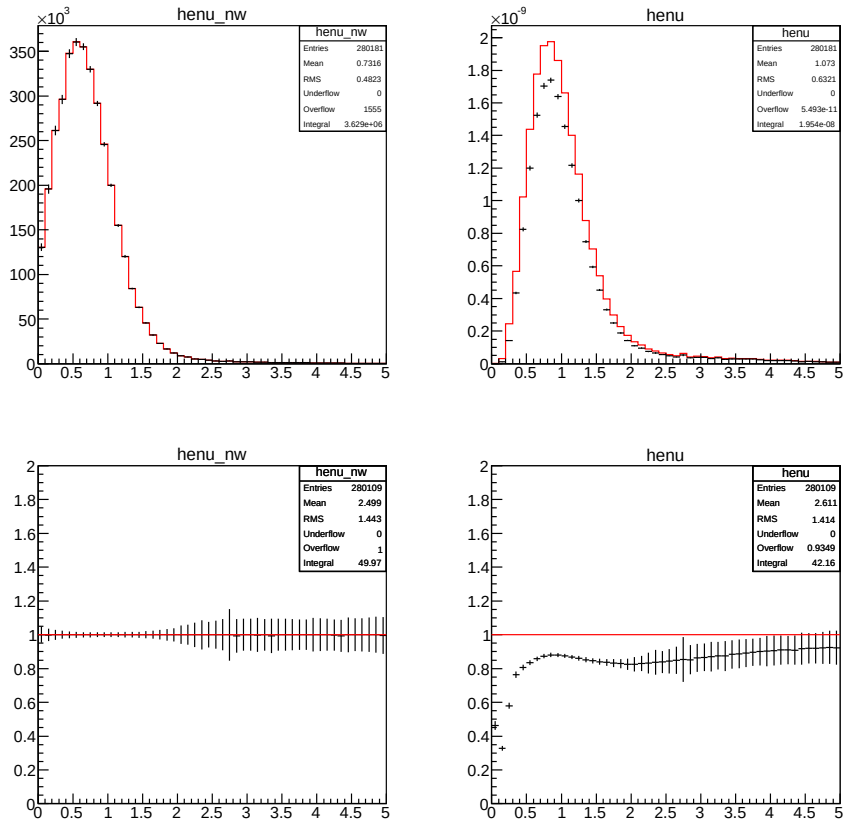

Figure C.1: The neutrino energy distributions at SciBar fiducial volume generated by NEUT (red curve) and NUANCE (black points). The left plots are the distributions before applying the cross-section weight, and the right plots are after applying the cross-section weights. Top plots are the comparisons in the absolute scale (the units of vertical axis is arbitrary), and the bottom plots show the ratio to the NEUT predictions.

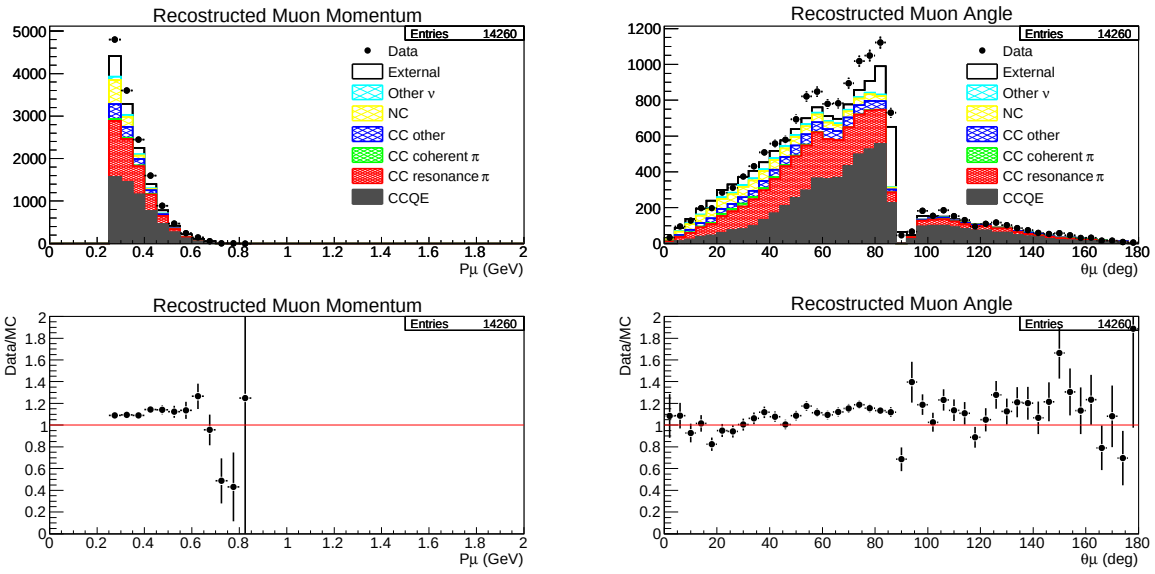

Figure C.2: Reconstructed p_μ (left) and θ_μ (right) distributions of SciBar-stopped sample. MC predictions are based on NEUT, and absolutely normalized by the number of POT.

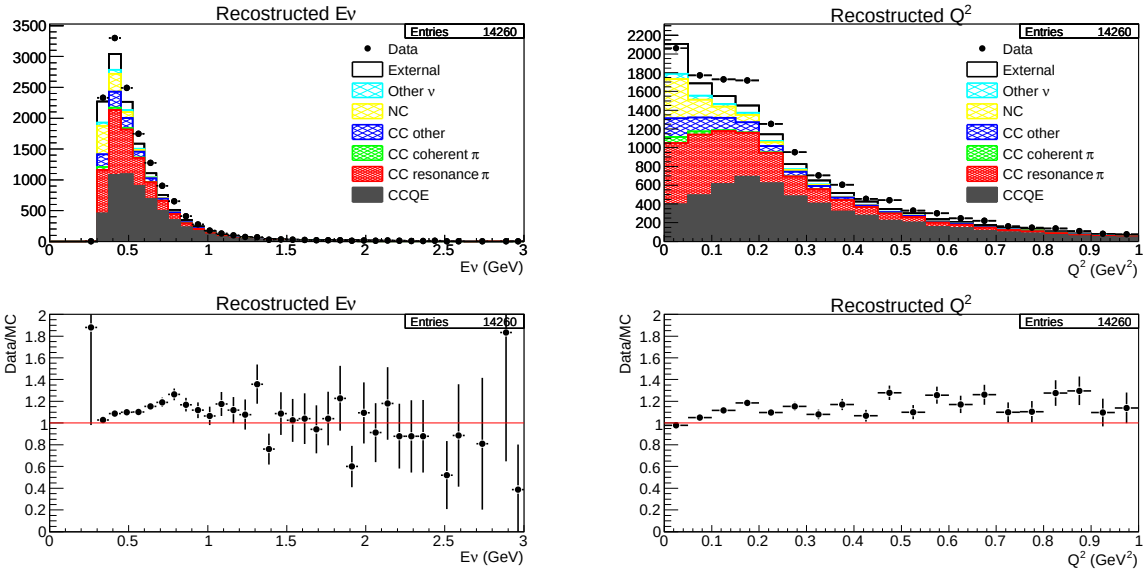

Figure C.3: Reconstructed E_ν (left) and Q^2 (right) distributions of SciBar-stopped sample. MC predictions are based on NEUT, and absolutely normalized by the number of POT.

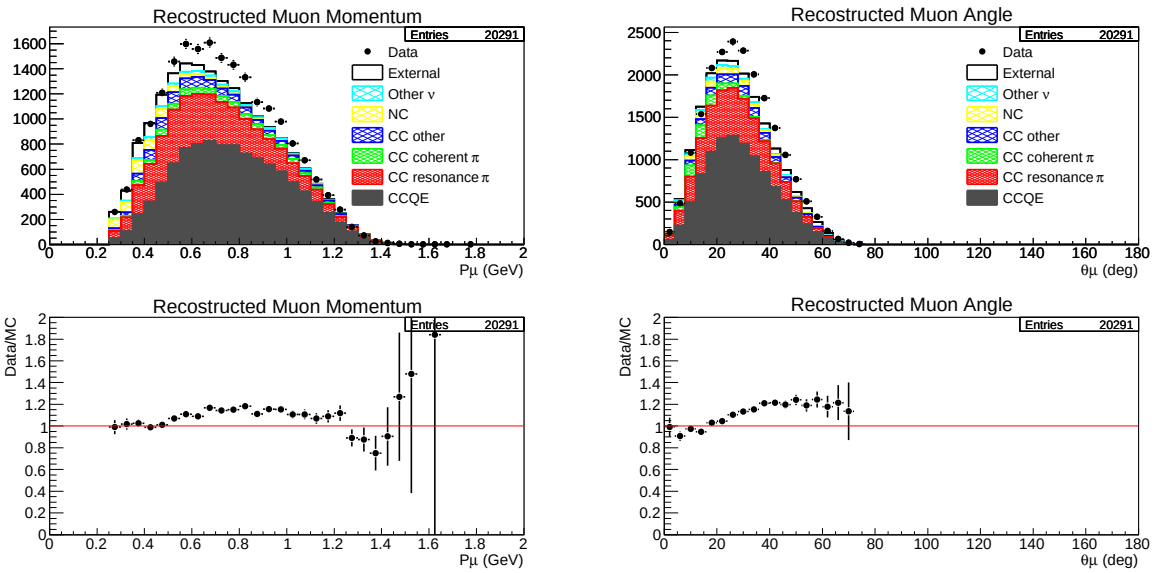

Figure C.4: Reconstructed p_μ (left) and θ_μ (right) distributions of MRD-stopped sample. MC predictions are based on NEUT, and absolutely normalized by the number of POT.

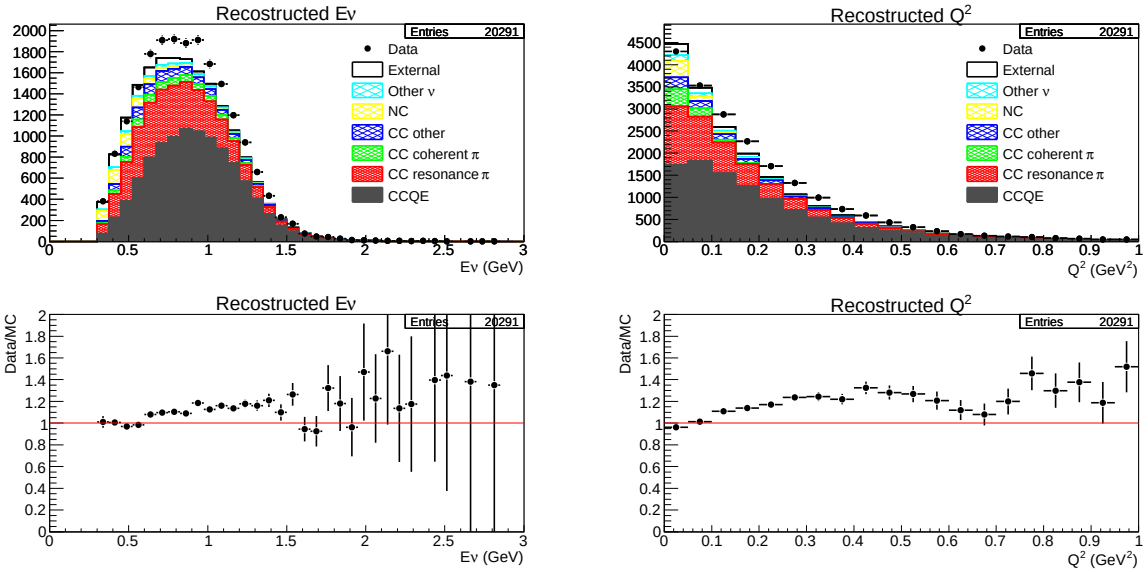

Figure C.5: Reconstructed E_ν (left) and Q^2 (right) distributions of MRD-stopped sample. MC predictions are based on NEUT, and absolutely normalized by the number of POT.

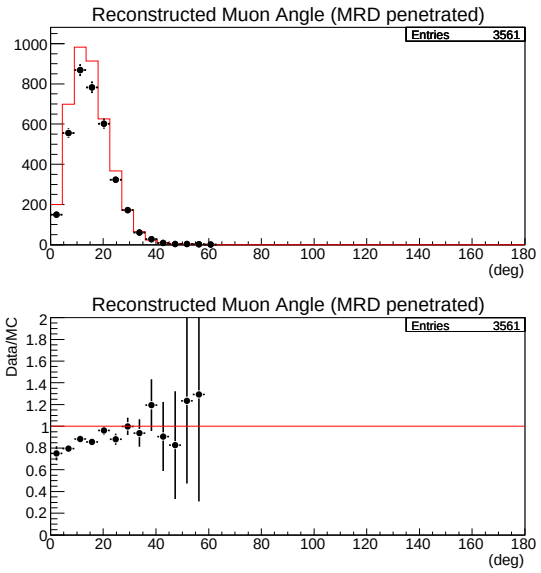

Figure C.6: Reconstructed muon angle for MRD-stopped sample. MC predictions are based on NEUT, and absolutely normalized by the number of POT.

C.3.2 Fit Result

Table C.1 shows the best fit parameters and its correlation coefficient. The χ^2 value after fitting is 191.6/153 d.o.f..

Table C.1: Best fit values and their error of the fit to the NEUT prediction. The bottom half shows the correlation coefficients for each parameters.

	f_0	f_1	f_2	f_3	f_4	f_5
Best fit	1.035	1.126	1.235	1.205	1.028	0.732
Error	0.175	0.079	0.056	0.066	0.070	0.061
f_0	1.0000	0.2939	0.0158	-0.3584	-0.4082	0.0230
f_1	0.2939	1.0000	-0.0568	-0.3164	-0.3863	-0.1149
f_2	0.0158	-0.0568	1.0000	-0.1029	-0.0814	-0.2588
f_3	-0.3584	-0.3164	-0.1029	1.0000	-0.1076	0.2047
f_4	-0.4082	-0.3863	-0.0814	-0.1076	1.0000	-0.3510
f_5	0.0230	-0.1149	-0.2588	0.2047	-0.3510	1.0000

Figure C.7 shows the the scale factor obtained by the spectrum fit with NEUT and NUANCE predictions. We found very different behavior for small E_ν scale factors between NEUT and NUANCE.

Figure C.8 shows the extracted number of events as a function of true neutrino energy, for combined sample of SciBar-stopped, MRD-stopped and MRD-penetrated events.

C.4 p_μ vs. θ_μ Distributions

Figures C.9 and C.11 show the MC predicted P_μ vs θ_μ distributions for the SciBar-stopped and MRD-stopped samples, respectively. Figures C.10 and C.12

show the distributions of (data-MC)/MC in P_μ vs θ_μ plane for the SciBar-stopped and MRD-stopped samples, respectively. Figure C.13 is the θ_μ distribution for the MRD-stopped sample.

Finally, Figure C.14 show the distributions of (data-MC)/MC divided by systematic (shown in the Figure 5.11) and statistical errors. Here we also see clear trend larger than systematic uncertainties in the data-MC difference even after fitting, just like the fitting with NUANCE predictions.

The further investigation of this described will be discussed in a separate technote.

C.5 Basic Distributions After Fit

C.5.1 SciBar-stopped Sample

Figures C.15 and C.16 shows the distributions of p_μ, θ_μ, E_ν and Q^2 distributions of SciBar-stopped sample from data and NEUT predictions. We see good agreement between data and MC after the fit.

C.5.2 MRD-stopped Sample

Figures C.17 and C.18 shows the distributions of p_μ, θ_μ, E_ν and Q^2 distributions of MRD-stopped sample from data and NEUT predictions after the fit. Again, We see good agreement between data and MC.

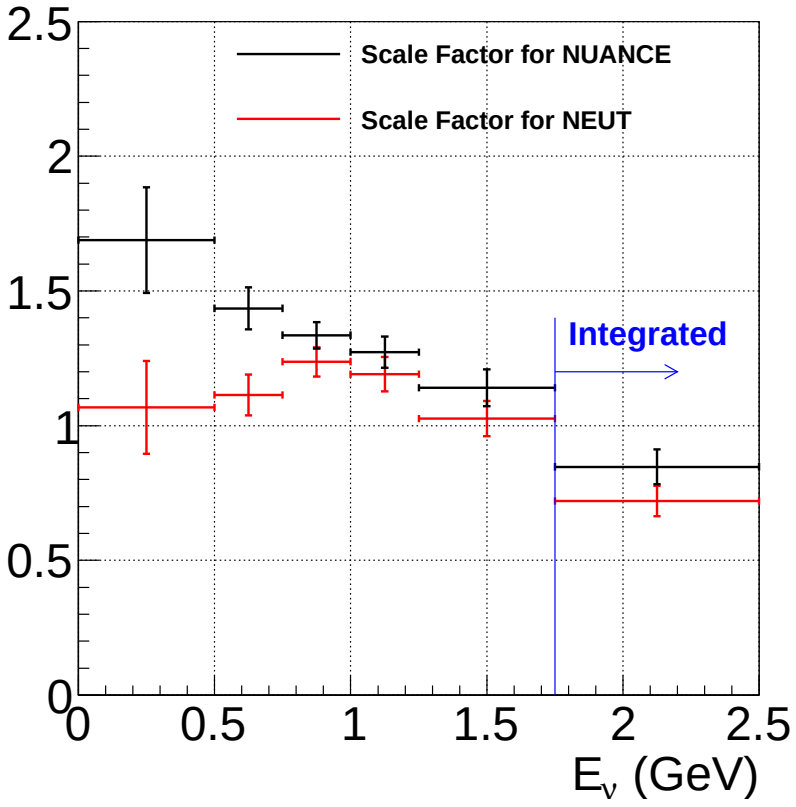

Figure C.7: The scale factors obtained by the scale spectrum fit with NEUT (red) and NUANCE (black) predictions.

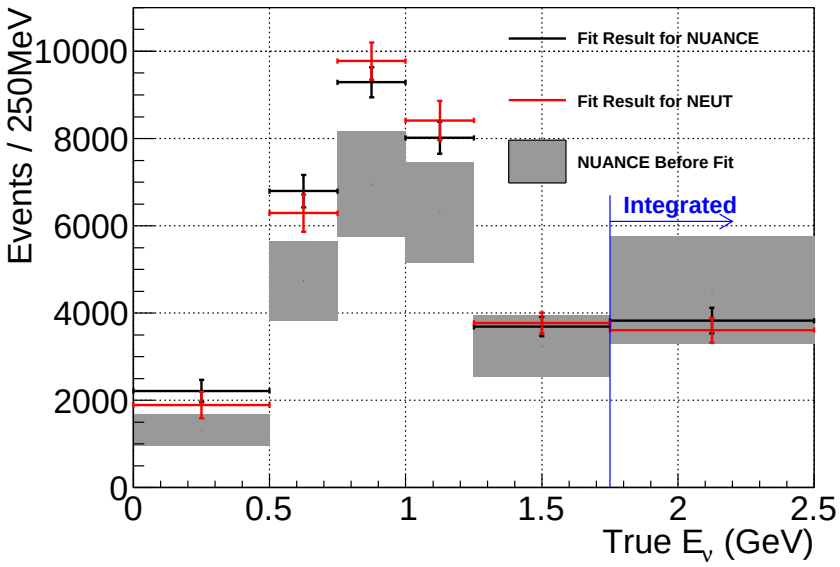

Figure C.8: The number of events as a function of true neutrino energy, for combined sample of SciBar-stopped, MRD-stopped and MRD-penetrated events.

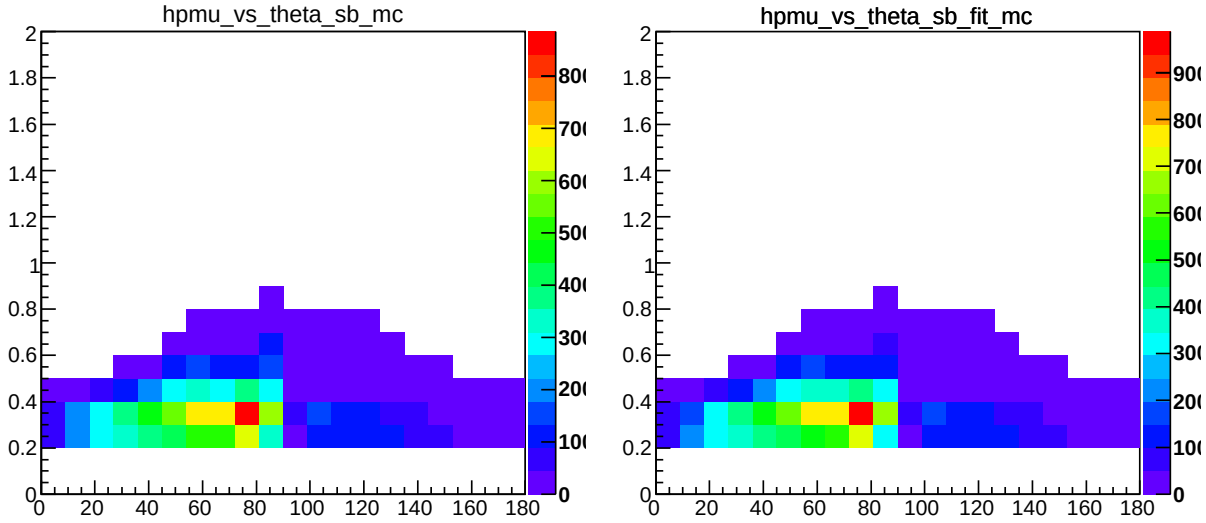

Figure C.9: MC distribution of SciBar-stopped P_μ vs. θ_μ distribution (left) before and (right) after fit. Only bins used for the shown in these plots.

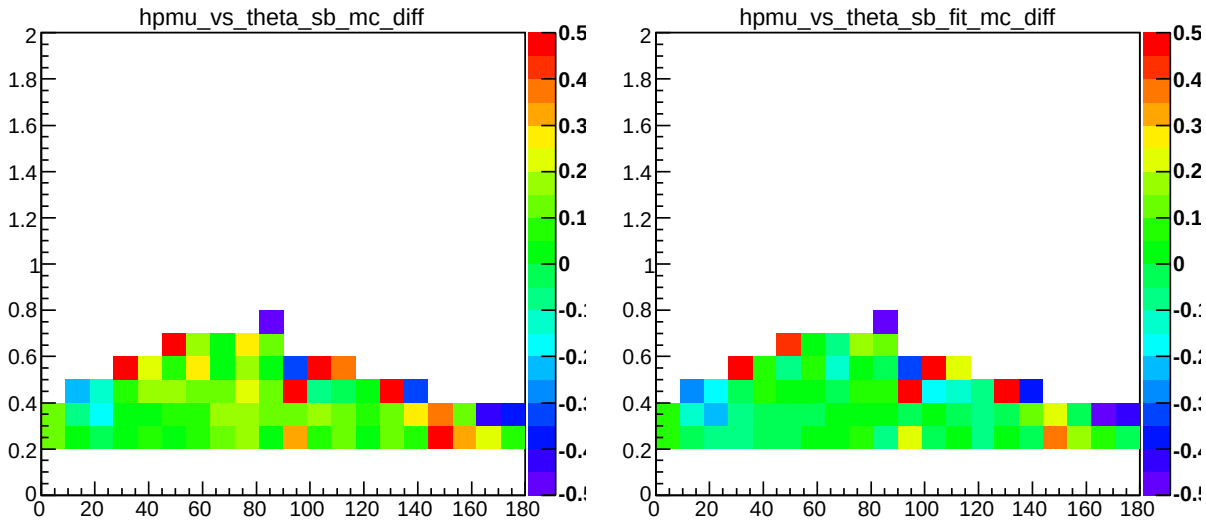

Figure C.10: Distribution of (Data-MC)/MC of the SciBar-stopped events at each P_μ vs. θ_μ bins (left) before and (right) after fit. Only bins used for the shown in these plots.

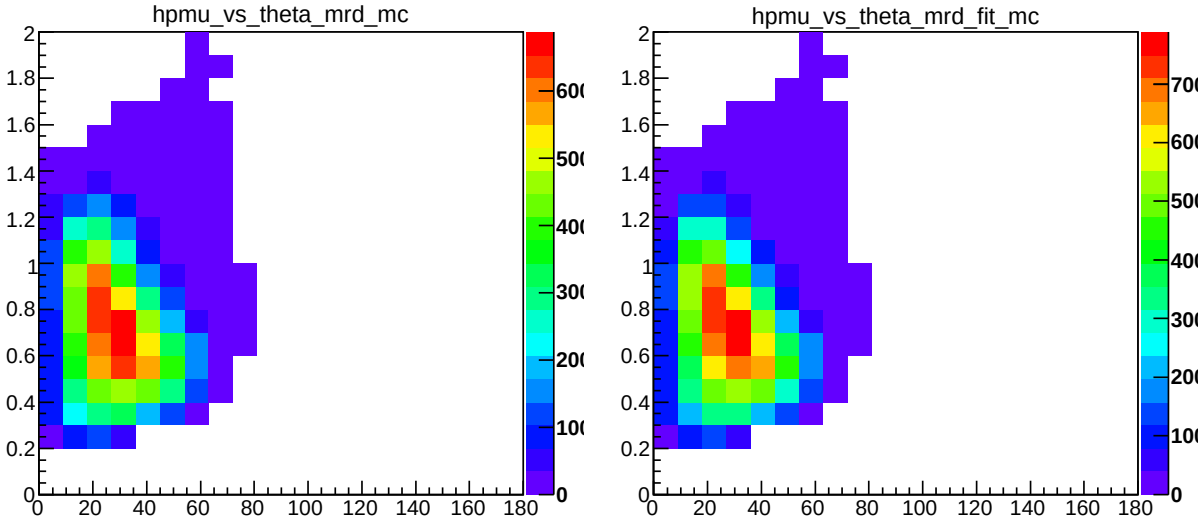

Figure C.11: MC distribution of MRD-stopped P_μ vs. θ_μ distribution (left) before and (right) after fit. Only bins used for the shown in these plots.

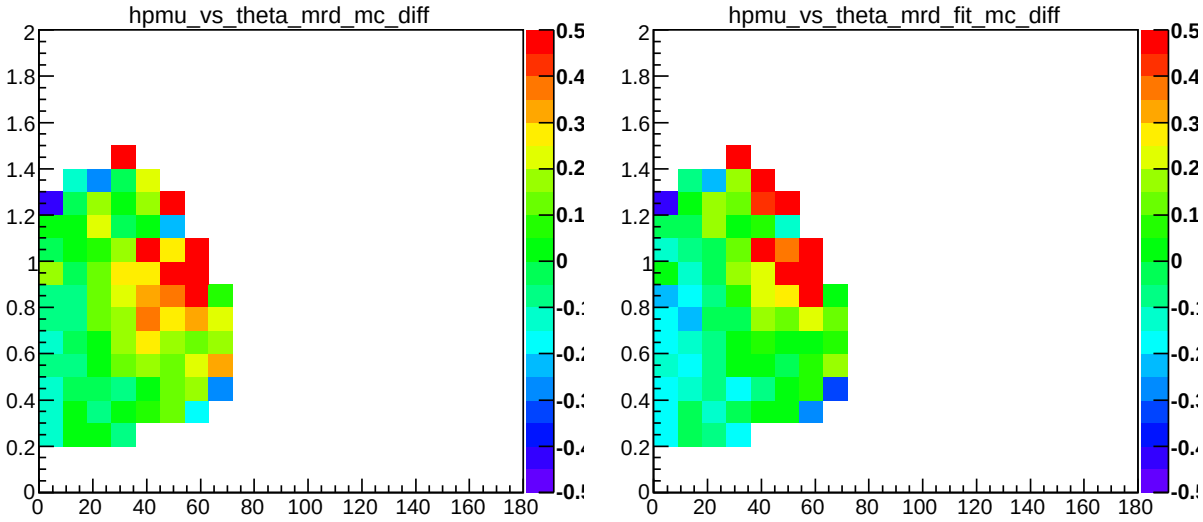

Figure C.12: Data over MC ratio of MRD-stopped P_μ vs. θ_μ distribution (left) before and (right) after fit. Only bins used for the shown in these plots.

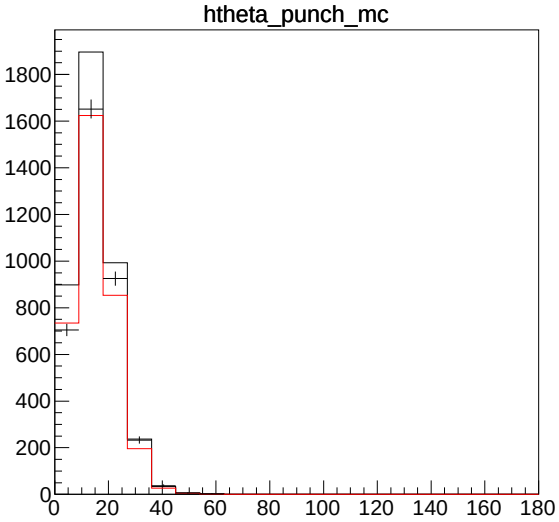

Figure C.13: θ_μ distribution for MRD-penetrated sample. Black dots shows the data point. Black line is the MC prediction before fit, and the red line is the one after fit.

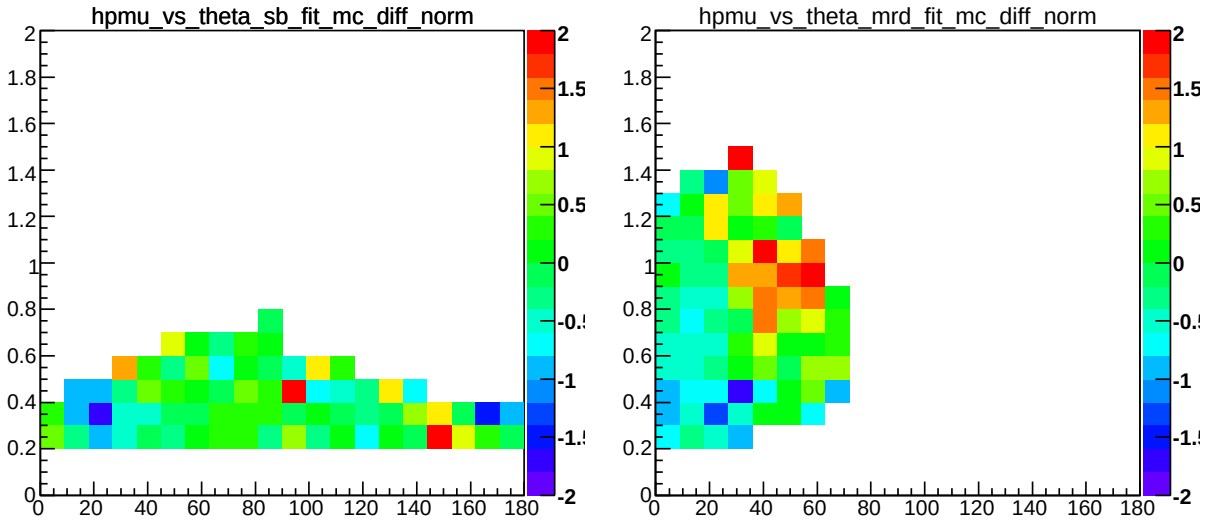

Figure C.14: The distributions of (Data-MC)/MC/(sys. + stat. error) at each P_μ vs. θ_μ bins. The left plot is that of SciBar-stopped sample, and the right one is that of MRD-stopped sample. Only bins used for the shown in these plots.

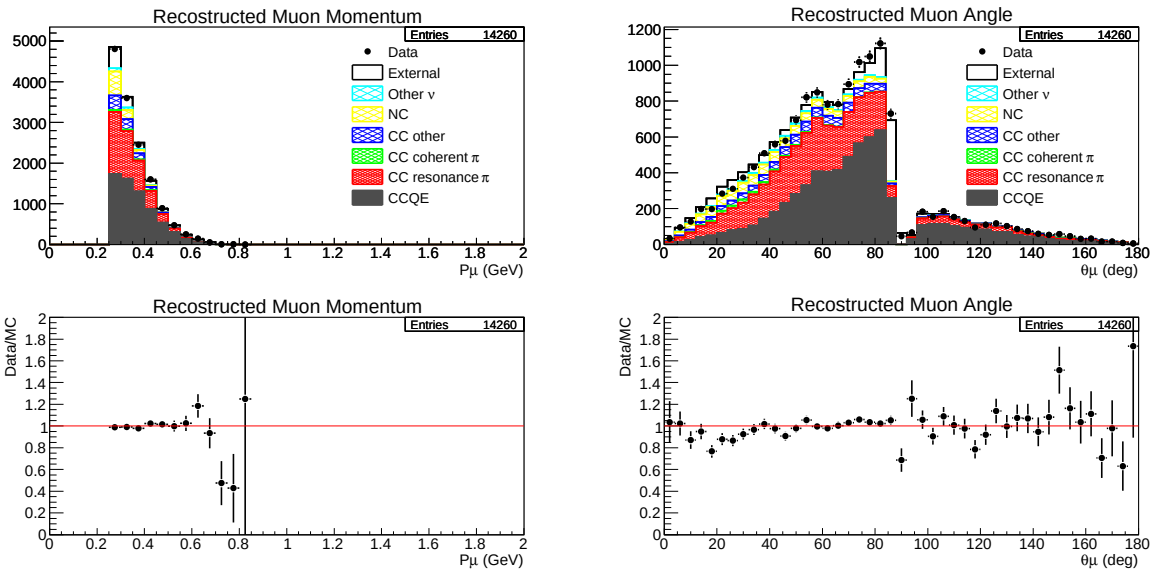

Figure C.15: Reconstructed p_μ (left) and θ_μ (right) distributions of SciBar-stopped sample. MC predictions are based on NEUT, and absolutely normalized by the number of POT.

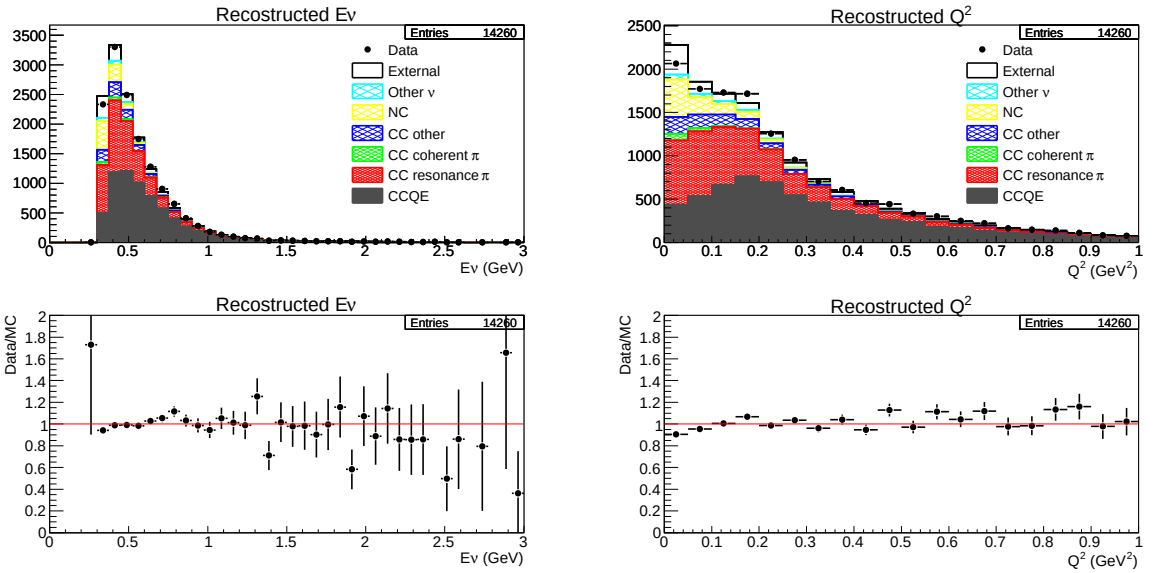

Figure C.16: Reconstructed E_ν (left) and Q^2 (right) distributions of SciBar-stopped sample. MC predictions are based on NEUT, and absolutely normalized by the number of POT.

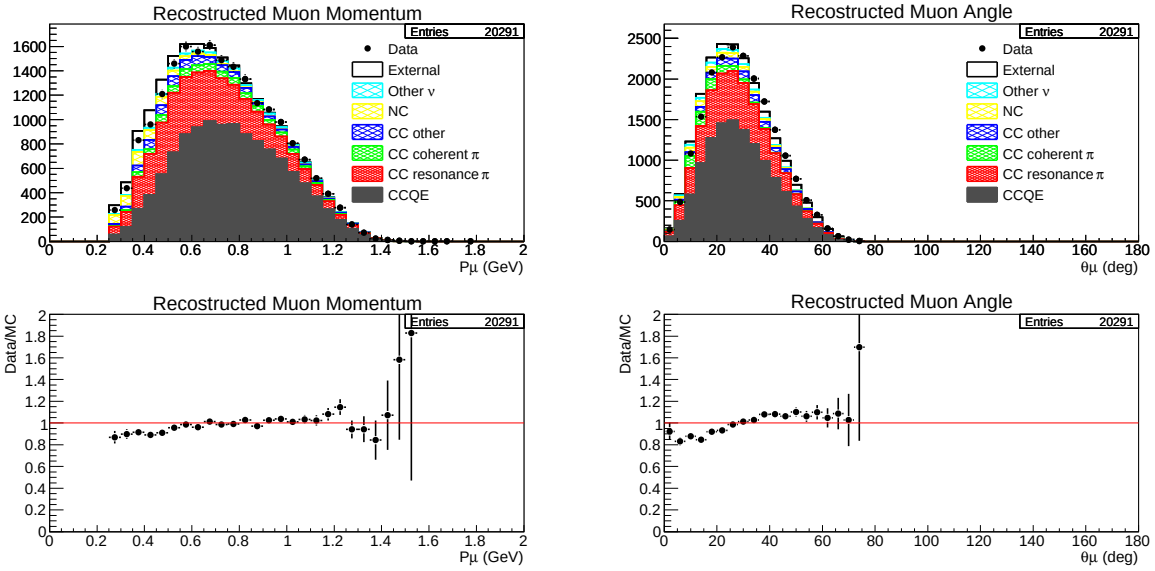

Figure C.17: Reconstructed p_μ (left) and θ_μ (right) distributions of MRD-stopped sample. MC predictions are based on NEUT, and absolutely normalized by the number of POT.

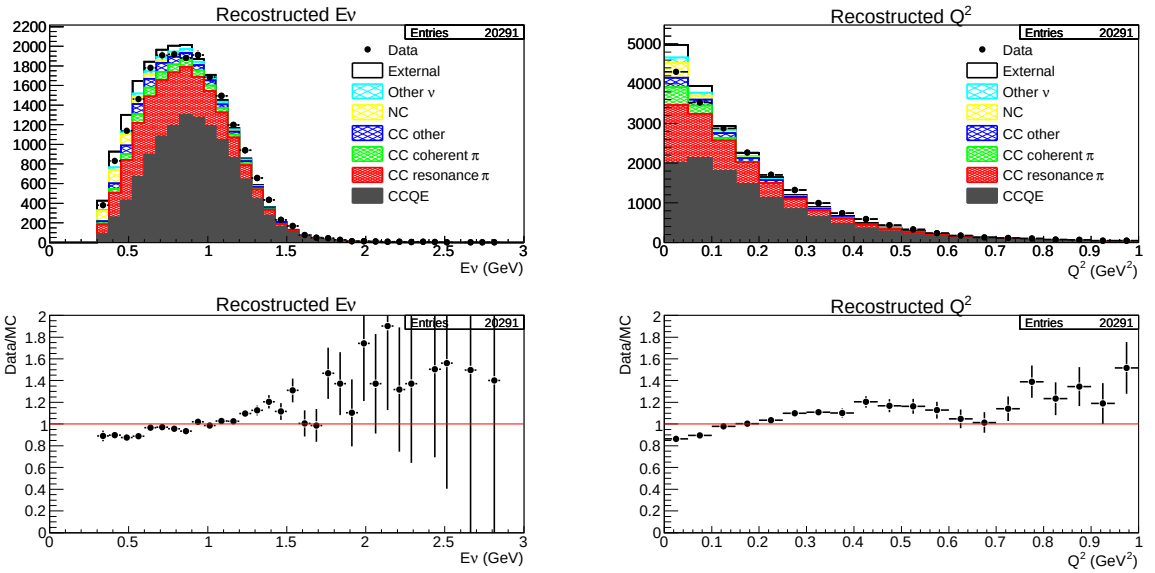

Figure C.18: Reconstructed E_ν (left) and Q^2 (right) distributions of MRD-stopped sample. MC predictions are based on NEUT, and absolutely normalized by the number of POT.

C.5.3 MRD-penetrated Sample

Figure C.19 shows the θ_μ distribution of MRD-penetrated sample from data and NEUT predictions after the fit.

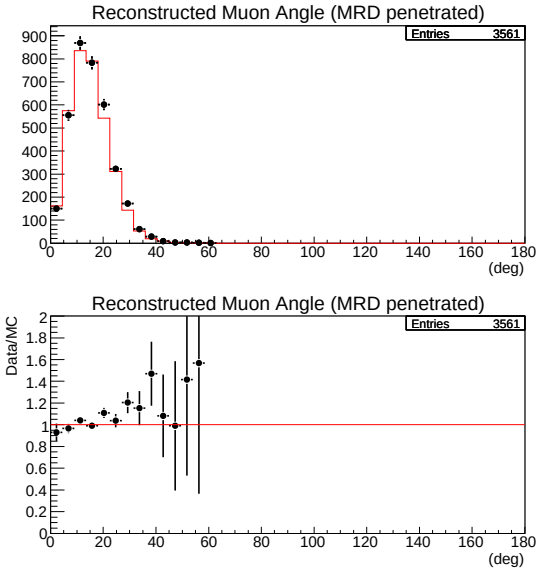

Figure C.19: Reconstructed muon angle for MRD-stopped sample. MC predictions are based on NEUT, and absolutely normalized by the number of POT.

Appendix D

Systematic Uncertainties for the Spectrum Fit

In this section, we describe the size of systematic uncertainty applied to the spectrum fit.

Figures D.1–D.15 show the size of individual systematic errors used for the spectrum fit. All errors in this section is added together to construct the total error shown in the Figures 5.11 and 5.12.

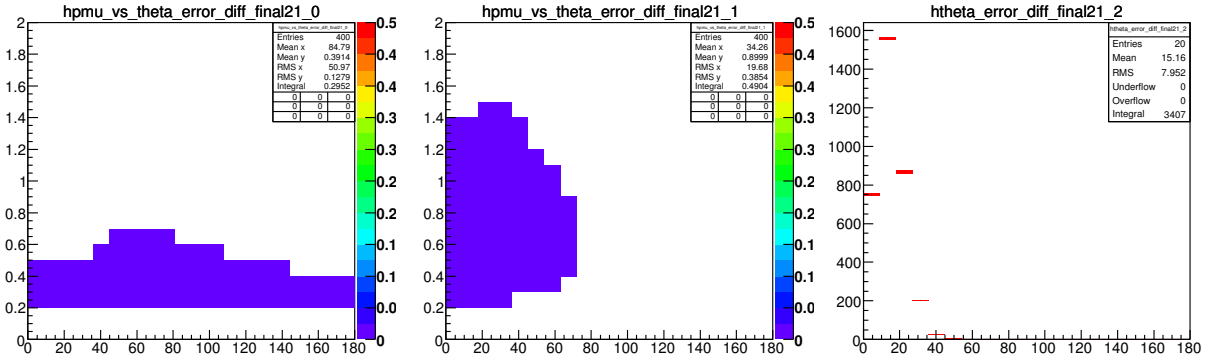

Figure D.1: Systematic uncertainties from π^+ production at the target. From the left, diagonal element of the errors for SciBar-stopped, MRD-stopped, and MRD-penetrated samples are shown.

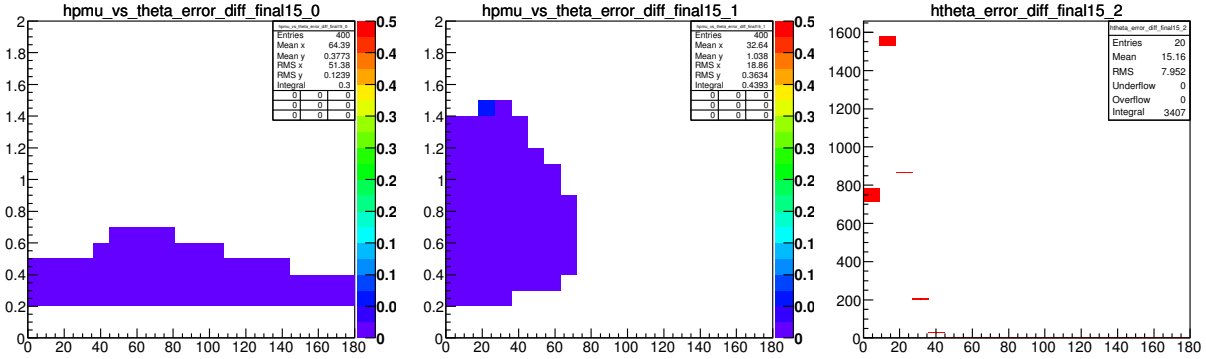

Figure D.2: Systematic uncertainties from K^+ production at the target. From the left, diagonal element of the errors for SciBar-stopped, MRD-stopped, and MRD-penetrated samples are shown.

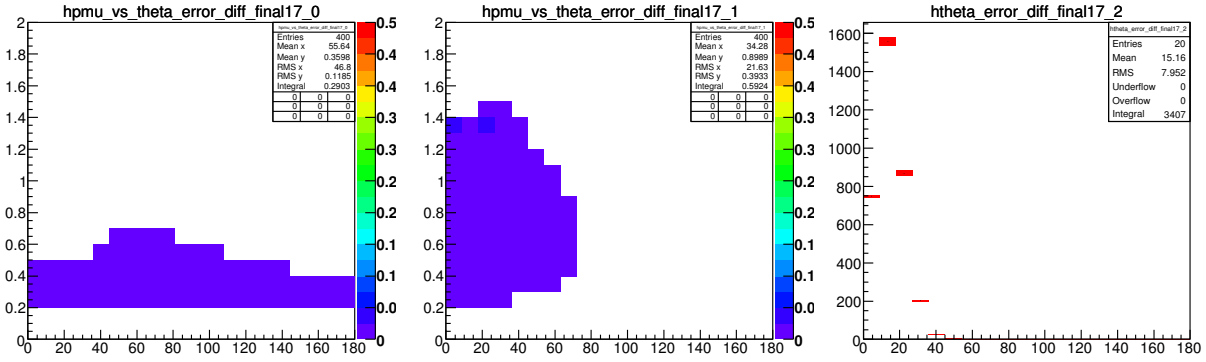

Figure D.3: Systematic uncertainties from other beam parameters, particularly from horn skin effect and horn current. From the left, diagonal element of the errors for SciBar-stopped, MRD-stopped, and MRD-penetrated samples are shown.

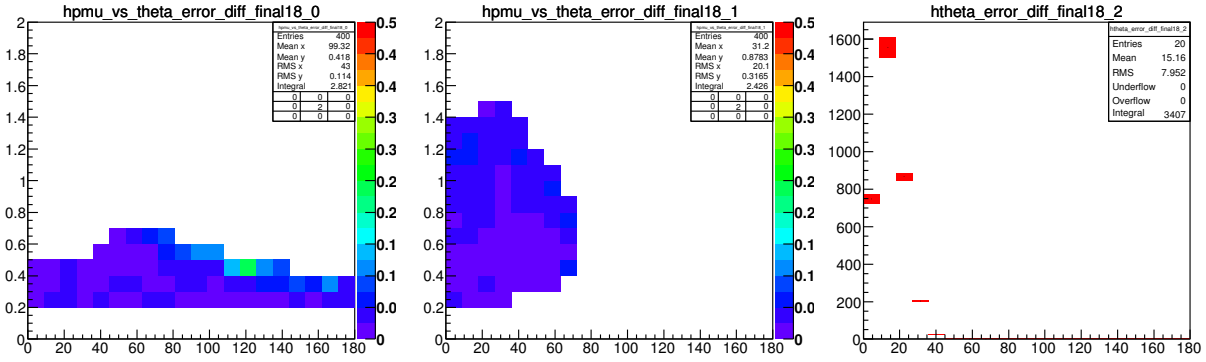

Figure D.4: Systematic uncertainties from p_F, E_B variations. From the left, diagonal element of the errors for SciBar-stopped, MRD-stopped, and MRD-penetrated samples are shown.

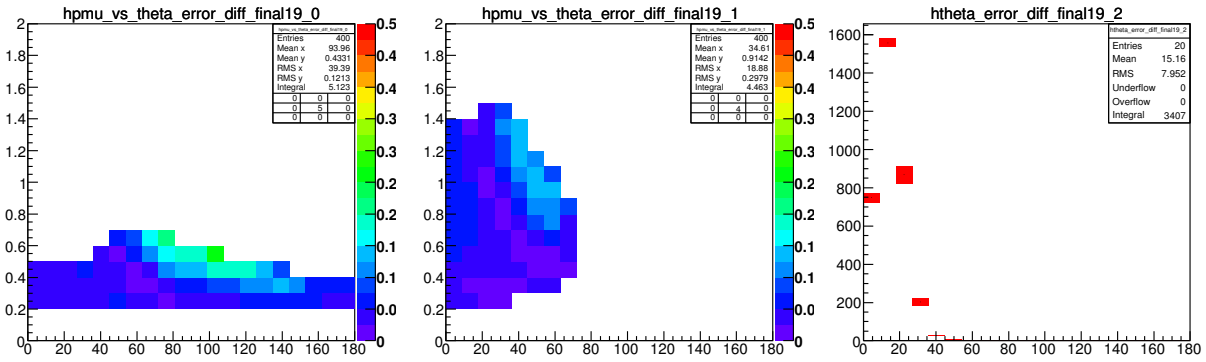

Figure D.5: Systematic uncertainties from CCQE M_A variation. From the left, diagonal element of the errors for SciBar-stopped, MRD-stopped, and MRD-penetrated samples are shown.

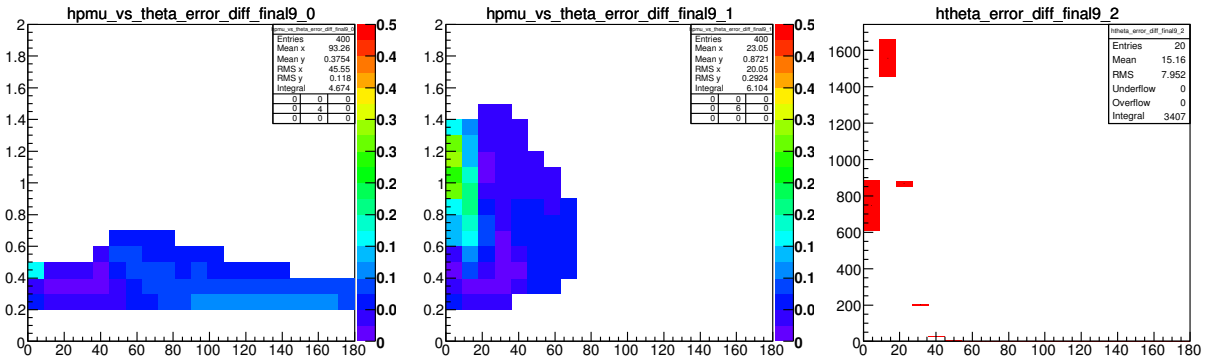

Figure D.6: Systematic uncertainties from CCQE κ variation. From the left, diagonal element of the errors for SciBar-stopped, MRD-stopped, and MRD-penetrated samples are shown.

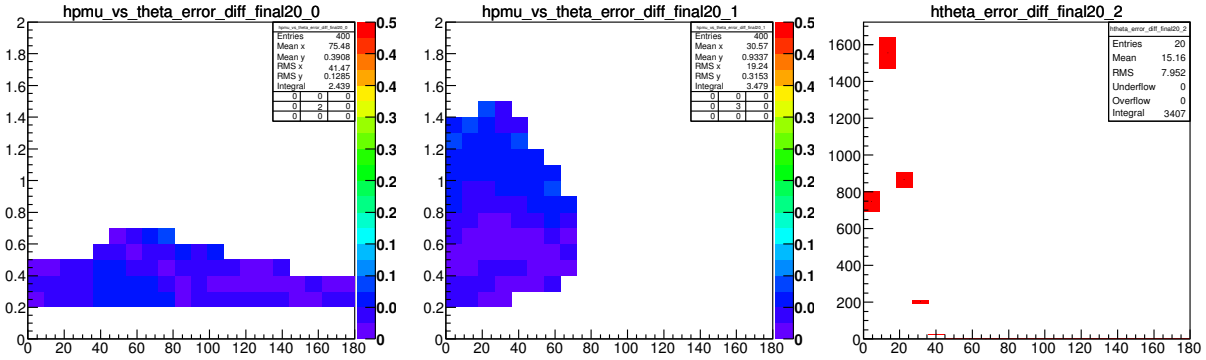

Figure D.7: Systematic uncertainties from CC-1π M_A variation. From the left, diagonal element of the errors for SciBar-stopped, MRD-stopped, and MRD-penetrated samples are shown.

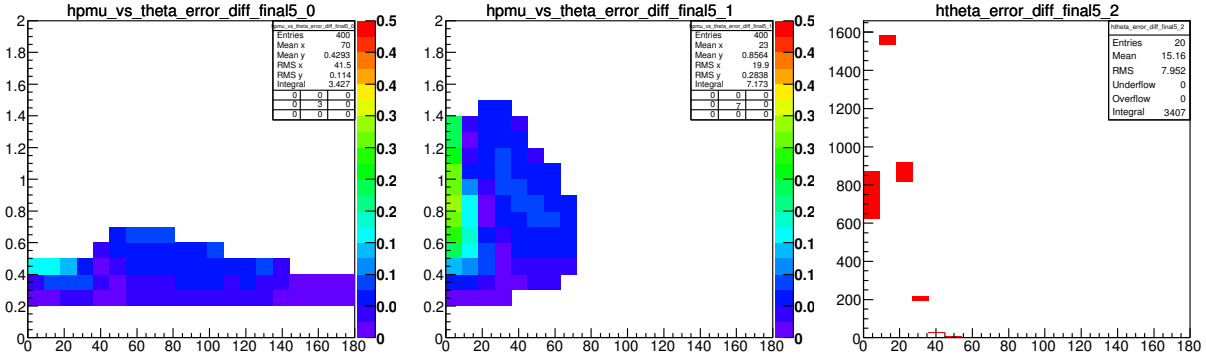

Figure D.8: Systematic uncertainties from CC-1π low Q^2 shape. From the left, diagonal element of the errors for SciBar-stopped, MRD-stopped, and MRD-penetrated samples are shown.

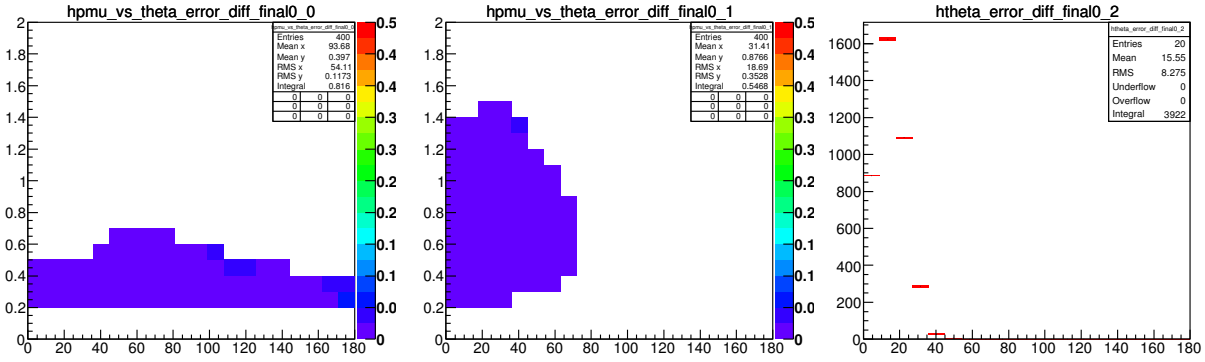

Figure D.9: Systematic uncertainties from pion interaction cross-section in SciBar. From the left, diagonal element of the errors for SciBar-stopped, MRD-stopped, and MRD-penetrated samples are shown.

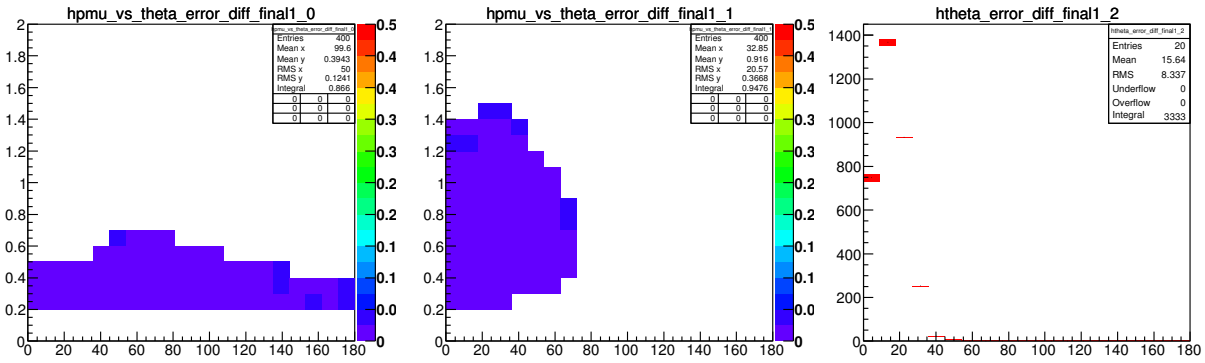

Figure D.10: Systematic uncertainties from pion absorption cross-section in nucleus. From the left, diagonal element of the errors for SciBar-stopped, MRD-stopped, and MRD-penetrated samples are shown.

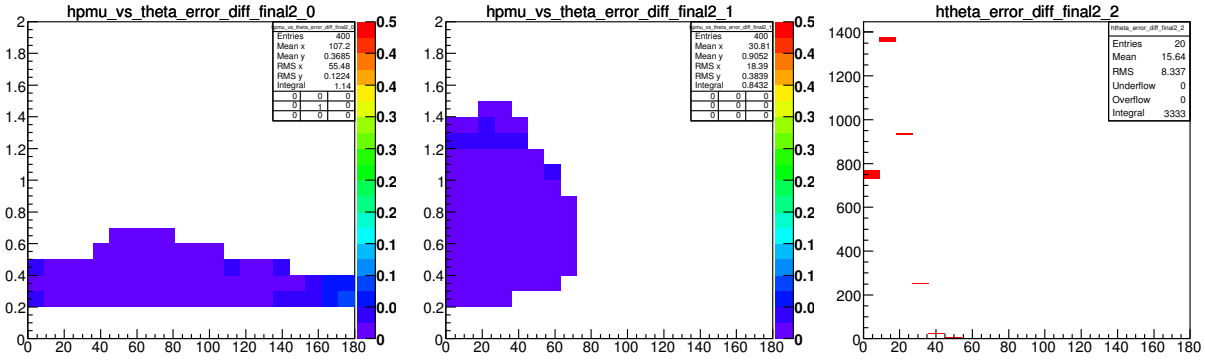

Figure D.11: Systematic uncertainties from pion charge exchange cross-section in nucleus. From the left, diagonal element of the errors for SciBar-stopped, MRD-stopped, and MRD-penetrated samples are shown.

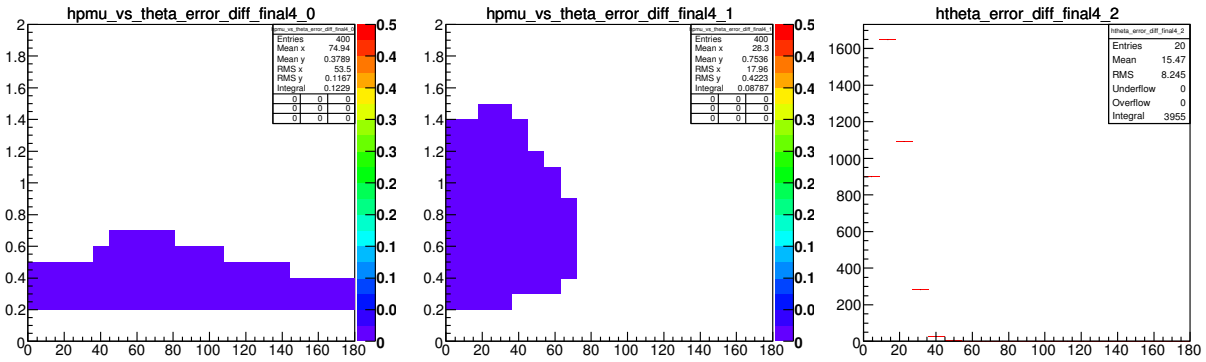

Figure D.12: Systematic uncertainties from dirt density variation. From the left, diagonal element of the errors for SciBar-stopped, MRD-stopped, and MRD-penetrated samples are shown.

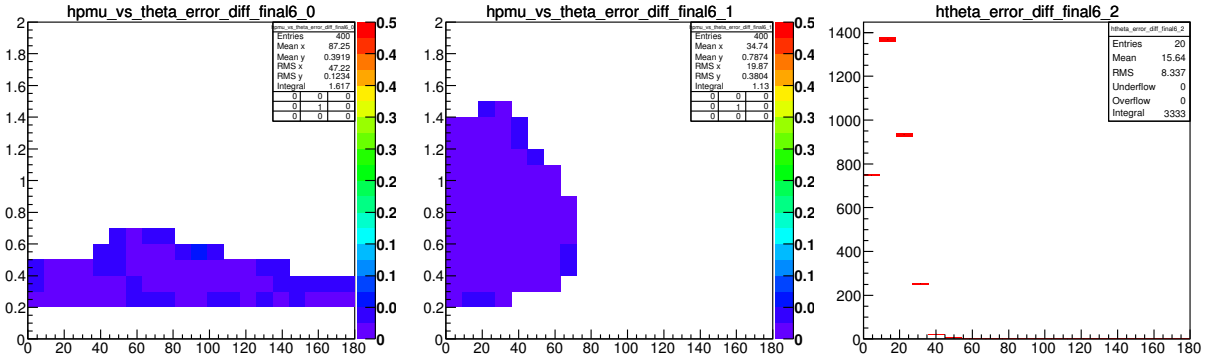

Figure D.13: Systematic uncertainties from SciBar dE/dx variation. From the left, diagonal element of the errors for SciBar-stopped, MRD-stopped, and MRD-penetrated samples are shown.

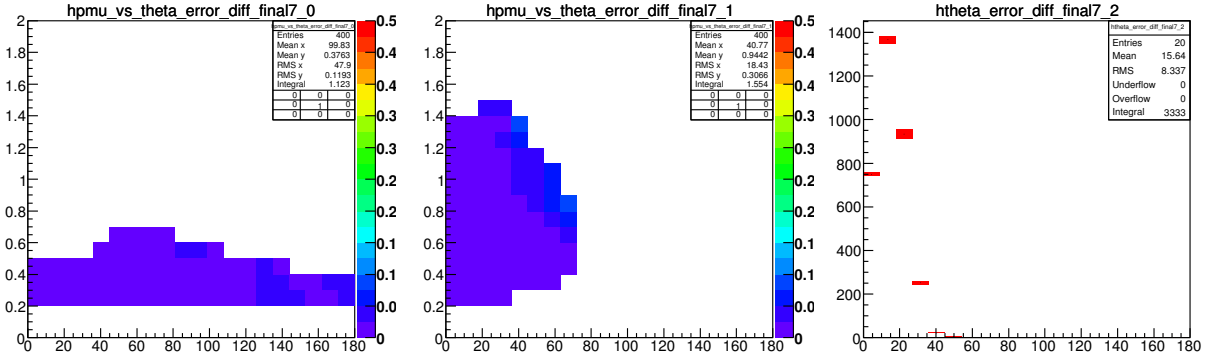

Figure D.14: Systematic uncertainties from EC dE/dx variation. From the left, diagonal element of the errors for SciBar-stopped, MRD-stopped, and MRD-penetrated samples are shown.

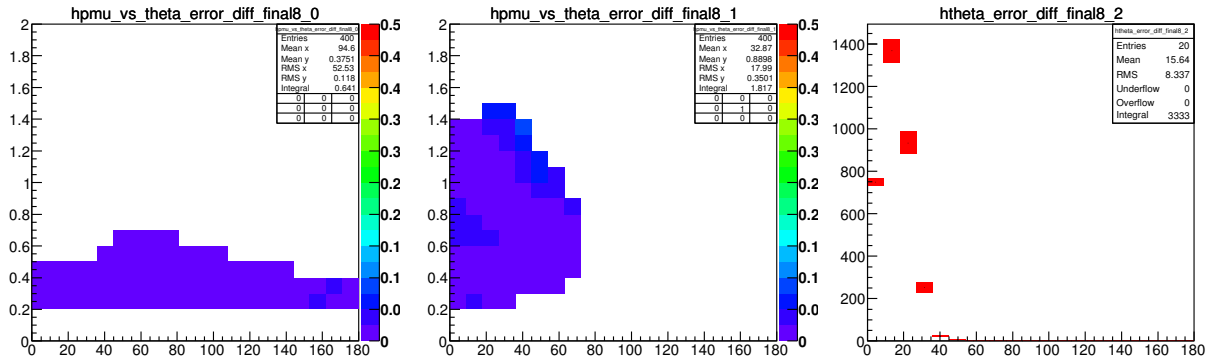

Figure D.15: Systematic uncertainties from MRD dE/dx variation. From the left, diagonal element of the errors for SciBar-stopped, MRD-stopped, and MRD-penetrated samples are shown.